



HEINRICH HEINE
UNIVERSITÄT DÜSSELDORF

**Physiologically Based Pharmacokinetic Modeling in
Pediatric Drug Development and Research:**

Methodology, Applications, and Limitations

INAUGURAL-DISSERTATION

zur Erlangung des Doktorgrades

der Mathematisch-Naturwissenschaftlichen Fakultät

der Heinrich-Heine-Universität Düsseldorf

vorgelegt von

Feras Khalil

aus Bochum

Düsseldorf, Januar 2014

Aus dem
Institut für Klinische Pharmazie
und Pharmakotherapie

Gedruckt mit der Genehmigung der
Mathematisch-Naturwissenschaftlichen Fakultät der
Heinrich-Heine-Universität Düsseldorf

Referent: Prof. Dr. Stephanie Lär
Korreferent: Prof. Dr. Jörg Breitzkreutz
Tag der mündlichen Prüfung: 10.04.2014

I. Erklärung zur Dissertation

Ich versichere an Eides Statt, dass die Dissertation von mir selbständig und ohne unzulässige fremde Hilfe unter Beachtung der „Grundsätze zur Sicherung guter wissenschaftlicher Praxis an der Heinrich-Heine-Universität Düsseldorf“ erstellt worden ist. Die Dissertation wurde in der vorgelegten oder in ähnlicher Form noch bei keiner anderen Institution eingereicht. Ich habe bisher keine erfolglosen Promotionsversuche unternommen.

Düsseldorf den

Feras Khalil

II. Danksagungen

Frau Prof. Dr. Stephanie Laer mochte ich ganz herzlich fur die Uberlassung dieses besonders interessanten und aktuellen Themas danken. Auch aufgrund Ihrer fachspezifischen, kompetenten und zuverlassigen Betreuung und Unterstutzung wahrend meiner Promotion und den damit verbundenen Erfahrungen und lehrreichen Tipps bin ich Ihnen zu besonderem Dank verpflichtet.

Herrn Prof. Dr. Jorg Breitreutz danke ich ganz herzlich fur die fachkundige Betreuung und die Ubernahme des Koreferates.

Fur die zuvorkommende Unterstutzung bei den Fragestellungen zum PK-SIM[®] Programm mochte ich Herrn Dr. Stefan Willmann von Bayer Technology Services meinen besonderen Dank aussprechen.

I would also like to thank Dr. Trevor Johnson and Dr. Jennifer Bonner for the support by questions related to SIMCYP[®] software.

Mein spezieller Dank gilt auch unserer Sekretarin am Institut fur Klinische Pharmazie und Pharmakotherapie, Frau Anita Mittler. Sie haben mich wahrend der gesamten Promotion stets unterstutzt und motiviert und mir damit die langen Tage an der Uni angenehmer und leichter gemacht.

Nicht zuletzt mochte ich sowohl meinen ehemaligen als auch meinen derzeitigen Kolleginnen und Kollegen am Institut fur Klinische Pharmazie und Pharmakotherapie der Heinrich-Heine-Universitat Dusseldorf fur das herzliche, angenehme Arbeitsklima und die kompetente Zusammenarbeit danken. Daruber hinaus mochte ich an dieser Stelle Dr. Sergej Ramusovic und Bjorn Burckhardt fur die spannenden Diskussionen und die freundliche Unterstutzung danken.

III. Zusammenfassung

Ein entscheidender Faktor für die sichere und effektive Pharmakotherapie von Kindern ist die Charakterisierung der optimalen Arzneistoffdosis. Die physiologiebasierten pharmakokinetischen (PBPK) Modelle stellen hierbei einen besonders vielversprechenden und äußerst innovativen Ansatz dar, um Hürden in der Arzneimittelentwicklung zu überwinden. In dieser Arbeit wird systematisch herausgearbeitet, wie diese mathematischen Modellbildungen entwickelt und validiert werden sollten. Für drei kardiovaskuläre Arzneimittel wurden pädiatrische PBPK-Modelle etabliert, sowie die aktuellen Möglichkeiten und Grenzen dieses Ansatzes analysiert. Zusätzlich wurde eines dieser Modelle zur Dosisfindung für eine konkrete klinische Studie mit Kindern genutzt.

Auf Grund der hohen Dichte an experimentellen Sotalol-Daten bei Erwachsenen und Kindern wurden anfangs mit zwei namhaften Computerprogrammen PBPK-Modelle entwickelt und die Prädiktivität der oralen Arzneimittelexposition über den kompletten pädiatrischen Altersbereich überprüft. Hierbei zeigte sich, dass insgesamt eine zuverlässige Vorhersage der Pharmakokinetik erzielt werden konnte. Jedoch war die Übereinstimmung der realen Expositionen der Neugeborenen mit deren Vorhersagen geringer als in allen anderen Altersgruppen. Innerhalb der Analyse stellte sich heraus, dass altersspezifische anatomischen und funktionellen Parametern innerhalb der Absorptionsmodelle der genutzten Software stärkere Berücksichtigung finden sollten. Die Prädiktivität von PBPK Modellen bezüglich oral applizierter Arzneiformen vor allem bei Neugeborenen könnte so optimiert werden. Im zweiten Teil wurde ein PBPK Modell für Amiodaron basierend auf klinischen Daten von Erwachsenen entwickelt und anschließend für die pädiatrische Anwendung skaliert. Diese stellt in der klinischen Praxis aufgrund verschiedener Faktoren eine besondere Herausforderung dar. Amiodaron zeigt unter anderem ein komplexes, von extensiver Verteilung ins Fettgewebe und extrem hoher Plasmaeiweißbindung geprägtes pharmakokinetisches Verhalten. Anhand dieses Modelles konnte der mechanistische Einfluss von pathophysiologischen Veränderungen sowie Enzym-Polymorphismen auf die Amiodaronexposition von Kindern untersucht werden, um das Verständnis der pädiatrischen Pharmakologie von Amiodaron zu verbessern. Abschließend wurde für den If-Kanalblocker Ivabradin mittels eines spezifischen PBPK Modells konkrete Dosisempfehlungen für geplante „first-in-children“ Studien getätigt. Da jegliche experimentelle Daten bei Kindern fehlten, verdeutlicht dieser Ansatz die Wichtigkeit und den herausragende Beitrag des Modelles.

Zusammenfassend zeigt diese Dissertation die vielseitige Anwendbarkeit von PBPK in der Simulation pädiatrischer Pharmakotherapien hervor und identifiziert zukünftige Entwicklungsmöglichkeiten dieser innovativen Methode.

IV. Summary

A decisive factor for a safe and effective pharmacotherapy in children is the determination of the optimal drug dose. The physiologically based pharmacokinetic (PBPK) models represent here a particularly promising and highly innovative approach to overcome hurdles in the clinical drug development process and accelerate the research in the vulnerable pediatric population. This thesis introduces novel pediatric PBPK models for three cardiovascular drugs in order to explore and analyze the current capabilities and limitations, and illustrate how such models can be used to support pharmaceutical industry in the dose selection for “first-in-children” clinical trials. It also proposes a systematic methodology for the development and validation of PBPK models to be used as a guidance when extrapolating adult data to children.

In the first part, a PBPK model for sotalolol, one of few substances for which a large set of observed pharmacokinetic (PK) data in both adult and children already exists, was developed to evaluate the accuracy of predicting oral drug exposure over the entire pediatric age range. The model identified neonates as the age group for which a priori predictions still have to be used with caution, but encouraged a wider and more confident use of such predictions in children over one year of age. It was also shown that the absorption models incorporated in the available modeling software packages still lack age-specific data for some of their anatomical and physiological parameters, and that more focus should be placed on addressing this drawback in the future. In the second part, a pediatric model for the prediction of amiodarone exposure was developed. The sparse pediatric PK data, the unfavorable side effects, as well as the complex PK profile of amiodarone hinder its optimal use in routine pediatric clinical practice and complicate the conduct of informative pediatric PK studies. The presented model can overcome these obstacles to provide valuable insights into amiodarone fate in children. It was also possible to demonstrate the potential effect of the pathophysiological changes, enzyme polymorphisms, and undocumented dosing changes on amiodarone exposure. In the last part, recommendations on dose selection for “first-in-children” trials of the heart rate-lowering drug ivabradine were proposed as a complete dosing scheme from birth to adolescence. It was shown that in order to obtain a relatively constant drug exposure, dose adaptation must be undertaken for children of different ages, and that, for example, children between 4 months and 4 years of age require double the adult weight-normalized dose to achieve the desired therapeutic levels.

In summary, this thesis demonstrates the versatility of PBPK in the simulation of pediatric pharmacotherapies and identifies future aspects of development of this innovative method.

V. Table of contents

I. Erklärung zur Dissertation	III
II. Danksagungen.....	IV
III. Zusammenfassung	V
IV. Summary	VI
V. Table of contents	VII
VI. List of Figures.....	X
VII. List of Tables.....	XII
VIII. List of abbreviations	XIV
IX. Motivation, Rationale, and Aim of the Thesis.....	XVI
Chapter 1: Physiologically Based Pharmacokinetic Modeling: Methodology, General Applications, and limitations	1
1.1. Introduction	1
1.2. PBPK model development	5
1.2.1. Overall model structure	5
1.2.2. Specification of tissues/organs to be modeled	6
1.2.3. Writing the PBPK model equations.....	7
1.2.4. PBPK-model parameterization.....	8
1.2.5. PBPK modeling software for simulation and parameter estimation.....	9
1.3. PBPK modeling applications.....	11
1.3.1. Overview of the general scope of application.....	11
1.3.2. PBPK modeling applications in pediatric populations	12
1.4. Limitations of PBPK modeling.....	15
1.5. Conclusion.....	17
Chapter 2: Pediatric physiologically based models to predict oral drug exposure across the entire pediatric age range	18
2.1. Introduction and rationale for this project.....	18
2.2. Objective of this project.....	19
2.3. Methods.....	21
2.3.1. Literature review about the modeled drug (Sotalol).....	21
2.3.2. PBPK modeling software and model parameterization	22
2.3.3. Pharmacokinetic/Clinical data in adults	24
2.3.4. Pharmacokinetic/Clinical data in children	28

2.3.5. Modeling strategy and simulation conditions	32
2.3.6. Clearance scaling.....	34
2.3.7. Evaluation of model performance	34
2.4. Results.....	37
2.4.1. Simulation results in adults.....	37
2.4.2. Simulation results in pediatrics.....	44
2.5. Discussion.....	51
2.5.2. Limitations.....	56
2.5.3. Implications and generalizations	56
2.6. Conclusion.....	57
Chapter 3: A Pediatric PBPK model to predict amiodarone intravenous exposure in severely ill pediatric patients	58
3.1. Introduction and rationale for this project.....	58
3.2. Objectives of this project	58
3.3. Methods.....	59
3.3.1. Literature search - the modeled drug.....	59
3.3.2. Used modeling software and model parameterization.....	60
3.3.3. Specific features of the adopted modeling strategy	62
3.3.4. Amiodarone pharmacokinetic and clinical data in adults	63
3.3.5. Amiodarone pharmacokinetic and clinical data in children	63
3.3.6. Evaluation of model performance	68
3.4. Results.....	70
3.4.1. Model simulation results in adults	70
3.4.2. Model simulation results in pediatrics	72
3.4.3. Results of the pediatric model modified for low protein levels	79
3.5. Discussion.....	80
3.6. Conclusions	86
Chapter 4: Ivabradine dose selection in “first-in-children” trials: an application of a pediatric PBPK model to support the clinical drug development process.....	87
4.1. Introduction	87
4.2. Objective of this project.....	88
4.3. Methods.....	89
4.3.1. Adult clinical data.....	89

4.3.2. Model parameterization and characterization.....	89
4.3.3. Model development strategy	92
4.3.4. Model evaluation	92
4.3.5. Investigating age-related differences in ivabradine exposure	93
4.4. Results.....	95
4.4.1. Predictability of IV ivabradine pharmacokinetics by the basic adult model	95
4.4.2. Ivabradine clearance scaling to children	109
4.4.3. Hypothetical ivabradine exposure in children.....	110
4.4.4. Recommendations for age-specific dose adaptation in children	114
4.5. Conclusion.....	116
X. Final summary of the thesis and perspectives	117
XI. References	121
XII. Curriculum Vitae	133

VI. List of Figures

- Figure 1-1:** The general concept and structure of a PBPK model
- Figure 1-2:** Example of the differential equations used in the PBPK models
- Figure 1-3:** Schematic drawing of a potential application of pediatric PBPK simulations to suggest sampling times (adopted from Willmann et al., 2003)
- Figure 2-1:** Demographics of the observed pediatric population who received oral sotalol
- Figure 2-2:** Plots of the observed sotalol plasma concentration profiles, children 1-40
- Figure 2-3:** Plots of the observed sotalol plasma concentration profiles, children 41-80
- Figure 2-4:** The general workflow for the development of a pediatric PBPK Model
- Figure 2-5:** Comparison of the visual predictive checks of simulation results in adults between the two modeling software from representative studies
- Figure 2-6:** Diagnostic goodness of fit plots for the sotalol model in adults
- Figure 2-7:** Visual predictive checks of simulation results of sotalol in representative pediatric patients using the two modeling software
- Figure 2-8:** Comparison between predicted and observed PK-parameters in the different pediatric age groups
- Figure 2-9:** Predicted versus observed plots for sotalol in the different pediatric age groups
- Figure 3-1:** Results of the analytical determination of amiodarone concentrations in 7 pediatric patients (patients 21-27)

- Figure 3-2:** Simulated systemic exposure of amiodarone in adults
- Figure 3-3:** Results of pediatric simulations using the PBPK amiodarone model (patients 1-9)
- Figure 3-4:** Results of pediatric simulations using the PBPK amiodarone model (patients 10-18)
- Figure 3-5:** Results of pediatric simulations using the PBPK amiodarone model (patients 19-27)
- Figure 3-6:** Box plots of percentage errors of model predictions in each individual pediatric patient
- Figure 3-7:** Comparison between the standard and protein-adjusted models of intravenous amiodarone prediction errors in the pediatric study population
- Figure 3-8:** Impact of abnormally low body weight and decreased muscle mass on AMI concentrations
- Figure 3-9:** Potential impact of suspected undocumented dosing change on AMI concentrations
- Figure 4-1:** Simulation results of individual adult patients receiving IV ivabradine, internal validation set
- Figure 4-2:** Simulation results of individual adult patients receiving IV ivabradine, external validation set
- Figure 4-3:** Summary of goodness of fit plots for the ivabradine model
- Figure 4-4:** Results of population simulations of the entire adult study population
- Figure 4-5:** Potential protocol deviation scenarios and their effect as simulated by the model
- Figure 4-6:** Scaled clearance of ivabradine across the pediatric age spectrum
- Figure 4-7:** Predicted exposure of ivabradine predicted exposure across the pediatric age spectrum
- Figure 4-8:** Effect of age-specific dose adaptations on ivabradine exposure in children

VII. List of Tables

- Table 2-1:** Sotalol model input parameters
- Table 2-2:** Summary of pharmacokinetic studies of intravenous sotalol used for modeling in adults
- Table 2-3:** Summary of pharmacokinetic studies of oral sotalol used for modeling in adults
- Table 2-4:** Summary of basic information on the observed pediatric population (the used pediatric data set)
- Table 2-5:** Numerical model evaluation for both developed models in adults
- Table 2-6:** Calculated PK parameters for observed and predicted sotalol plasma profiles after IV drug application in adults
- Table 2-7:** Calculated PK parameters for observed and predicted sotalol plasma profiles after oral drug application in adults
- Table 2-8:** Evaluation metrics and calculated observed to predicted ratios of AUC_{last} , C_{max} , t_{max} , and k_e of the entire pediatric collective using both models
- Table 2-9:** List of the anatomical, physiological, and drug specific parameters used in the absorption model
- Table 3-1:** Amiodarone model input parameters
- Table 3-2:** Summary of the characteristics of the PK studies used for modeling in adults
- Table 3-3:** Demographics and dosing information of the entire pediatric cohort used for amiodarone model evaluation
- Table 3-4:** Laboratory findings of the entire pediatric cohort used for amiodarone model evaluation
- Table 3-5:** Model simulation results of IV amiodarone application in adults

- Table 3-6:** List of the potential reasons for the deviations in four pediatric patients together with their impact on the calculated model evaluation metrics
- Table 3-7:** Model evaluation metrics of pediatric simulations
- Table 4-1:** General characteristics of the patient population who received ivabradine
- Table 4-2:** Ivabradine model input parameters
- Table 4-3:** Comparison of predicted and observed PK parameters of ivabradine in adults
- Table 4-4:** List of individualized and fixed parameters
- Table 4-5:** Numerical metrics of ivabradine model evaluation
- Table 4-6:** Input parameters for the adult virtual population
- Table 4-7:** Predicted ivabradine exposure across the age spectrum
- Table 4-8:** List of recommended first dose of ivabradine in each pediatric age group

VIII. List of abbreviations

[P]	concentration of plasma protein
ADAM	advanced dissolution, absorption, and metabolism
AE	absolute error
ALT	alanine transaminase
APE	absolute percentage error
ASD	atrial septal defect
AST	aspartate transaminase
AUC _{0-inf}	area under the plasma concentration-time curve from time zero to infinity
AUC _{last}	area under the plasma concentration-time curve from the first to the last concentration points
B:P ratio	blood-to-plasma concentration ratio
BCS	Biopharmaceutics Classification System
BMI	body mass index
BSA	body surface area
BW	body weight
CI	confidence interval
CID	PubChem Compound Identification number
CL	drug clearance
C _{last}	last measured concentration in a plasma profile
CL _H	hepatic clearance
CL _{int}	intrinsic clearance
CL _R	renal clearance
C _{max}	maximum concentration
CREAT	serum creatinine level
CRP	C-reactive protein
CYP	cytochrome P450
DEA	desethylamiodarone
DORV	double outlet right ventricle
EMA	European Medicines Agency
f _u	fraction unbound
GET	gastric emptying time
γ-GT	gamma-glutamyl transpeptidase
HF	heart failure
HPLC	high performance liquid chromatography
ICRP	International committee on radiological protection for human values

IV	Intravenous
IVIVE	in vitro-in vivo extrapolation
k_e	elimination rate constant
K_m	substrate concentration at which the reaction velocity is half of maximum
K_p	tissue-to-plasma distribution coefficient
LOD	limit of detection
logD	logarithmic distribution coefficient
log <i>P</i>	logarithmic octanol-water partition coefficient
LOQ	limit of quantification
M&S	modeling and simulation
MAPE	mean absolute percentage error
MDAPE	median absolute percentage error
MDPE	median percentage error
MM-Kinetics	Michaelis-Menten kinetics
MPE	mean percentage error
MRD	mean relative deviation
MW	molecular weight
P_{app}	apparent permeability coefficient
PBPK	physiologically based pharmacokinetic
PD	pharmacodynamics
PDA	patent ductus arteriosus
PE	percentage error
PK	pharmacokinetic
pK_a	acid dissociation constant
$P \times SA$	permeability-surface area product
Q_H	hepatic blood flow
Ratio _(Obs/Pred)	observed to predicted ratio
RMSE	root mean square error
SD	standard deviation
SITT	small intestinal transit time
SVT	supraventricular tachycardia
$t_{1/2}$	half-life
TGA	transposition of the great vessels
t_{max}	time of maximum concentration
UV	ultra violet
V_{max}	maximum reaction velocity
VSD	ventricular septal defect

IX. Motivation, Rationale, and Aim of the Thesis

Physiologically based pharmacokinetic (PBPK) modeling is an innovative technique that can bridge drug pharmacokinetics from adults to children, and explore, *a priori*, age-related PK changes, thereby offering many advantages for healthcare providers and researchers in the field of pediatrics. However, uncertainty and debate persist on whether data generated through PBPK modeling are suitable for use across all pediatric age groups, and the extent to which the complexity of the PK profile of a drug can influence the data. This thesis aims to fill important gaps in this knowledge by exploring current limitations of PBPK modeling in pediatric populations, demonstrating applications, and highlighting areas for improvement in order to ensure proper and wider implementation of this technique in routine pediatric clinical practice, research, and drug development.

In order to achieve this objective, it was necessary to establish a comprehensive base of background information on the structure, possible applications, general limitations, and available modeling software tools and packages (Chapter 1). In the second chapter, the first challenge was to identify the pediatric age groups for which PBPK model-generated data still have to be used with caution. This was done by evaluating the accuracy of the model in predicting the dose-exposure relationship after oral administration across the entire pediatric age/development continuum using two commonly used PBPK modeling software packages. Another challenge was addressed in the third chapter by exploring whether a pediatric PBPK model can be developed to predict the systemic exposure of amiodarone, a very effective drug that is used in refractory cases but which possesses a complex PK and side effect profile, in severely ill pediatric patients. A model for such a drug can not only explore age-related PK changes, but also aid in optimizing therapy of individual patients. In the last chapter, a PBPK model was developed to provide *a priori* data to support dose selection for “first-in-children” trials of the heart rate-lowering drug ivabradine. Such information can be integrated into the pediatric investigation plan (PIP), since the regulatory agencies do recognize modeling and simulation (M&S) as an important part of any submitted documents.

Chapter 1:

Physiologically Based Pharmacokinetic Modeling: Methodology, General Applications, and limitations

1.1. Introduction

Modeling and simulation is an acknowledged methodology by industry, academia, and regulators to support and optimize clinical trials and/or to be used as a data analysis tool during various stages of the drug-development process (Bellanti and Della Pasqua 2011; Manolis and Pons 2009; Rowland et al. 2011). The terms “modeling” and “simulation” are closely related; however, modeling is the science of using mathematics to describe and quantify a system or a process, whereas “simulation” refers to the use of these models to make quantitative predictions (Manolis et al. 2011). In the field of pharmacokinetics, one has to differentiate between the conventional PK compartmental modeling, the so-called top-down approach, and the PBPK modeling, the bottom-up approach. Both of these approaches can be extended to incorporate a pharmacodynamic component and, thus, to link drug exposure with a certain effect.

The conventional PK compartmental models have important clinical applications particularly in establishing therapeutic dosage regimens and addressing responsible factors for the observed variability in drug behavior in a certain population. However, such models are inherently limited in the information they provide, as they are data-driven, i.e., dependent in their structure and parameters on the experimental data available. In addition, they do not have an obvious relationship with the anatomical structure or the physiological function of the species under study. This makes these models unsuitable to be used beyond the experimental data, e.g., for age extrapolation, or to explore changes in drug pharmacokinetics under different physiological, pathological, or pharmacological conditions.

In contrast, PBPK models are mechanistic models that are independent of the measured concentrations but are elaborated based on the known anatomy and physiology of the living organism being modeled; PBPK models utilize actual

anatomical and physiological measures that are involved in the complex absorption, distribution, metabolism, and excretion processes (Khalil and Läer 2011). Such physiologically realistic models provide a rational basis for inter-species, inter-individual, or across-age scaling, and are able to offer greater insight into drug disposition in the body, as they can describe the time course of drug concentration in various body tissues. PBPK models can also be used as a predictive tool to a priori explore changes in drug behavior under altered physiological conditions or in pathological conditions. For these reasons, PBPK models are considered superior to classical compartmental models in many respects.

Although the concept of PBPK modeling was introduced years ago, it had not achieved the scope of development and implementation that it deserves until recently, as evidenced by the large increase in publications in this field over the past few years (Nestorov 2007). The general concept of PBPK modeling is to mathematically describe relevant physiological, physicochemical, and biochemical processes that determine the PK behavior of a compound in as much detail as is appropriate or needed. In order to accomplish this, principles of anatomy and physiology are employed to represent the species to be modeled as a structure composed of physiologically relevant compartments, with each compartment often representing a single organ or tissue. Following the anatomical structure of the organism, these compartments are interconnected via the blood circulation loop, and the mass-balance equations for each compartment describing the fate of the substance within it are established. To solve these equations, the PBPK model uses physiological and substance-specific parameters. In the end, PBPK models can describe and/or predict drug pharmacokinetics in certain individuals, or under certain physiological or pathological conditions, where the primary result of a simulation is a set of concentration-time curves illustrating the temporal behavior of the drug in blood/plasma and/or other relevant organs. **Figure 1-1** illustrates the general concept behind a PBPK model.

The objective of this chapter (Khalil and Läer 2011) is to introduce the necessary background information on this modeling technique by providing a

simplified general overview of the structure of PBPK models as well as the various software packages that can be used in model development. I have also highlighted some of the technique's weaknesses and provided an overview of its multiple applications that show the potential of PBPK models.

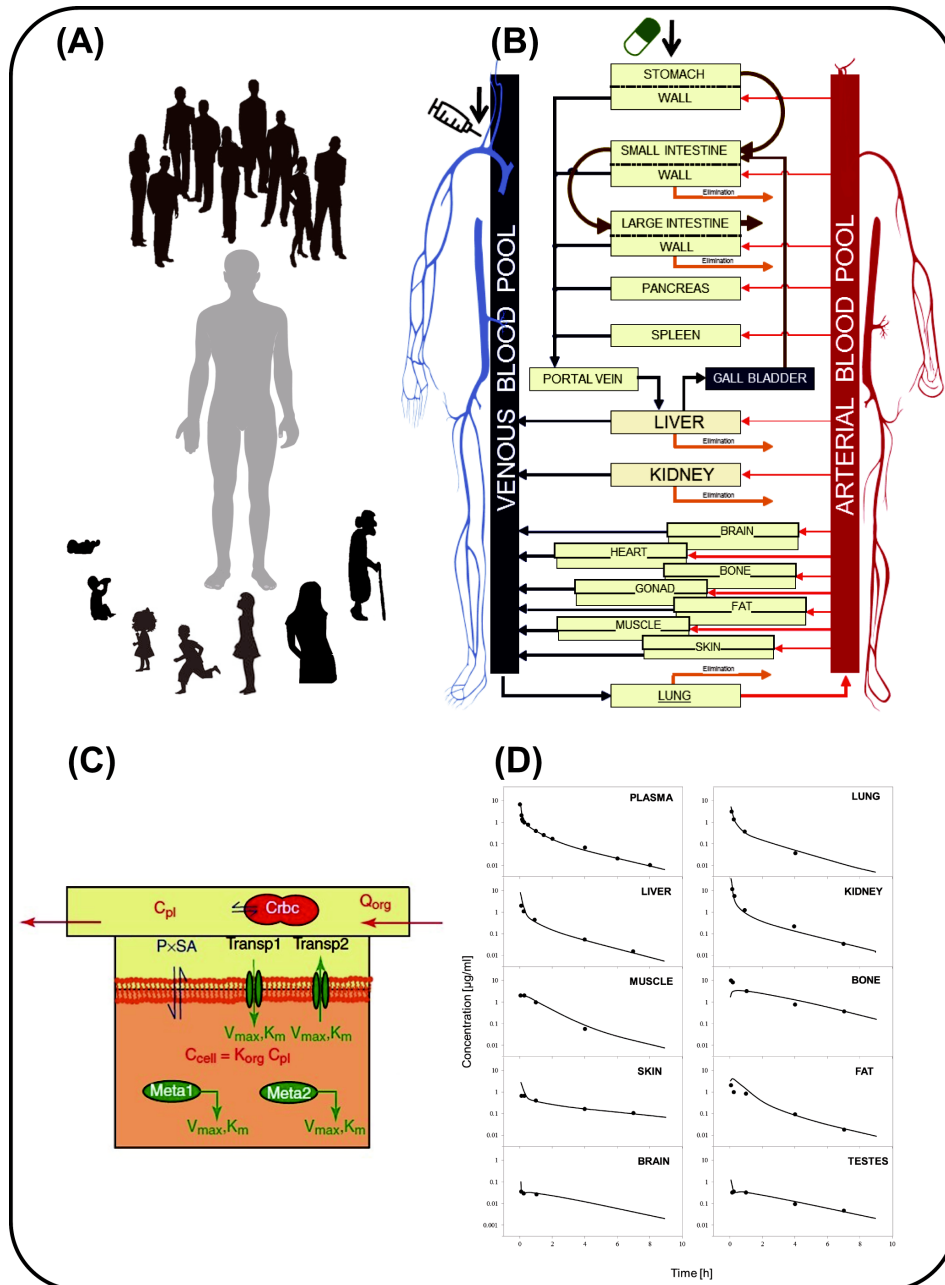


Figure 1-1. The concept for building a PBPK model modified according to Willmann et al. (2003). (A): Organisms (e.g., humans of different ages or populations) are the basis for the model. (B): The organism is divided into a number of compartments, each representing a single organ. To describe the distribution of compounds in the body, the organs are connected via their arteries and veins to the arterial and venous blood pool. The rate of inter-compartmental mass transport is determined by organ-specific blood flow rates. The organs are mathematically connected. (C): Division of each organ into three sub-compartments representing the vascular space with blood cells and the interstitial and cellular space. The interstitial space is assumed to be in direct contact with the plasma. The exchange of substances between the cellular and interstitial compartment can occur by permeation across the membranes via passive diffusion as well as active influx and efflux transport processes governed by saturable Michaelis-Menten (MM) kinetics with V_{max} and K_m as parameters. Metabolism of substances (Meta1, Meta2) occurs via active enzymes (MM-kinetics). Finally, the model consists of a large number of coupled differential equations. (D): Output of the model: Concentration-time curves shown are simulated and observed ciprofloxacin concentrations in various organs after ciprofloxacin 5mg/kg was intravenously administered to a rat.

1.2. PBPK model development

Generally, the five major steps in PBPK model development include: 1) specifying general model structure, 2) specifying the tissue being modeled, 3) writing model equations, 4) defining model parameters, and 5) simulations and/or parameter estimation.

1.2.1. Overall model structure

PBPK models emulate the structure of the living organism being studied and represent the various organs and tissues as compartments that are connected via a blood circulation loop which is subdivided into arterial and venous pools. The natural basis for the choice of compartments is the available data on the anatomy and physiology of the biological system from the cellular to the organismal levels. However, this does not by itself determine how many body regions, or compartments, are needed, since the important aspects of the drug's PK events must be evaluated. The choice also depends upon the model's purpose and the physicochemical (e.g., binding, lipid solubility, ionization) and pharmacological (e.g., mechanism of transport, site[s] of action) properties of the modeled drug (Bischoff 1975). For example, if the drug is not lipid soluble, the details of the adipose tissues of the body are not particularly important and if only the absorption of the drug is of interest, a model that includes only those body tissues or organs involved in the absorption process may be sufficient. The complexity of the models and the amount of incorporated information increase with an increasing number of represented tissues/organs; however, due to the fact that the main features of drug distribution can often be described with models that have surprisingly few details, a common strategy in structuring PBPK models, called "lumping," is implemented (Nestorov et al. 1998; Brochot et al. 2005). Tissues that share similar physiological, physicochemical, and biochemical properties are grouped as one compartment, while tissues with distinct properties—such as the liver, where metabolism occurs, or target tissues—are separated from the lumped compartments. Eventually, PBPK models do vary, ranging from partial-body PBPK models, which only include certain body systems

or tissues, to whole-body PBPK models where almost all body tissues are included and represented either as separated or lumped compartments.

1.2.2. Specification of tissues/organs to be modeled

Following the determination of the overall model structure, modeling of each particular tissue or organ must subsequently be specified (i.e., sub-compartments representing each organ/tissue must be identified and described). The vast majority of PBPK models involve one to four compartments for each tissue or organ. The compartmentalization decision is based on existing information regarding tissue kinetics and the biochemical processes involved once the drug gets into the tissue (Nestorov 2007). It is important to distinguish between the different assumptions made at this level.

A perfusion rate-limited tissue model assumes that, on entry with the blood circulation, the drug is distributed freely and instantly across the membranes without diffusion barriers; thus, it is the rate of delivery by the blood that is rate limiting. If, on the other hand, diffusion barriers to the distribution of a compound in the tissue are presumed and can be physiologically identified—for example, capillary membranes (such as the blood-brain barrier for some hydrophilic molecules) or cellular membranes, or both—the more complex permeability rate-limited tissue model is used with at least a two-compartment tissue structure. Furthermore, the assumption of a well-stirred model is that there is no concentration gradient within a tissue/organ compartment. This contrasts with the dispersion model, in which a diffusion barrier cannot be identified but concentration gradients nevertheless exist. Examples of a perfusion rate-limited, well stirred, one-compartment tissue model and a permeability rate-limited, two-compartment tissue model are given in **Figure 1-2**.

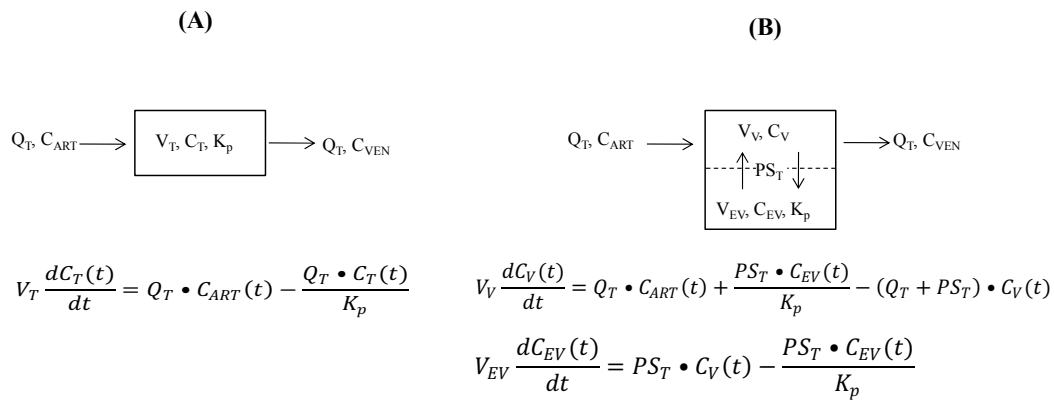


Figure 1-2. Diagrams and equations for a perfusion rate limited, one compartment model (Left Panel, A) and a permeability rate limited, two compartment model with the permeability at the vascular membrane (Right Panel, B) of noneliminating organs, adapted from Nestorov et al. (1998). Q= blood flow; C= concentration; V= volume; Kp= tissue:plasma distribution coefficient; PS= permeability surface area coefficient; subscripts T, ART, VEN, V and EV indicate tissue, arterial, venous, vascular compartment and extravascular compartment respectively.

1.2.3. Writing the PBPK model equations

The PBPK model equations are derived from the law of mass action—i.e., they are mass balance equations, as the kinetic processes are mass transfer phenomena. Four types of mathematical descriptions of the tissues within PBPK models have been used (Nestorov 2003): i) algebraic, which are used when the processes are assumed to equilibrate instantly and can be considered static (e.g., alveolar and inhaled air concentrations); ii) linear ordinary differential, which are the most commonly used descriptions in describing dynamic PK processes; iii) non-linear differential, which are used to represent non-linear processes within a particular tissue (e.g., concentration-dependent clearance and/or binding); and iv) partial differential, which are used with the dispersion tissue model. Examples of the types of differential equations that can be used in a PBPK model are shown in **Figure 1-2.**

1.2.4. PBPK-model parameterization

Once model equations are written, their parameters must be specified and/or estimated. The parameters for incorporation into PBPK models are generally either physiological or compound-dependent.

Physiological parameters characterize the anatomical structure and physiological processes of the species being modeled, and include parameters such as organ/tissue volumes, cardiac output and blood flows, tissue composition, surface area, pH values, and/or transit times for the gastrointestinal tract. The values of these parameters are known to vary among species and subjects, or with age and physiological/pathological state. Despite the large volume of available literature reporting such physiological data in numerous species—notably, annals of the International Committee on Radiological Protection (ICRP) for human values (Valentin 2002) and Brown et al. for animal values (Brown et al. 1997)—allometric scaling (i.e., extrapolation from another species or another age group) is still used when various physiological parameters that are needed for a PBPK model are incomplete or entirely lacking. Although physiological parameters are most often assumed to be compound-independent, drugs can sometimes affect the physiology of the biological system as seen, for example, in the change of cardiac output and blood flow due to the induction of anesthesia (Wada et al. 1996; Sasaki and Wagner, Jr 1971). Therefore, the potential pharmacological effects of some compounds on physiological variables must be accounted for in such circumstances.

The second set of parameters necessary for a PBPK model are compound-dependent and include information such as permeability-surface area products (PxSA) and partitioning of the substance between body tissues and the blood/plasma (KpT). These parameters can be obtained either from in vitro experiments, by extrapolating the experimental in vivo values from animals to humans, or by estimation/prediction using specific algorithms. Multiple specialized PBPK modeling software programs include such algorithms to calculate tissue:plasma partition coefficients—for instance, those developed by Poulin and

Theil, Rodgers and Rowland, or Schmitt (Poulin and Theil 2000; Rodgers and Rowland 2006; Schmitt 2008). In the latter case, easily obtained compound characteristics such as molecular weight (MW), lipophilicity ($\log P$ or $\log D$ value), ionization (pK_a value), and plasma fraction unbound (f_u) are alternative inputs since these algorithms use the previous information along with tissue composition (lipids, proteins, water) to estimate partition coefficients.

Clearance is a compound/species-specific parameter that greatly influences the PK behavior of a drug; thus, a measure of clearance is a necessary PBPK model input. It is up to the researcher to decide how to provide the PBPK model with this information. An experimental blood or plasma clearance is often used as a direct input; however, as many PBPK models are able to perform in vitro–in vivo extrapolations (IVIVE), in vitro data can also be used—e.g., data from in vitro experiments on microsomes or hepatocytes (in the form of half-lives or residual fractions). In the latter case, depending on the type of input parameter, PBPK models use additional information such as liver volume, liver blood flow, or microsomal binding to calculate the in vivo hepatic intrinsic clearance.

1.2.5. PBPK modeling software for simulation and parameter estimation

In the last step, the entire system is coupled and equations that describe the model are coded in a particular software language for subsequent parameter estimation and/or simulation. Several commercial software tools for developing PBPK models are available; however, it is important to distinguish between general mathematical and engineering modeling software and specialized PBPK modeling software packages.

General modeling software packages, such as MATLAB® (MATLAB), ModelMaker™, Berkeley Madonna™, and acsIX™ provide a programming language for the model code, numerical solutions for the ordinary differential equations that define the system being modeled, and a graphical output of the simulation results. These software packages offer much flexibility to the PBPK model developer, but more advanced modeling and programming skills and experience are required; thus, they are less suitable for beginners. However, both

acslX™ and Berkeley Madonna™ software attempt to incorporate features to make them more intuitive for beginners by providing, for example, a graphical interface and a PBPK library to assemble models from already programmed code.

PK-Sim® (PK-Sim), Simcyp® (Simcyp), and GastroPlus™ (Gastroplus), which are specialized PBPK modeling software packages, provide less flexibility in model development. However, they also require less mathematical and modeling experience. Such software tools provide the user with either a click-and-drag assembly of the model structure or an already built model, and can either simulate particular PK-relevant processes (e.g., intestinal absorption or metabolism) or constitute a generic whole body PBPK model. Many packages offer additional features; for example, Simcyp® and PK-Sim® allow simulation of complex absorption, distribution, metabolism, and excretion outcomes involving multiple drug interactions as well as parent drug and metabolite profiles. They also allow the simulation of virtual patient populations such as obese/morbidly obese individuals and patients with renal impairment or liver cirrhosis, and include a clearance prediction model that incorporates knowledge about growth, development, and maturation of various organs and tissues involved in drug metabolism and elimination across pediatric age groups to predict clearance in children using values from adults (Jamei et al. 2009a; Willmann et al. 2003; Willmann et al. 2005). However, although specialized PBPK modeling software packages do not require the programming skills required by general purpose software packages, they are still relatively complex to use. This is not only due to the diversity of input options and many menus/windows that require knowledge about these parameters, where they are located, and how to work with them, but also because users of such software tools are required to have a substantial background knowledge of clinical pharmacology – for instance, pharmacokinetics topics such as absorption, distribution, metabolism, and the elimination processes of drugs as well as pharmacogenetics, pharmacodynamics (PD), and the molecular processes involved in these topics – to understand the differences among the various models offered and the model equations and assumptions so that the appropriate models are used to conduct PK analysis.

1.3. PBPK modeling applications

1.3.1. Overview of the general scope of application

Although PBPK modeling was originally generated in the pharmaceutical field, it has more applications in environmental toxicology and risk assessment, and has become a commonly and widely used technique. However, PBPK modeling can be used for a variety of other purposes and is becoming more popular in the fields of pharmacology and drug development (Parrott and Lave 2008; Rowland et al. 2011; Espie et al. 2009). Even during early drug discovery programs and the preclinical phase, PBPK modeling can be used, together with *in vitro* data and physicochemical characteristics, to anticipate the pharmacokinetics of potential drug candidates in animals, which may permit a reduction of unnecessary animal testing and significant time savings (Germani et al. 2007). Another example of the use of PBPK modeling demonstrated the utility of a PBPK/pharmacodynamic model in the selection of the most promising compound from five potential clinical candidates (Parrott et al. 2005). Given that PBPK models integrate relevant information from various sources, including those that are substance-dependent and physiologically relevant, they have been widely used for *in vivo* of drug kinetics in different species or for different routes of administration (Parrott et al. 2005; Shiran et al. 2006; Buck and Mackie 2007). The PBPK modeling technique has also emerged as a learning tool that can help users understand the influence of different processes and/or parameters involved in determining drug disposition and PK behavior (Sun and Pang 2010). PBPK modeling is widely used in describing and/or predicting drug PK profiles by simulating different dosing regimens that allows established therapies to be evaluated and optimized. It also has been used to describe and/or predict drug pharmacokinetics under different physiological and pathological conditions; for example, in pregnancy (Hays et al. 2000; Kawahara et al. 1998; Ward et al. 1997; Andrew et al. 2008), under surgery (Bjorkman et al. 2001), and in liver cirrhosis (Edginton and Willmann 2008; Johnson et al. 2010). The effects of food (Jones et al. 2006), aging (Li and Gwilt 2003; Yang et al. 2006), rest and physical exertion (Dennison et al. 2005; Hamelin et al. 2005; Reddy et al. 2003), and gender

differences (Clewell et al. 2004) have also been explored using PBPK modeling. Another application of PBPK modeling is in the estimation of the PK of both a parent drug and its metabolite (Clewell et al. 2000; Clewell et al. 2001; El-Masri and Kenyon 2008). It has also been used successfully to predict the magnitude of complex drug-drug interactions and to clarify the change in drug pharmacokinetics upon concomitant drug administration (Rowland et al. 2010; Vossen et al. 2007; Zhang et al. 2009), which is important within the pharmaceutical industry to improve safety and reduce the attrition rate of new drugs. Additionally, PBPK models are advantageous in that they enable prediction of exposure to a drug and/or toxic substances not only in the plasma or blood, but also in remote and/or inaccessible compartments such as the brain (Liu et al. 2005) or tumor tissues (Gallo et al. 2004). It is easy to quantify drug concentrations in different tissues and/or body fluids when simulating and/or predicting using Simcyp® or PK-Sim® modeling software.

1.3.2. PBPK modeling applications in pediatric populations

Interest in in-silico PBPK modeling in the field of pediatric drug development has been increasing since the initiation of the Pediatric Exclusivity Program in 1997 by the US Food and Drug Administration (FDA), which was later followed by new regulations on medicinal products for pediatric use in both the USA and the European Union. This interest is because PBPK modeling provides a useful tool to bridge pediatric and adult pharmacology. A child-specific PBPK model can deliver information about age-dependent changes in the pharmacokinetics of drugs in children, explore “what if” scenarios to determine the most likely cause of altered pharmacokinetics, and potentially help in guiding pediatric clinical trials by suggesting, for example, first dose/dose range or optimal sampling times (Parrott and Lave 2008; Grass and Sinko 2002).

1.3.2.1. Building a pediatric PBPK model to perform simulations and predict drug pharmacokinetics in children

This important application of PBPK models will be discussed in more detail in this thesis. The scope of **Chapters 2 and 3** is to develop and evaluate pediatric

PBPK models to perform simulations and predict the pharmacokinetics of two different antiarrhythmic drugs: sotalol and amiodarone. These models show an important application of PBPK modeling to predict drug exposure in children of different ages and to explore age-related changes in the PK behavior for two drugs that possess different physicochemical and PK profiles. Moreover, the different routes of administration of sotalol and amiodarone allow us to examine the ability and the limits of such models to predict systemic drug exposure after oral and intravenous (IV) dosing.

1.3.2.2. Using the pediatric PBPK model to suggest dosing in children

An example of how a pediatric PBPK model can be used to suggest age-specific dose recommendations to support drug development research will be given in **Chapter 4** for the heart rate-lowering drug, ivabradine. The pediatric PBPK model will be developed and used to run simulations in virtual pediatric populations of different ages to estimate the exposure after a weight-normalized dose based on adult data. This will detect any necessary age-specific dose adaptations required to achieve a relatively constant drug exposure in adults and children (**Chapter 4**). The suggested dosing adjustments across pediatric age groups in this example of ivabradine are yet to be validated with prospectively collected data and are, therefore, hypothetical. Nevertheless, upon establishing and validating the use of PBPK modeling for this purpose, the data generated may help clinical trials become more “confirmatory” rather than “exploratory.” The modeling exercise will thus potentially save time and effort, and reduce the number of trials needed to be performed in children

1.3.2.3. Using the pediatric PBPK model to suggest sampling times

Willmann (2009) provides an example of using a PBPK model to determine optimal sampling times in children, comparing the possible difference between suggested pediatric sampling times based on adult concentration-time data and suggested sampling times based on simulations by a PBPK model (**Figure 8**). The latter, as shown in the study, can potentially help detect the best sampling times for a PK analysis and help avoid taking blood samples when the drug concentration

is out of detection range. This is of great importance, especially in neonates and infants, as taking blood samples is more difficult than in adults and poses the main challenge in conducting pediatric clinical trials. The primary reason for using a PBPK model to provide such information in advance is to help conduct these trials optimally. Whether these techniques can reduce the number of children required for clinical trials and thereby save time, effort, and costs remains to be proven.

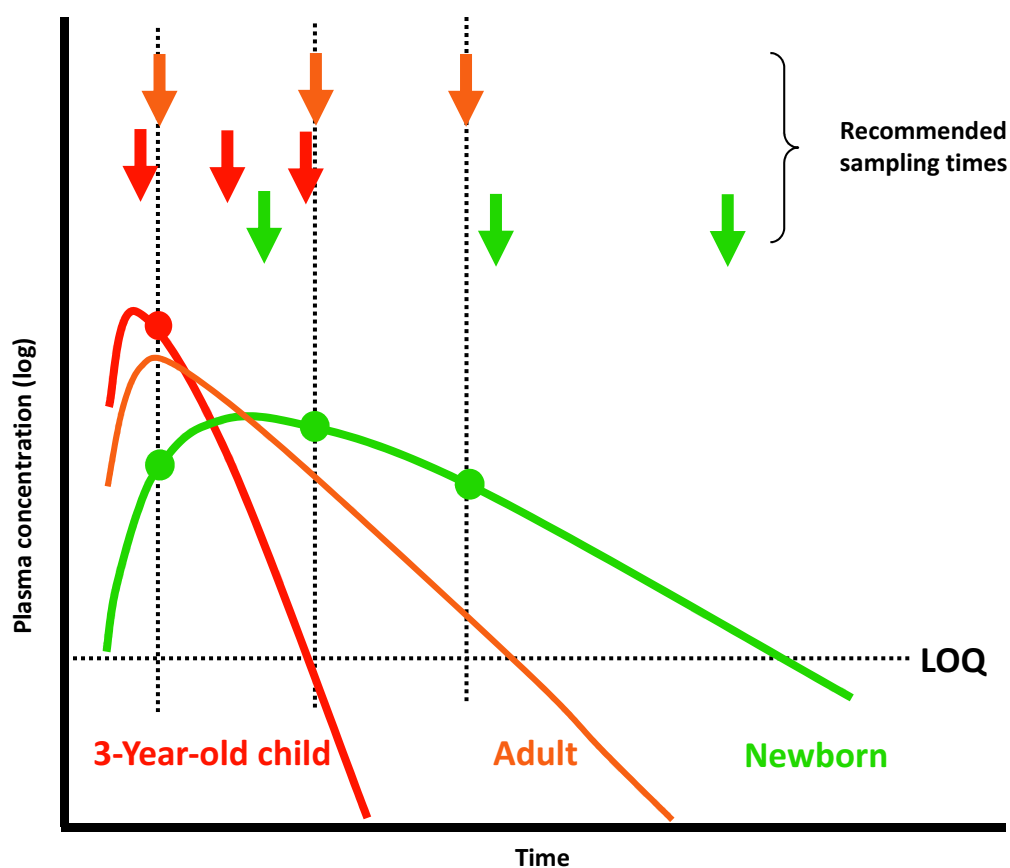


Figure 1-3. Schematic drawing of a potential application of PBPK simulations for children of different ages to find optimal blood sampling time points for PK investigations in a future pediatric trial according to Willmann (2009). Arrows indicate optimal sampling time for a 3-year-old child, a newborn, and an adult. LOQ: Limit of quantification.

Finally, it is worth mentioning that the ultimate gold standard is to prospectively validate predictions/simulations generated by pediatric PBPK models. To our knowledge, in vivo data for validation had been collected up to

now before the predictions of the models had been made. To qualify a model ultimately, data should be collected after predictions are made and then compared. Unfortunately, there is a definite shortage of clinical examples that verify the use of PBPK models prospectively. Such examples need to be developed to gain confidence in using PBPK models in clinical situations.

1.4. Limitations of PBPK modeling

A salient feature of PBPK modeling is that it requires comprehensive data about the physiological, biochemical, and physicochemical processes that occur in biological systems in different age groups or under specific physiological and pathological conditions. These data are not available from a single source, which may lead to some confusion and to a problem in establishing a reliable source of accurate and consistent information. The PBPK models reflect current scientific knowledge and while some processes are known to be well characterized, others are partly or poorly characterized as a consequence of information gaps that may exist. Information gaps or poor characterization of some physiological processes, such as the abundance of transporters or the absorption process in newborns and infants, may cause the model to fail to optimally describe the PK behavior of some drugs in these populations. It is therefore important to emphasize that the validity and quality of the simulations depend on the corresponding model and its incorporated data as well as its purpose, and uncertainty concerning the data used to build the model should be properly described. Moreover, as simulations are associated with prediction errors and uncertainty, they require accurate judgment and interpretation of their inferences to frame them in the right context. In addition, simulation results should be supported by experimental data, and should not be used to replace data from well-conducted studies as the primary source of evidence (Manolis and Pons 2009). It should be recognised that poor quality modeling and simulation practices could lead to a biased model or overestimation of the predictive power of the model. An extensive and continuous evaluation of the model will help minimize bias and enable early identification of biased models. Finally, the researcher/user of this modeling technique should understand the physiological and pharmacological rationale behind the model and should be

aware that PBPK modeling, despite its potential benefits and various manifestations, does not provide the ultimate solution and should recognize that there remains a shortage of prospective examples that verify that this technique is as good in clinical practice as in theory.

1.5. Conclusion

This chapter provided a brief overview of the methodology, applications, and limitations of PBPK modeling. The applications of the PBPK modeling technique are diverse, as PBPK models can potentially be used at different stages of drug development from early discovery phases and preclinical development up to clinical phase studies. Simulations by PBPK models are developed to potentially save time, effort, and costs, avoid unnecessary experimentation in animal models, explore the effect of various factors on drug pharmacokinetics, address the magnitude of drug-drug interactions, and help optimize the conduct of clinical trials in special populations such as neonates and infants where optimal planning is needed to minimize and overcome the multiple ethical and technical difficulties. Modeling is therefore an essential key for success of drug development efforts. However, prospective examples that assure the clinical value of such a modeling technique are needed and are important to increase the acceptance of these techniques in the planning phases of clinical trials or for the practical application of the individual drug treatment. The PBPK models do have inherent limitations and weaknesses. For instance, because they reflect current scientific knowledge, some physiological processes are poorly characterized and information gaps may exist. In addition, the validity of the simulations depends on the corresponding model and its incorporated data, and obtained results are associated with prediction errors and uncertainty. The use of PBPK modeling techniques is still relatively narrow, but the introduction of many universally applicable software tools with a more user-friendly interface that do not require an extensive modeling and/or mathematical background has facilitated its use and contributed significantly to its wider implementation in different scientific areas over the last few years. Researchers need, however, to have a substantial background knowledge of clinical pharmacology, pharmacokinetics, and PD, as well as the molecular processes involved in these topics to understand the differences between the various models offered and the model equations and assumptions so that the appropriate models are used to conduct PK analysis and to accurately interpret and apply the results.

Chapter 2:

Pediatric physiologically based models to predict oral drug exposure across the entire pediatric age range

2.1. Introduction and rationale for this project

Physiologically based pharmacokinetic (PBPK) models can deliver valuable information during various stages of drug development and research (Parrott and Lave 2008; Rowland et al. 2011; Espie et al. 2009; Johnson and Rostami-Hodjegan 2011). Their ability to incorporate information about maturation, growth, and age-dependent changes in anatomical and physiological processes facilitates their use to extrapolate drug pharmacokinetics from adults to children and to explore age-related changes (Khalil and Läer 2011; Bouzom und Walther 2008). In recent years, the implementation of PBPK models in pediatric drug development has become more attractive (Läer et al. 2009; Bellanti and Della Pasqua 2011; Jadhav and Kern 2010; Manolis et al. 2011; Barrett et al. 2012), encouraged by an increased awareness of and interest in pediatric research, especially after the new regulations on medicinal products for pediatric use in both the United States and the European Union (International Conference on Harmonisation 2000; Commission of the European Communities 2006).

Despite the marked potential of PBPK models, uncertainties still exist in the pediatric community about the accuracy of their predictions, especially after oral drug administration in pediatric patients of different ages (Barrett et al. 2012). The lack of sufficient published pediatric PBPK models evaluated adequately for the prediction of oral drug absorption and disposition is the main reason for this uncertainty. For the IV application, 6 pediatric whole-body PBPK models evaluated with a total of 10 different drugs have already been reported (Ginsberg et al. 2004; Bjorkman 2005; Edginton et al. 2006b; Kersting et al. 2012; Maharaj et al. 2013). In contrast, there are only 2 publications with reported pediatric PBPK model predictions evaluated for 6 drugs after oral drug application as of the date of writing (Johnson and Rostami-Hodjegan 2011; Parrott et al. 2011), of which only one of them evaluated the model with neonatal experimental data for the modeled drug (Parrott et al. 2011). In addition, there are other reported pediatric

PBPK models that were, however, either not evaluated with experimental data (Dumont et al. 2013; Edginton and Ritter 2009), or focused only on one aspect of the drug PK with no comprehensive concentration-time profiles or information about predicted drug absorption or exposure (e.g., the model may have predicted only the clearance of the drugs) (Johnson et al. 2006; Edginton et al. 2006a). Given all of these facts, more examples of evaluated pediatric PBPK models for oral drugs are still needed.

In recognition of this unmet need, a PBPK model drug with an already available large-scale clinical PK data set that covers all pediatric age groups is preferable. Sotalol, an orally administered antiarrhythmic drug used in the treatment of supraventricular tachycardia, and which has >90% oral bioavailability and almost complete renal elimination, has been very well studied in both adults and children and fulfills this requirement (Hanyok 1993; Tjandramaga 1980; Anttila et al. 1976; Salazar et al. 1997; Uematsu et al. 1994; Somberg et al. 2010; Rehm et al. 1987; Poirier et al. 1990; Kimura et al. 1996; Kahela et al. 1979; Ochs et al. 1985; Läer et al. 1997; Liebau 1999; Läer et al. 2005). The extensive pediatric data on sotalol facilitate a good assessment of the model predictability from adolescents down to neonates, and provide individual full concentration-time profiles with information on drug absorption. On the other hand, the rich adult data after both IV and oral administration will enable the validation of the model first in adults before scaling it to children, thus forming a solid basis for age extrapolation. Finally, because commercial PBPK modeling packages are often used nowadays by researchers as a basis for their models, and because no single source for the integrated data currently exists, the decision to use two commonly used modeling software tools for model development has been taken to minimize bias introduced by software and to examine the extent to which the use of different modeling software packages can influence the results obtained.

2.2. Objective of this project

This study (Khalil and Läer 2014) was undertaken to investigate how whole-body PBPK models developed using two dedicated PBPK modeling tools can

describe the oral pharmacokinetics of sotalol from adults to neonates, and to detect the pediatric age groups for which the model predictability is the lowest. A secondary goal was to observe any differences in the performance of these two models during routine use by researchers in this field.

2.3. Methods

2.3.1. Literature review about the modeled drug (Sotalol)

Sotalol is an antiarrhythmic drug with Class II (beta-adrenoreceptor blocking) and Class III (cardiac action potential duration prolongation) properties that is used for the treatment of supraventricular and ventricular arrhythmia in adults and children, and which has been shown to be successful in the treatment of refractory cases.

2.3.1.1. Physicochemical properties of sotalol

Sotalol is a relatively small hydrophilic compound with a molecular weight of 272.36 (g/mol) (PubChem Compound CID= 5253). Multiple measures of sotalol lipophilicity are already reported in the literature in terms of *LogP* or *LogD*: 0.03 (Taylor and Cruickshank 1985), 0.039 (Woods and Robinson 1981; McDevitt 1987), 0.2 (PubChem Compound CID= 5253), and 0.37 (Yang et al. 2007). Sotalol does not bind to plasma proteins (Anttila et al. 1976) and has pK_a values of 9.72 and 8.28 for the basic and acidic functions, respectively (Cheymol et al. 1997). Sotalol is a chiral drug that is marketed as the racemate D,L-sotalol. It has already been demonstrated that D,L-sotalol and D-sotalol have similar PK properties in humans (Carr et al. 1992; Funck-Brentano 1993; Poirier et al. 1990).

2.3.1.2. Sotalol pharmacokinetics in adults

The apparent volume of distribution of sotalol has been reported in various literature reviews to be 1.34 l·kg⁻¹ (Poirier et al. 1990), 1.3 l·kg⁻¹ (Riddell et al. 1987), and 1.2-2.4 l·kg⁻¹ (Hanyok 1993; McDevitt 1987; Antonaccio and Gomoll 1990; Funck-Brentano 1993; Sundquist et al. 1979). No significant biotransformation of sotalol takes place in humans since sotalol does not undergo any metabolism in the liver. The primary route of sotalol elimination is renal excretion, with more than 90% of each dose being excreted unchanged in the urine (Hanyok 1993; Antonaccio and Gomoll 1990). Therefore, appropriate adjustment of the dose must be made for patients with impaired renal function or increased renal blood flow (e.g., in pregnancy). A small amount is thought to be

excreted in the feces, bile, or other intestinal secretions (Hanyok 1993; Antonaccio and Gomoll 1990). The total clearance of sotalol has been reported to range between 0.09 and 0.328 l·h⁻¹·kg⁻¹; for example, it has been reported to be 0.13 l·h⁻¹·kg⁻¹ (Poirier et al. 1990), 0.15 l·h⁻¹·kg⁻¹ (Rehm et al. 1987), 0.13 l·h⁻¹·kg⁻¹ (Liebau 1999), 0.09 l·h⁻¹·kg⁻¹ (Tjandramaga 1980), 0.12 l·h⁻¹·kg⁻¹ (Kowey et al. 1997; Meier 1982), 0.14 l·h⁻¹·kg⁻¹ (Riddell et al. 1987), and 0.09–0.328 l·h⁻¹·kg⁻¹ (McDevitt 1987) in various studies. The reported values of sotalol half-life (t_{1/2}) range between 7 and 18 h; for example, the half-life has been reported to be 7.45 h (Poirier et al. 1990), 6.85 and 7.21 h (Rehm et al. 1987), 5-13 h (Tjandramaga 1980), 7-15 h (Meier 1982), 7.5-15 h (Riddell et al. 1987), 7-18h (McDevitt 1987; Antonaccio and Gomoll 1990; Funck-Brentano 1993), 8.06 (Läer et al. 1997), and 8.46 h (Liebau 1999). Sotalol shows linear pharmacokinetics over the therapeutic dose range.

Sotalol is almost completely absorbed after oral administration and undergoes no first-pass hepatic metabolism, as a result of which its absolute bioavailability is 90-100% (Hanyok 1993; Tjandramaga 1980), and the drug is classified as a Biopharmaceutics Classification System (BCS) class I drug with a high permeability/high solubility profile (Yang et al. 2006; Alt et al. 2004). Sotalol reaches its maximum concentration within 2 to 4 hours after an oral dose (Läer et al. 1997; Liebau 1999). Sotalol exposure given as the area under the plasma concentration time curve (AUC) after a typical oral dose of 160 mg has been reported to be 15.6-15.9 mg·h·l⁻¹ in healthy adults (Läer et al. 1997; Liebau 1999).

2.3.2. PBPK modeling software and model parameterization

To develop a whole-body PBPK model of sotalol, two specialized modeling software tools were used separately: software package 1 was Simcyp® simulator (v.12.1 [academic license]; Simcyp Ltd, Sheffield, UK) for adults and pediatrics (Simcyp), while software package 2 was PK-Sim® (v.4.2.2 [academic license]; Bayer Technology Services GmbH, Leverkusen, Germany) with its integrated clearance scaling module (PK-Sim). In brief, these tools provide a general PBPK model structure to describe drug absorption and disposition in the body and incorporate a large data set of anatomical and physiological parameters with their age-

dependencies to the extent permitted by the current scientific knowledge. The detailed structure and methodology of these PBPK models have been published elsewhere (Jamei et al. 2009a; Willmann et al. 2003).

To complete the model parameterization, the required physicochemical properties of sotalol, along with other drug-dependent parameters, were collected from a comprehensive literature search. Both models used the same values for molecular weight, lipophilicity (octanol-water partition coefficient [logP] value), acid dissociation constant (pKa), fraction unbound (fu), and clearance (CL), as listed in **Table 2-1**, which summarizes the final model input parameters.

Table 2-1. Input parameters for sotalol PBPK models using both modeling software packages

Parameter	Simcyp®-value	PK-Sim®-value	Ref. value	Reference
Molecular weight (g/mol)	272.36	272.36	272.36	PubChem 5253
LogP _(o:w)	0.37	0.37	0.2, 0.37	PubChem 5253, Yang 2007
Ionization constant	pK _{a1} = 8.28 ^a pK _{a2} = 9.72	pK _{a1} = 8.28 ^a pK _{a2} = 9.72	pK _{a1} = 8.28 ^a pK _{a2} = 9.72	Rodgers 2007
f _u	1	1	1	Hanyok 1993, McDevitt 1987
Blood:plasma ratio	1.02	0.86	1.07	Rodgers 2007
CL _{IV, total}	7.875 L/h	0.1125 L/h/kg	0.09–3.2 L/h/kg	Poirier 1990, Riddell 1987
Fraction of renal clearance	100%	100%	90-100%	Hanyok 1993, Tjandramaga 1980
Permeability (cm/s) [†]	2.01 × 10 ⁻⁴ †	12.6 × 10 ⁻⁶ †	-	-

LogP= octanol-water partition coefficient; fu= fraction unbound; CL_{IV, total}= total intravenous clearance.

^a pK_a= acid dissociation constant; pK_{a1}: for acidic function; pK_{a2}: for basic function.

[†] Human jejunum permeability (P_{eff, man}) as permeability measure in software 1; In vitro intestinal permeability (P_{app}) as permeability measure in software2. Both measures were manually adjusted to give the same value of fraction-absorbed (f_a) and a bioavailability of 90%.

The total clearance of sotalol was set to be 0.1125 L/h/kg and assigned to be cleared completely through the renal route. Both the value and the route of

clearance are consistent with the literature (Hanyok 1993; Tjandramaga 1980; Poirier et al. 1990). The partition coefficients in the tissues were calculated with both software packages using Rodgers and Rowland's distribution model (Rodgers and Rowland 2006). The input values assigned to the blood-to-plasma concentration (B:P) ratio differed between software 1 and software 2 (1.02 versus 0.86, respectively), since these values gave the best visual fit during the IV model development (see Modeling strategy). However, the models predicted similar V_{ss} values of 1.3 and 1.22 L/kg, respectively, in an average adult male weighing 70 kg, both of which are in good agreement with the reported literature values (Hanyok 1993; Poirier et al. 1990; McDevitt 1987; Riddell et al. 1987). Drug absorption was predicted by the advanced dissolution, absorption, and metabolism (ADAM) model in Simcyp® (Jamei et al. 2009b), and by a built-in absorption model in PK-Sim (Willmann et al. 2004), with various input measures offered by the two software packages to account for the drug intestinal permeability. Sotalol is known to be a biopharmaceutics classification system (BCS) Class I drug with high solubility and high permeability profile. However, the in vitro measured apparent permeability coefficient (P_{app}) of sotalol is very low and does not correlate with the high values of the absorbed dose fraction (>90%) obtained from PK studies in humans (Yang et al. 2007; Alt et al. 2004). Therefore, the value of the intestinal permeability measure for each model was adjusted separately in order to give the same absorbed fraction and a bioavailability of 90% in adults. Finally, the default mean values used in both models for gastric emptying time (GET) and small intestinal transit time (SITT) were 0.5 h and 4 h, respectively.

2.3.3. Pharmacokinetic/clinical data in adults

The MEDLINE database was searched for PK studies of sotalol in healthy adults with known age, gender, height, and weight information, as well as clear dosing information and available plasma concentration-time profiles. The search retrieved a total of 27 data sets originating from 11 clinical trials published by 8 different scientific groups between 1976 and 2010 in 5 countries. These data were used in model development and evaluation (**Tables 2-2, 2-3**) (Anttila et al. 1976; Salazar et al. 1997; Uematsu et al. 1994; Somberg et al. 2010; Rehm et al. 1987;

Poirier et al. 1990; Kimura et al. 1996; Kahela et al. 1979; Ochs et al. 1985; Läer et al. 1997; Liebau 1999). Each experimental data set represents a mean observed concentration-time profile in an average of 5-6 healthy volunteers who received either IV or oral doses of sotalol-HCl. These data were either provided by the author (Läer et al. 1997; Liebau 1999) or were scanned from the figures in the respective publications (Anttila et al. 1976; Salazar et al. 1997; Uematsu et al. 1994; Somberg et al. 2010; Rehm et al. 1987; Poirier et al. 1990; Kimura et al. 1996; Kahela et al. 1979; Ochs et al. 1985).

Table 2-2. Demographics and dosing information of the population in clinical studies of intravenously administered sotalol

Study reference	Applied Dose	Duration of IV dose	No. of subjects	Gender composition	Age (years)	Height (cm)	Weight (kg)
				(% males)	Mean (Range)	Mean (Range)	Mean (Range)
Anttila et al. 1976	20 mg	5 min	8	50%	(24–53)	NR	(58–86)
Rehm et al. 1987	1.5 mg/kg	5 min	8	100%	25 (21–32)	179 (169–185)	67.8 (57–78.8)
Rehm et al. 1987	2 mg/kg	5 min	8	100%	25 (21–32)	179 (169–185)	67.8 (57–78.8)
Poirier et al. 1990	2 mg/kg	5 min	6	100%	23.8 (22–25)	NR	69.5 (59–77)
Uematsu et al. 1994 [†]	1 mg/kg	10 min	6	100%	32.5 (22-43)	NR	61.7 (47.9-77)
Uematsu et al. 1994 [†]	1.5 mg/kg	10 min	6	100%	32.5 (22-43)	NR	61.7 (47.9-77)
Salazar et al. 1997	0.5mg/kg	2 min*	4	100%	25 (18-36)	177 (168-188)	76.5 (68.6-86.2)
Salazar et al. 1997	1.5 mg/kg	2 min*	4	100%	25 (18-36)	177 (168-188)	76.5 (68.6-86.2)
Salazar et al. 1997	3 mg/kg	2 min*	4	100%	25 (18-36)	177 (168-188)	76.5 (68.6-86.2)
Salazar et al. 1997	0.5mg/kg	2 min*	4	0%	35 (28-38)	163 (155-166)	65 (53.9-81)
Salazar et al. 1997	1.5 mg/kg	2 min*	4	0%	35 (28-38)	163 (155-166)	65 (53.9-81)
Salazar et al. 1997	3 mg/kg	2 min*	4	0%	35 (28-38)	163 (155-166)	65 (53.9-81)
Somberg et al. 2010	75 mg	2.5 h	15	40%	32 (19-45)	166.1 (152-178)	69.6 (60-80.5)

All of these studies are single dose studies conducted in healthy volunteers.

NR= not reported

[†] Japanese population

* Average value of the duration of the infusion

Table 2-3. Demographics and dosing information of the population in clinical studies of orally administered sotalol

Study reference	Applied Dose (mg)	Condition	No. of subjects	Gender composition	Age (years)	Height (cm)	Weight (kg)
				(% males)	Mean (Range)	Mean (Range)	Mean (Range)
Anttila et al. 1976	160 mg	fasting	8	50%	(24–53)	NR	(58–86)
Kahela et al. 1979	160 mg	fasting	5	80%	28-56	NR	(74-86)
Ochs et al. 1985	320 mg	fasting	9	89%	21-29	NR	NR
Poirier et al. 1990	100 mg	fasting	5	100%	23.8 (22–25)	NR	69.5 (59–77)
Uematsu et al. 1994 [†]	50 mg	fasting	18*	100%	32.5 (22-43)	NR	61.7 (47.9-77)
Uematsu et al. 1994 [†]	100 mg	fasting	18*	100%	32.5 (22-43)	NR	61.7 (47.9-77)
Uematsu et al. 1994 [†]	200 mg	fasting	18*	100%	32.5 (22-43)	NR	61.7 (47.9-77)
Uematsu et al. 1994 [†]	300 mg	fasting	18*	100%	32.5 (22-43)	NR	61.7 (47.9-77)
Kimura et al. 1996 [†]	40 mg	fasting	6	100%	22-45	NR	52.4-69.8
Kimura et al. 1996 [†]	80 mg	fasting	6	100%	22-45	NR	52.4-69.8
Kimura et al. 1996 [†]	160 mg	fasting	6	100%	22-45	NR	52.4-69.8
Läer et al. 1997	160 mg	fasting	7	100%	26 (24–30)	185 (178–192)	73 (63–80)
Liebau 1999	160 mg	fasting	9	100%	27 (23–34)	187 (184–192)	78 (72–86)
Somberg et al. 2010	80 mg	fasting	15	40%	32 (19-45)	166.1 (152-178)	69.6 (60-80.5)

All of these studies are single dose studies conducted in healthy volunteers.

NR=not reported

[†] Japanese population

* Total number of subjects in the study

2.3.4. Pharmacokinetic/clinical data in children

Data from 80 pediatric patients of different age groups with known age, gender, height, weight, dosing information, and measured plasma profiles were used. The majority of these data are already published (Läer et al. 2005). These patients, ranging from age 11 days to 17.7 years (average: 3.51 years, including 13 premature infants) received various doses of sotalol (1.0-9.9 mg/kg/day) for the treatment of supraventricular tachycardia. The demographics for each age group are presented in **Table 2-4**, while the height and weight of these children plotted against age are presented in **Figure 2-1**. This pediatric data set was classified using a system similar to the WHO classification, however, using 6 different age groups: a) Neonates: 0-28 days, n = 14; b) Infants: 1-11 months, n = 33; c) Toddlers: 12-23 months, n = 6; d) Preschoolers: 2-5 years, n = 10; e) School-aged: 6-11 years, n = 13; and f) Adolescents: 12-18 years, n = 4. This classification was used for presenting results in children. Finally, the raw data of the measured concentrations are shown in **Figures 2-2 and 2-3**.

Table 2-4. Demographics of the simulated children classified into age groups

Age Group	Nr. of children	Gender	Age (years)	Height (cm)	Weight (kg)
		(% M)	Mean (Range)	Mean (range)	Mean (Range)
Newborns	14	71%	0.05 (0.03–0.07)	50.3 (35–65)	3.3 (2.1–4.3)
Infants	33	76%	0.40 (0.08–0.97)	61.2 (45.5–79)	5.8 (2.2–9.7)
Toddlers	6	83%	1.35 (1.05–1.69)	79.5 (74–88)	9.8 (7.7–12.3)
Preschooler	10	30%	3.33 (2.1–4.2)	96.4 (84–139)	14.9 (10.6–31)
School-aged	13	62%	9.08 (6.4–11.7)	136 (120–158)	35.8 (22.1–78.4)
Adolescents	4	75%	14.40 (13.0–17.8)	162 (142–183)	53.5 (30.1–84.3)

% M = percentage of males in each age group

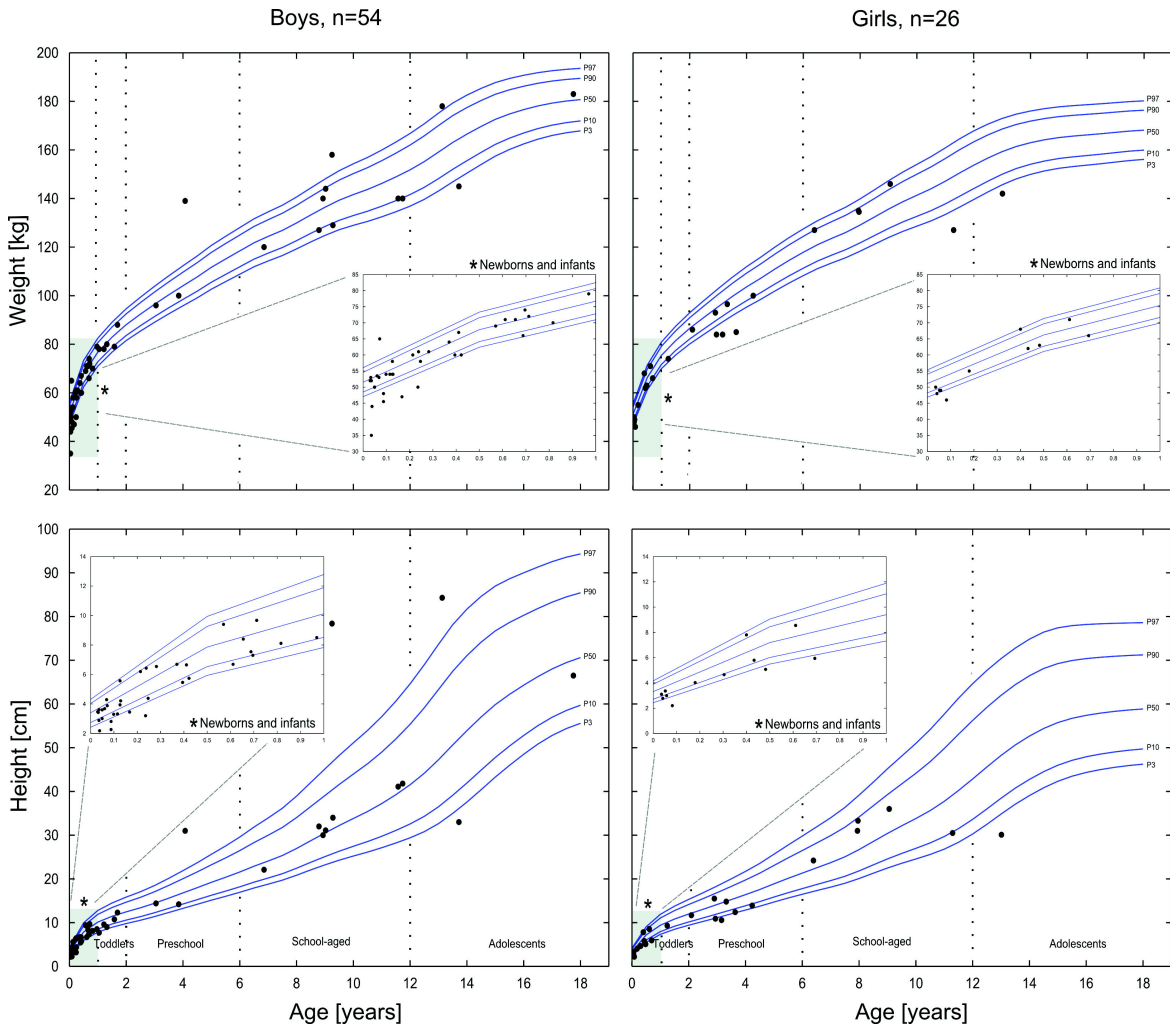


Figure 2-1. The height and/or weight (dots) of each of the 80 children (boys: n=54, left panel; girls: n=26, right panel) in the observed population originally exposed to sotalol. In addition, lines show pediatric age- and gender-specific percentiles (3rd, 10th, 50th, 90th, and 97th), which represent the normal values of a representative German population (Kromeyer-Hauschild 2001). The inlay panels show the demographics of the segment from birth to the end of the first year to highlight the values of newborns and infants.

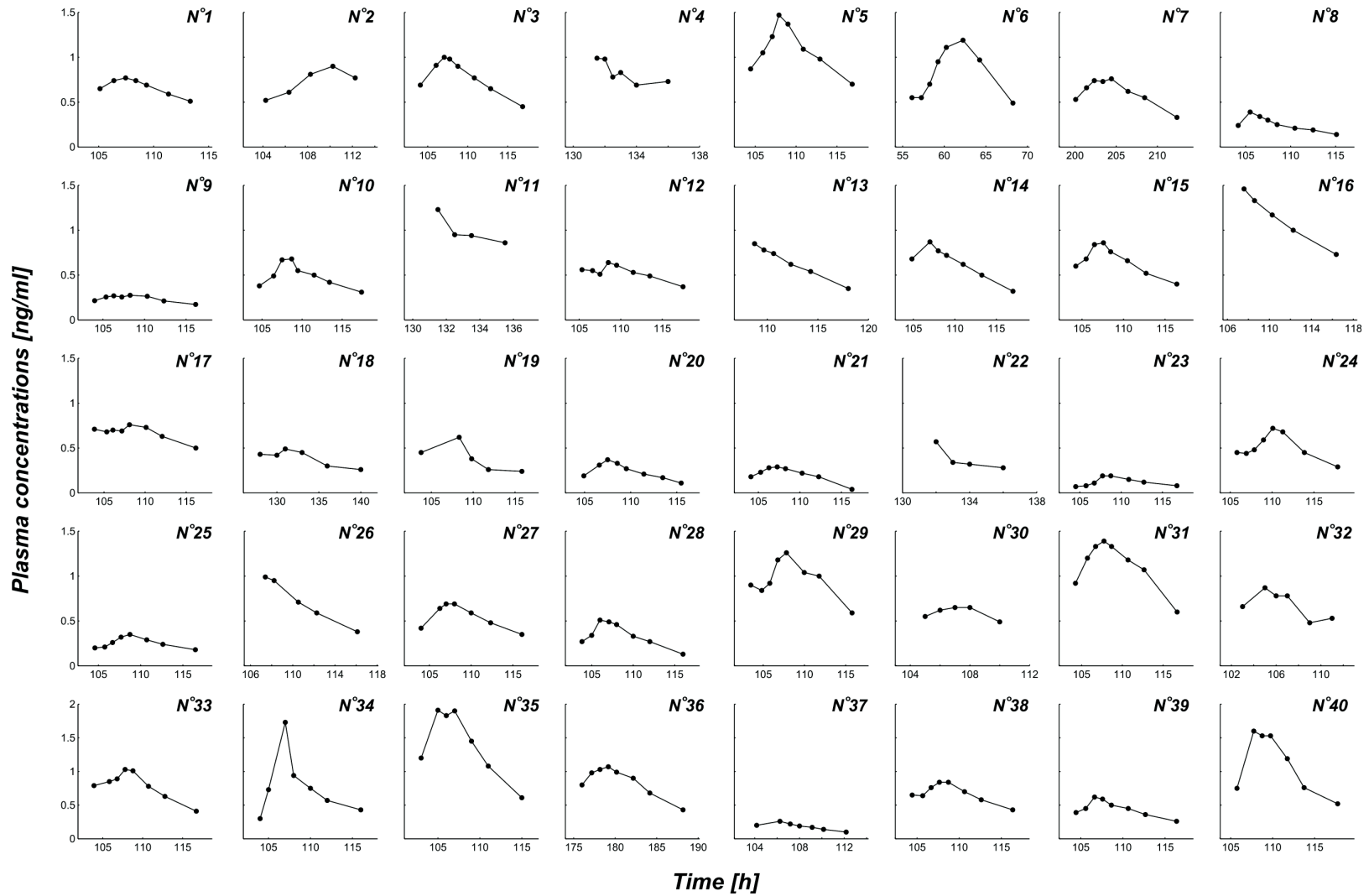


Figure 2-2. Plots of the observed sotalol plasma concentration profiles in children, ID=1-40. Concentrations are measured in steady-state.

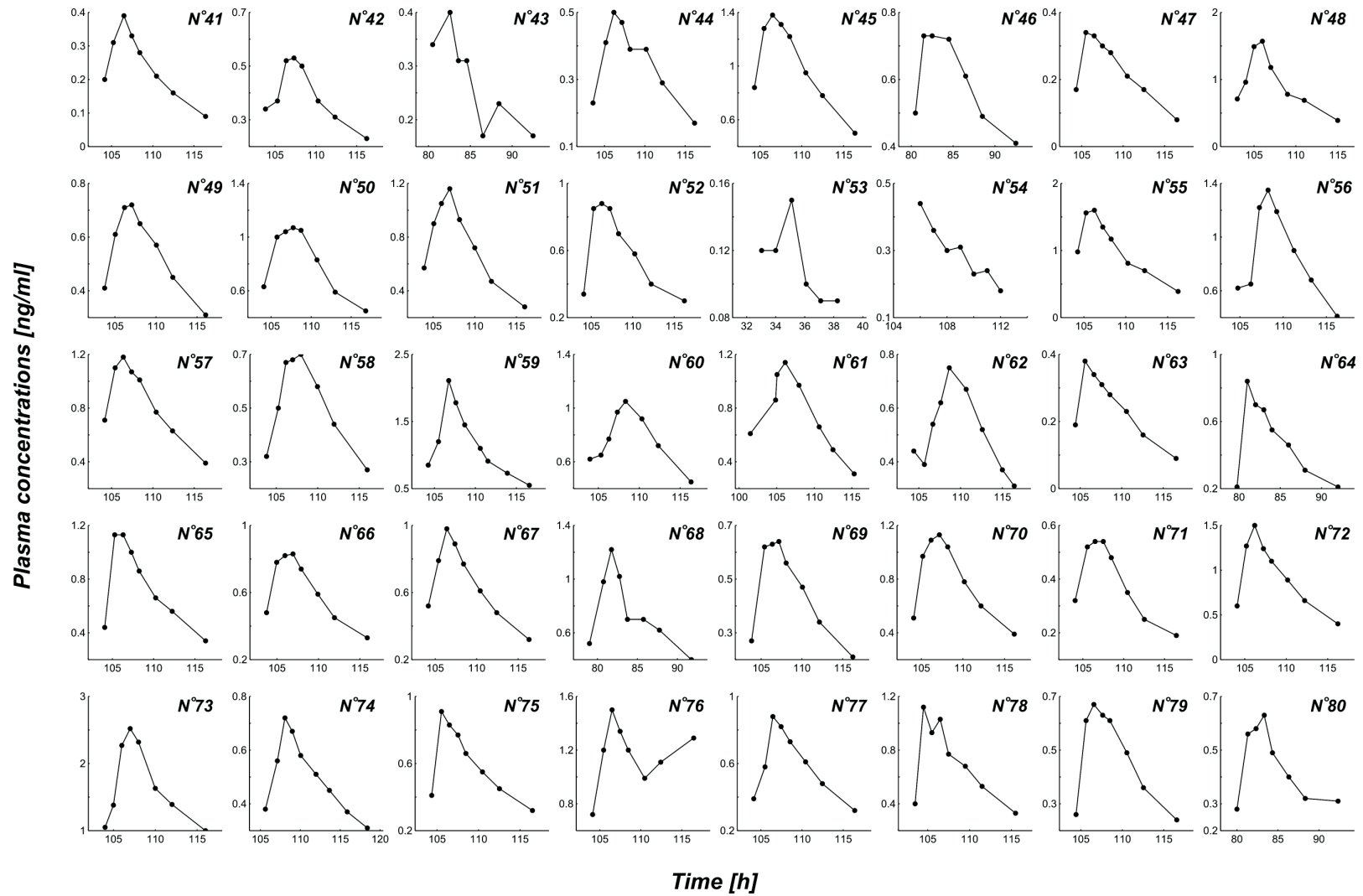


Figure 2-3. Plots of the observed sotalol plasma concentration profiles in children, ID=41-80. Concentrations are measured in steady-state.

2.3.5. Modeling strategy and simulation conditions

The adopted modeling strategy is shown in **Figure 2-4**. An adult model was first developed for the IV application, as this allows for the kinetics of drug disposition to be simulated in the absence of the complexities of the absorption process. Thus, the best set of input parameters, the most suitable distribution model, and the most appropriate clearance that collectively gave the best visual description of the observed data used at this stage were assigned. For the oral application, parameter values from the previous step were retained and the values of additional parameters that control and influence drug absorption, such as intestinal permeability, GET, and SITT were added. In the previously mentioned steps (i.e., model building), only one fifth (n=5) of the collected adult data set was used, whereas the remaining data (n=22) were used later for a subsequent model verification. The adult model was slightly refined with regard to logP and CL inputs before the evaluation of the final model. The final adult model was then scaled down for applicability to children, taking into consideration the age-dependencies of anatomical and physiological processes/parameters and the ontogeny of clearance pathways—which are already integrated into the modeling software—to predict pediatric sotalol exposure (see also: clearance scaling).

The comparison of model results with observed data was based on simulations of virtual populations, where the main results of these simulations are concentration-time profiles. In adults, each virtual population consisted of 100 virtual subjects having the same age range, race, gender composition, and dosing as their corresponding real population. The resulting mean predicted plasma concentrations were then compared with the mean observed concentrations for model evaluation. Population simulations performed with a higher number of virtual subjects (n=1000) did not produce any significant difference from the previous ones which used 100 replicates, and did not influence any differences seen between the results of both models. In children, a similar approach was used by performing a population simulation of 100 virtual children each with the same age, race, gender, and dosing information as that of a real child; however, the resulting median plasma concentrations were used along with the individual

observed concentrations in the model evaluation. For all previous simulations, variability ranges for CL, GET, and SITT were assigned to account for the inter-individual variability. These values were either set by the software, as in the case of software 1 as follows: CL: mean value \pm 30% CV, GET: mean value \pm 38% CV, SITT: Weibull distribution around the mean value with $\alpha=2.92$ and $\beta=4.04$, or were assigned manually based on a comprehensive literature search as in the case of software 2 as follows: log-normal distribution with geometric standard deviation of 1.3 for CL, GET: uniform distribution of 0.2–1.9 h in adults (Graff et al. 2001; Gentilcore et al. 2006), 0.2–2.1 h in children (van Den Driessche and Veereman-Wauters 2003; Barbosa et al. 2005; Barnett et al. 1999; Staelens et al. 2008), and SITT: normal distribution with a mean value of 4 ± 1 h in both adults and children (Graff et al. 2001; Khin et al. 1999).

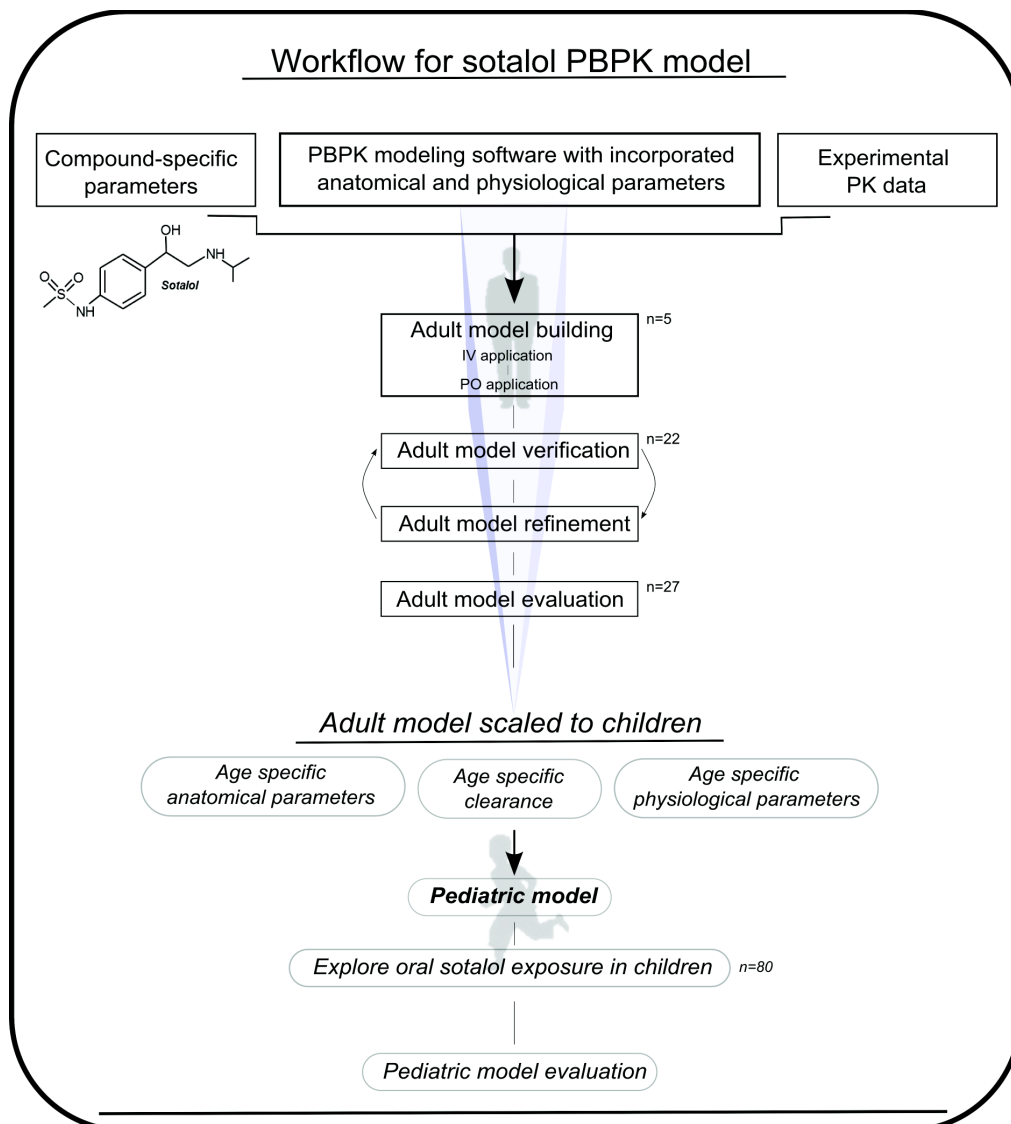


Figure 2-4. Schematic workflow of the developed PBPK models

2.3.6. Clearance scaling

The modeling tools used here employ a physiology-based scaling of adult clearance to children. In short, data-sets of experimentally obtained clearances of various substances which were primarily eliminated through one process were previously collected and used to develop and validate ontogeny patterns accounting for the maturation of various elimination pathways—including renal elimination pathways—over the pediatric age continuum (Johnson et al. 2006; Edginton et al. 2006a). These ontogeny profiles are incorporated into the used modeling tools and employed along with age-specific differences in bodyweight and composition (i.e., percentages of water, phospholipids, and neutral lipids), weight of and blood flow through eliminating organs, and protein binding in order to scale adult clearance values (model inputs) to children of different ages. This physiology-based scaling of clearance was shown to accurately predict clearance in children from birth to adolescence (Johnson et al. 2006; Edginton et al. 2006a), and was found to be superior to allometric scaling.

2.3.7. Evaluation of model performance

2.3.7.1. Graphical analysis and comparison of PK parameters

Visual predictive checks for superimposed predicted and observed plasma concentration-time profiles, as well as goodness of fit plots were used for the graphical analysis of each model results.

Moreover, the area under the plasma concentration-time curve from the first to the last concentration point (AUC_{last}), the maximal concentration (C_{max}) with the time to reach it (t_{max}), and the elimination-rate constant (k_e) were calculated via a non-compartmental analysis for each observed profile and its corresponding predicted value from each model. These parameters were chosen as the primary parameters to be calculated for pediatric PK data as the drug was given orally and the plasma concentration-time profile was measured under steady-state conditions. AUC_{last} was calculated via the trapezoidal method, k_e as the slope of the last 3 concentrations on a natural logarithmic scale (in children:

only for plasma profiles observed for over 10 hours, $n=66/80$), whereas C_{max} and t_{max} were manually determined as in the definition. An observed/predicted ratio ($ratio_{Obs/Pred}$) was then calculated and the final results were reported as mean $ratio_{S(Obs/Pred)}$ with a nonparametric 95% confidence interval (CI) derived from 10,000 bootstrap repetitions. A two-fold error range from the observed values for model predictions was set as a reference. Such a range is commonly reported by other researchers and is considered appropriate for a predictive model (Ginsberg et al. 2004; Edginton et al. 2006b; Parrott et al. 2011).

In addition, further PK parameters were also calculated and reported for adult data, as these data were obtained after single doses of both IV and oral application, which further facilitated the ability of the developed model to reflect sotalol disposition in the body. First, the AUC_{last} was extrapolated to infinity (AUC_{0-inf}) by adding the terminal AUC calculated by dividing the last measured concentration (C_{last}) by the calculated elimination rate-constant ($AUC_{terminal}=C_{last}/k_e$). As a result, the clearance was calculated as $Dose/AUC_{0-inf}$. If the previous clearance calculation was made for oral drug plasma concentration profiles, the calculated value indicates an oral clearance (CL/F). Finally, the elimination half-life ($t_{1/2}$) was calculated as $k_e/\ln 2$.

2.3.7.2. Statistical and numerical evaluation

Statistical calculations were performed using MATLAB 2012a (The Mathworks Inc., Natick, MA). To numerically describe the predictive performance of the model, various numerical metrics were reported in order to quantify either the model accuracy or precision (Sheiner and Beal 1981).

Mean Error (ME), Mean Percentage Error (MPE), and Median Percentage Error (MDPE) serve to measure the accuracy of the model. The closer the value of any of these metrics is to 0, the better the model accuracy. For example, a value of 0% for either MPE or MDPE indicates the absence of a bias towards under- or over-prediction of sotalol concentrations when compared to observed data. The ME indicates the average absolute value of error for each simulated concentration point.

On the other hand, Mean Absolute Error (MAE), Mean Absolute Percentage Error (MAPE), and Median Absolute Percentage Error (MDAPE) serve to measure the precision of the model. The closer the value of any of these metrics is to 0, the better the model accuracy. A value of 0% indicates that predicted and observed values for sotalol are identical.

Mean Error (ME) was calculated as the mean of all errors for each concentration point. Errors (= residuals) were calculated for every concentration point in each drug administration in adults and children as follows:

$$E = (C_{PRED} - C_{OBS}) \quad \text{Equation (2-1)}$$

Mean Absolute Error (MAE) was calculated as the mean for all absolute errors for each concentration point. Absolute errors were calculated as:

$$AE = |C_{PRED} - C_{OBS}| \quad \text{Equation (2-2)}$$

The Mean and the Median Percentage Errors (MPE and MDPE) were also calculated. Percentage error (PE) was calculated for all concentration points in each drug administration as follows:

$$PE = \frac{(C_{PRED} - C_{OBS})}{C_{OBS}} \times 100\% \quad \text{Equation (2-3)}$$

The mean and the median of all absolute percentage errors (MAPE and MDAPE) were also reported. Absolute percentage errors (APE) were calculated for all concentration points in each drug administration as follows:

$$APE = \frac{|C_{PRED} - C_{OBS}|}{C_{OBS}} \times 100\% \quad \text{Equation (2-4)}$$

Nonparametric 95% confidence intervals derived from 10,000 repetitions of random data sampling and recalculation (bootstrap repetitions) were additionally reported for the median percentage error (MDPE) and median absolute percentage error (MDAPE), respectively.

2.4. Results

2.4.1. Simulation results in adults

A total of 11 different adult single-dose PK studies of either IV or oral sotalol were collected. Because some of these studies investigated sotalol pharmacokinetics after different doses or type of application, or in different individuals, the total number of obtained adult data sets was 27. For each of these data sets, sotalol exposure was simulated using both models developed by SIMCYP® (software 1) or PK-SIM® (software 2).

A visual comparison between mean simulated and mean observed plasma concentration-time profiles for four representative data sets in adults is shown in **Figure 2-5**. In general, the 2 presented models were able to accurately describe sotalol exposure after IV and oral application over a total dose range of 20 to 320 mg (0.2–4.5 mg/kg body weight [BW]), and for both Caucasians and Asians. The resulting AUC_{last} ratios_(Obs/Pred) were within 0.8-1.25 in 100% (27/27) and in 92.6% (25/27) of the observed values using software packages 1 and 2, respectively, and with all predictions contained within the range 0.5-2. Moreover, the adult model did not show any difference in the predictability of sotalol exposure after IV or oral application. The mean AUC_{last} ratio_(Obs/Pred) for all simulated data sets using software 1 was 0.997 and 0.94 after IV and oral applications, respectively. These results were similar using software 2 as the mean AUC_{last} ratio_(Obs/Pred) was 0.94 for the IV and 0.987 for the oral application. **Figure 2-6** shows the predicted vs observed plots for plasma concentrations, AUC_{last} , C_{max} , t_{max} , and k_e .

The calculated numerical metrics indicate good accuracy of both models (**Table 2-5**). Software package 1 showed no bias with a MDPE value (95th bootstrap CI) of 1.36% (-1.37-3.17), in comparison to a slight bias of 3.17% (1.63-5.23) in the model generated using software package 2, which is, however, minimal and has no clinical relevance. Finally, both models showed similar precision (deviation less than 10%) as the MDAPE for all predicted concentration points was 9.91% (8.79-10.96), and 9.76% (8.56-10.85) using software packages 1 and 2, respectively (**Figure 2-6**).

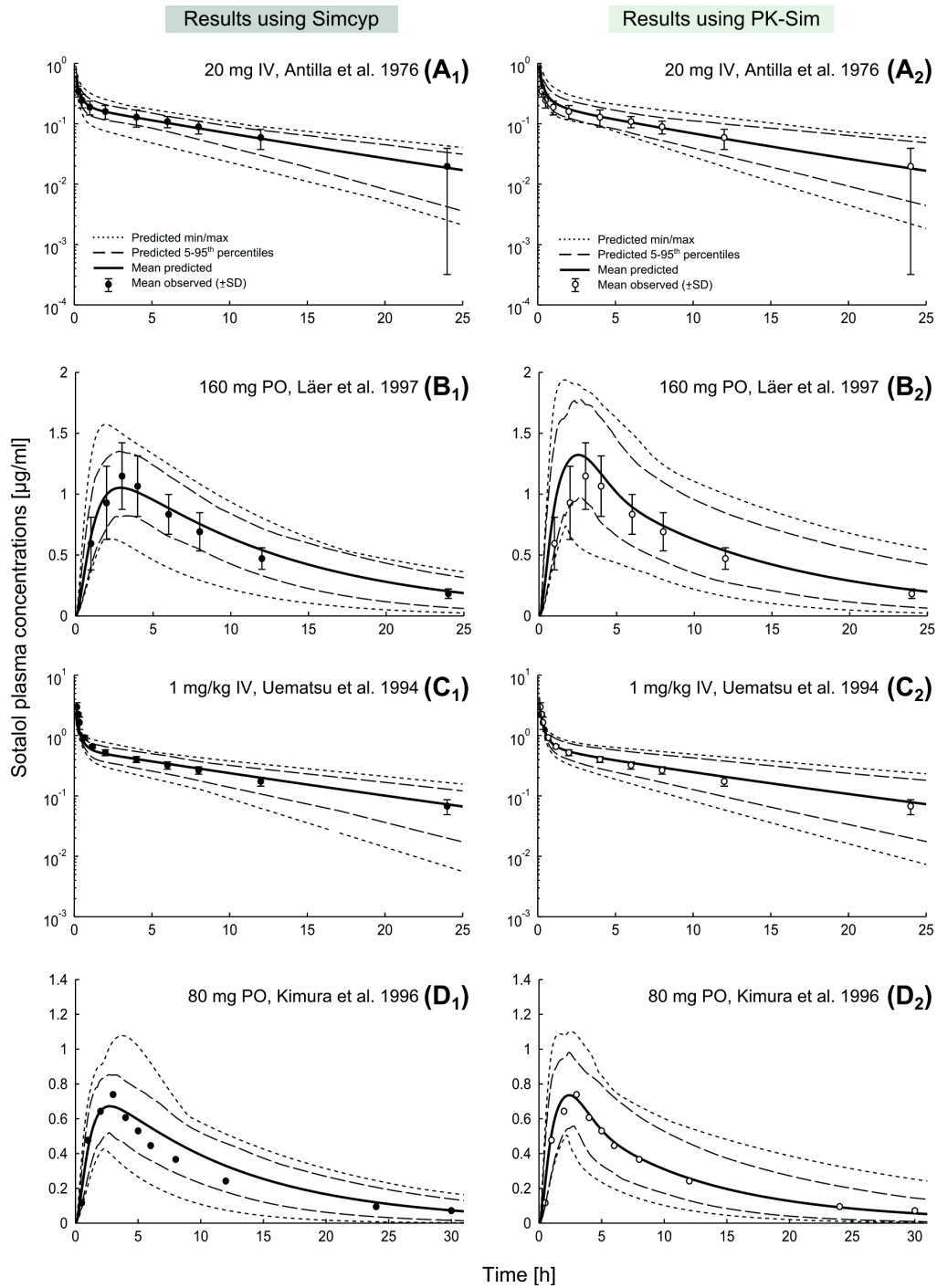


Figure 2-5. Comparison of predicted (lines; mean, 5–95th percentile, min/max) and mean observed (dots; \pm standard deviation [SD]) concentrations of IV and oral sotalol after various dosing strategies in both Caucasians [(a), (b)] and Asians [(c), (d)]. Simulations were performed using software 1 (SIMCYP®, left column, filled circles) and software 2 (PK-Sim®, right column, empty circles). Observed data are obtained from four different single dose PK studies in healthy adult volunteers.

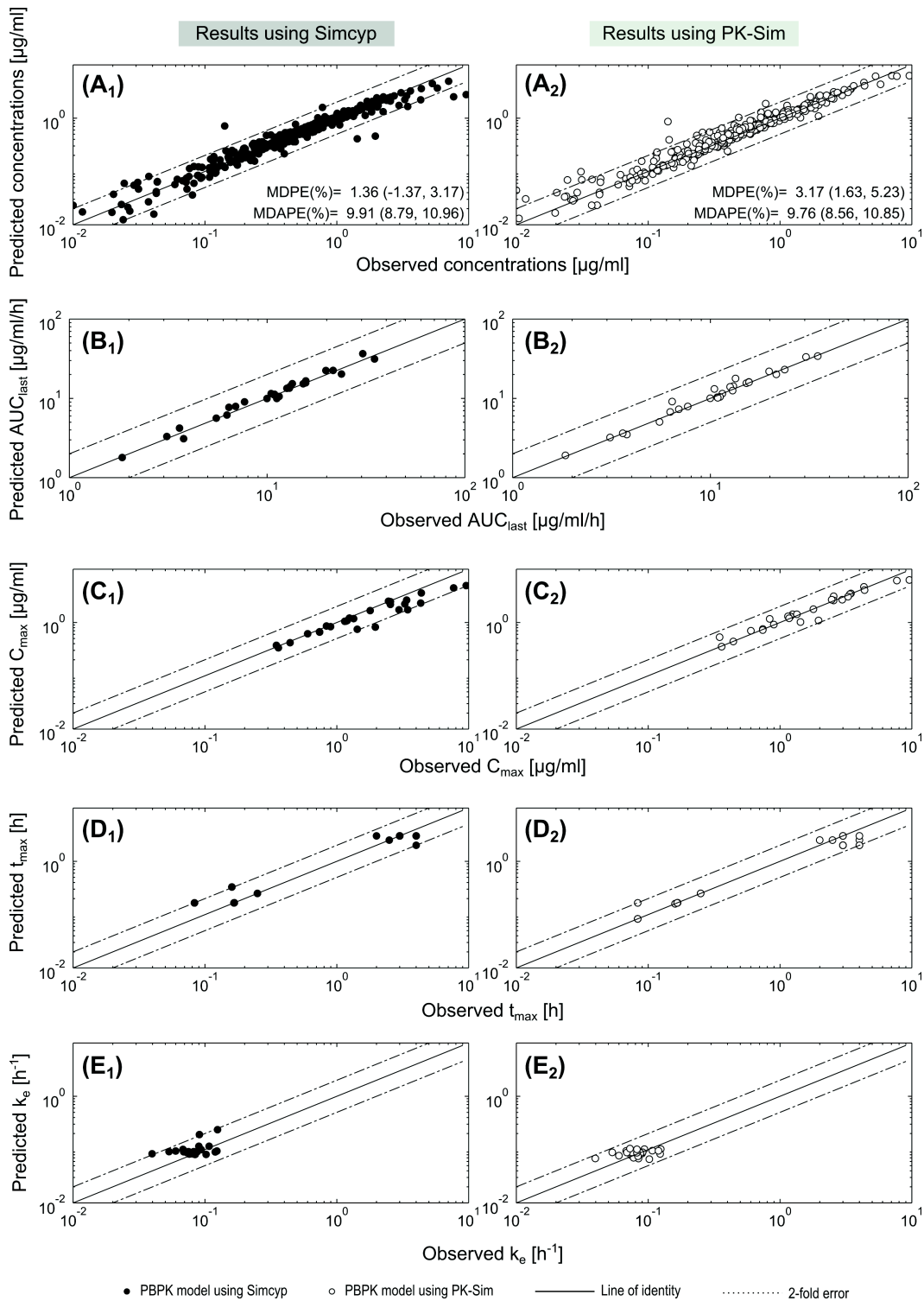


Figure 2-6. Goodness of fit plots for simulations of adult data by both sotalol PBPK models. a) Predicted vs observed concentrations plot, (b–e) predicted vs. observed AUC_{last} , C_{max} , t_{max} , and k_e plots. Results are obtained by using software 1 (SIMCYP®, left column, filled circles) and software 2 (PK-Sim®, right column, empty circles). Line= Line of unity; dashed lines= twofold error range; MDPE= median percentage error (95% confidence interval [CI]); MDAPE= median absolute percentage error (95% CI).

Table 2-5. Numerical model evaluation for both developed models in adults

Study	Dose (mg)	ME (µg/ml)		MAE (µg/ml)		MPE (%)		MAPE (%)		MDPE (%)		MDAPE (%)	
		Simcyp	PKSIM	Simcyp	PKSIM	Simcyp	PKSIM	Simcyp	PKSIM	Simcyp	PKSIM	Simcyp	PKSIM
Anttila 1976	20†	0.003	0.036	0.007	0.039	-1.488	10.897	5.332	17.007	-1.692	2.470	5.369	9.741
Rehm 1987	105†	-0.143	0.064	0.190	0.064	9.823	37.321	22.026	37.321	9.528	14.237	16.155	14.237
Rehm 1987	140†	-0.144	0.131	0.223	0.131	22.807	62.448	33.029	62.448	14.081	19.784	20.066	19.784
Poirier 1990	140†	-0.051	0.067	0.111	0.072	-1.685	6.159	8.477	7.104	-1.385	6.303	7.052	6.303
Uematsu 1994	70†	-0.263	-0.051	0.275	0.080	-11.213	2.592	16.440	8.369	-4.926	4.593	12.283	7.744
Uematsu 1994	105†	-0.127	-0.018	0.127	0.054	-8.534	-0.231	8.534	4.204	-7.520	0.070	7.520	4.134
Salazar 1997*	35†	-0.122	-0.045	0.122	0.076	-19.833	-4.698	19.833	9.870	-11.324	-3.732	11.324	6.422
Salazar 1997*	105†	-0.026	0.059	0.041	0.105	-8.188	-0.428	9.282	10.508	-4.313	-3.535	4.636	9.751
Salazar 1997*	210†	-0.652	-0.254	0.668	0.384	-16.034	-2.471	16.987	8.578	-4.794	0.758	4.877	6.569
Salazar 1997	35†	-0.098	-0.041	0.115	0.056	-2.863	2.225	26.411	19.823	-4.455	-9.321	16.542	13.444
Salazar 1997	105†	-0.139	-0.073	0.158	0.079	1.506	0.149	16.636	15.133	0.498	-6.924	6.481	8.766
Salazar 1997	210†	-0.317	0.013	0.440	0.200	3.363	7.009	17.795	10.003	4.363	2.433	11.742	3.063
Somberg 2010	75†	0.053	0.161	0.055	0.161	18.816	52.364	21.689	52.364	15.977	43.679	19.062	43.679
Anttila 1976	160‡	0.075	0.158	0.099	0.173	10.469	20.436	18.157	27.117	8.856	10.756	14.515	13.395
Kahela 1979	160‡	0.009	0.066	0.045	0.083	1.836	8.406	6.545	11.513	2.350	0.114	6.344	3.366
Ochs 1985	320‡	-0.003	0.163	0.161	0.284	-5.477	12.588	18.907	24.764	-4.985	4.454	19.104	14.176
Poirier 1990	100‡	0.011	0.045	0.041	0.060	3.678	14.999	17.068	23.236	8.665	4.042	12.329	10.878
Uematsu 1994	50‡	-0.012	-0.019	0.024	0.024	-3.727	-8.251	8.655	9.454	-2.808	-9.769	6.818	9.769
Uematsu 1994	100‡	0.004	0.007	0.039	0.062	0.022	-1.374	7.944	15.307	3.138	-6.444	6.825	10.483
Uematsu 1994	200‡	0.034	0.009	0.091	0.154	9.558	6.606	13.146	21.182	4.395	-9.961	7.181	12.398
Uematsu 1994	300‡	0.231	0.214	0.243	0.255	58.050	61.971	58.523	64.068	22.308	18.808	22.308	18.808
Kimura 1996	40‡	0.011	0.001	0.029	0.011	13.111	3.423	22.033	7.690	8.016	-3.114	16.315	3.397
Kimura 1996	80‡	0.032	0.022	0.056	0.031	14.567	9.012	20.529	15.314	12.150	3.277	12.745	4.621
Kimura 1996	160‡	0.006	0.071	0.059	0.083	6.684	11.466	10.848	18.293	6.300	-0.488	8.959	7.684
Läer 1997	160‡	0.021	0.132	0.058	0.141	4.587	15.330	7.869	19.848	6.655	11.412	7.781	13.376
Liebau 1999	160‡	-0.020	0.010	0.064	0.053	-1.758	-2.974	9.383	9.858	-3.691	0.839	8.513	5.716
Somberg 2010	80‡	0.037	0.056	0.050	0.062	13.204	16.140	26.288	29.249	11.968	14.201	17.225	19.606

† IV drug application; * female group; ‡ Oral drug application; ME= Mean Error; MPE=Mean Percentage Error; MDPE= Median Percentage Error; MAE= Mean Absolute Error; MAPE= Mean Absolute Percentage Error; MDAPE= Median Absolute Percentage Error. Simcyp= predicted value by Simcyp® software; PKSIM=predicted value by PK-Sim® software.

The results of a comprehensive PK analysis that was performed for each observed profile and its corresponding predicted values by each PBPK model after IV and oral drug administrations are reported in **Table 2-6** and **Table 2-7**, respectively. This comprehensive analysis was necessary to characterize the processes of sotalol absorption, distribution, and elimination in the human body in order to insure a proper reflection of these processes by the adult model prior to its extrapolation to the pediatric age.

After IV dosing, the adult model developed using software 1 predicted the clearance of sotalol in the simulated studies to range from 8.77 to 11.19 L/h with an average of 9.72 L/h, whereas the software 2 model predicted it to range from 7.57 L/h to 9.78 L/h with an average of 8.90 L/h. The model 1 software predicted the volume of distribution and the elimination half-life in the simulated studies to average 94.94 L and 6.87 h, respectively. In contrast, the model 2 software predicted them to average 106.85 L and 8.39 h, respectively. Moreover, the average $AUC_{0-\infty}$ was predicted to be 0.100 and 0.107 $\mu\text{g/mL/h}$ per each administered milligram of sotalol using the software 1 and software 2 models, respectively. All of the previously mentioned results are in very good agreement with reported values in the literature (see section 2.3.1.2) and the calculated PK parameters for the used studies (**Table 2-6**). After a typical 160 mg oral dosing of sotalol, the median values of $AUC_{0-\infty}$, C_{max} , and t_{max} were predicted to be 15.72 $\mu\text{g/mL/h}$, 1.09 $\mu\text{g/mL}$, and 3 hours, respectively, by software 1 and 16 $\mu\text{g/mL/h}$, 1.30 $\mu\text{g/mL}$, and 2 hours, respectively, by the software 2 model, which were also in very good agreement with the calculated values of the observed plasma profiles (**Table 2-7**). If such PBPK models for sotalol had been available some years ago, some of the recent adult PK studies would have been of little or no use.

Table 2-6. Calculated PK parameters for observed and predicted sotalol plasma profiles after IV drug application in adults

Study	IV Dose	AUC _{0-inf} (µg/ml/h)			Clearance (L/h)			Volume of distribution (L)			Elimination half-life (hour)		
		OBS	Simcyp	PKSIM	OBS	Simcyp	PKSIM	OBS	Simcyp	PKSIM	OBS	Simcyp	PKSIM
Anttila 1976	20 mg	2.06	1.97	2.08	9.71	10.16	9.63	103.69	101.82	94.57	7.40	6.94	6.80
Rehm 1987	1.5 mg/kg	10.61	11.71	13.61	9.89	8.97	7.72	117.17	110.46	113.57	8.21	8.54	10.20
Rehm 1987	2 mg/kg	13.50	15.61	18.48	10.37	8.97	7.57	101.67	110.48	114.45	6.80	8.54	10.47
Poirier 1990	2 mg/kg	16.00	15.96	16.52	8.75	8.77	8.48	112.57	105.37	115.24	8.91	8.33	9.42
Uematsu 1994	1 mg/kg	7.07	6.90	7.58	9.90	10.14	9.24	117.86	111.85	105.80	8.25	7.65	7.94
Uematsu 1994	1.5 mg/kg	12.01	11.08	11.94	8.74	9.48	8.79	105.75	115.46	102.68	8.39	8.44	8.10
Salazar 1997†	0.5mg/kg	4.00	3.13	3.80	8.74	11.19	9.22	70.21	47.35	90.19	5.56	2.93	6.78
Salazar 1997†	1.5 mg/kg	11.44	10.12	10.73	9.18	10.37	9.78	85.38	89.80	102.35	6.45	6.00	7.25
Salazar 1997†	3 mg/kg	24.65	20.58	24.03	8.52	10.20	8.74	94.80	88.33	103.75	7.71	6.00	8.23
Salazar 1997‡	0.5mg/kg	3.37	3.37	3.60	10.37	10.38	9.72	114.29	54.22	109.17	7.64	3.62	7.78
Salazar 1997‡	1.5 mg/kg	11.00	11.48	10.82	9.54	9.15	9.70	77.46	97.27	116.83	5.62	7.37	8.34
Salazar 1997‡	3 mg/kg	21.37	23.25	23.14	9.83	9.03	9.07	163.88	96.07	117.87	11.56	7.37	9.00
Somberg 2010	75 mg	6.55	7.80	9.28	11.45	9.62	8.08	155.00	105.77	102.59	9.38	7.62	8.80

AUC_{0-tlast}= Area under the plasma concentration-time profile from time 0 to infinity. OBS= Observed value; Simcyp= predicted value by Simcyp® software; PKSIM=predicted value by PK-Sim® software

† Female group; ‡ male group; Reference body weight used is 70 kg.

Table 2-7. Calculated PK parameters for observed and predicted sotalol plasma profiles after oral drug application in adults

Study	Dose (mg)	AUC _{0-inf} (µg/ml/h)			C _{max} (µg/ml)			t _{max} (h)			Oral Clearance (L/h)		
		OBS	SIMCYP	PKSIM	OBS	SIMCYP	PKSIM	OBS	SIMCYP	PKSIM	OBS	SIMCYP	PKSIM
Anttila 1976	160	16.32	15.72	16.00	1.25	1.21	1.43	3	3	2	9.80	10.17	10.00
Kahela 1979	160	16.72	16.58	16.92	1.20	1.09	1.30	4	2	2	9.57	9.65	9.45
Ochs 1985	320	35.85	31.92	35.23	2.55	2.18	2.59	4	3	2.5	8.93	10.03	9.08
Poirier 1990	100	11.01	10.14	10.37	0.74	0.66	0.76	4	3	2	9.08	9.86	9.64
Uematsu 1994	50	6.05	6.05	5.49	0.44	0.42	0.44	3	3	2	8.26	8.26	9.10
Uematsu 1994	100	12.16	12.11	10.93	0.90	0.84	0.91	3	3	2	8.22	8.26	9.15
Uematsu 1994	200	23.35	24.22	21.71	1.79	1.67	1.78	3	3	3	8.57	8.26	9.21
Uematsu 1994	300	30.97	37.39	34.12	2.47	2.51	2.68	4	3	3	9.69	8.02	8.79
Kimura 1996	40	3.85	4.83	4.06	0.36	0.34	0.35	3	3	2	10.40	8.29	9.86
Kimura 1996	80	8.73	9.73	8.50	0.74	0.67	0.72	3	3	2	9.16	8.22	9.42
Kimura 1996	160	16.56	17.48	16.69	1.34	1.18	1.43	3	3	2	9.66	9.15	9.59
Läer 1997	160	14.81	15.54	15.45	1.15	1.05	1.30	3	3	3	10.80	10.30	10.35
Liebau 1999	160	15.87	15.57	13.75	1.17	1.06	1.20	3	3	2	10.08	10.28	11.63
Somberg 2010	80	7.32	8.02	7.38	0.60	0.61	0.70	2	3	2.5	10.93	9.98	10.84

AUC_{0-tlast}= Area under the plasma concentration-time profile from time 0 to infinity. C_{max}= Maximum concentration in the plasma profile; t_{max}= time of the maximum concentration; Oral clearance= CL/F; OBS= Observed value; Simcyp= predicted value by Simcyp® software; PKSIM=predicted value by PK-Sim® software.

2.4.2. Simulation results in pediatrics

Using both modeling software applications, the extrapolated model corresponding to the pediatric population showed acceptable correlated predictions to in vivo data in adolescents down to infants, with a pronounced deviation in neonates. A comparison between median simulated and observed plasma profiles for 6 representative pediatric patients of each age group is shown in **Figure 2-7**.

Only in neonates, both models were unable to predict a mean ratio_(Obs/Pred) of all four PK parameters within the predefined two-fold error range (**Figure 2-8**). Using software 1, the mean ratios_(Obs/Pred) were 2.56 (95% CI: 2.10–3.49) and 2.15 (95% CI: 1.77–2.99) for AUC_{last} and C_{max}, respectively. Using software 2, the mean ratio_(Obs/Pred) of t_{max} was 2.37 (95% CI: 1.76–3.25). The elimination-rate constant was reasonably predicted by both models as indicated by a mean ratio of 0.55 and 0.81 for the 2 software models, respectively.

In all remaining age groups, the mean ratios_(Obs/Pred) for the chosen PK parameters were within a two-fold error range irrespective of the model used, which indicates a good predictive performance and a proper description of the age-related PK changes of sotalol. The 95% CI of the mean ratios for all PK parameters was contained within the range of 0.5 to 2, except for t_{max} in some age groups (**Figure 2-8**).

Furthermore, both models showed a general tendency to underestimate sotalol concentrations as seen with the negative MDPE values in almost all age groups and the lower accuracy and precision values when compared to the adult model (see **Figure 2-9**). The least accuracy in predicting individual concentration points was seen in neonates for software 1 (MDPE= -54.8%) and in infants for software 2 (MDPE= 29.2%), whereas for both models the highest accuracy was seen in adolescents. On the other hand, the pediatric model imprecision was less than 40% in all groups except in neonates using software 1 (MDAPE = 54.8%) and in infants using software 2 (MDAPE = 43.6%), with the best model precision seen

in adolescents using both software packages (MDAPE = 15.7%, 15.6% for software 1 and software 2, respectively).

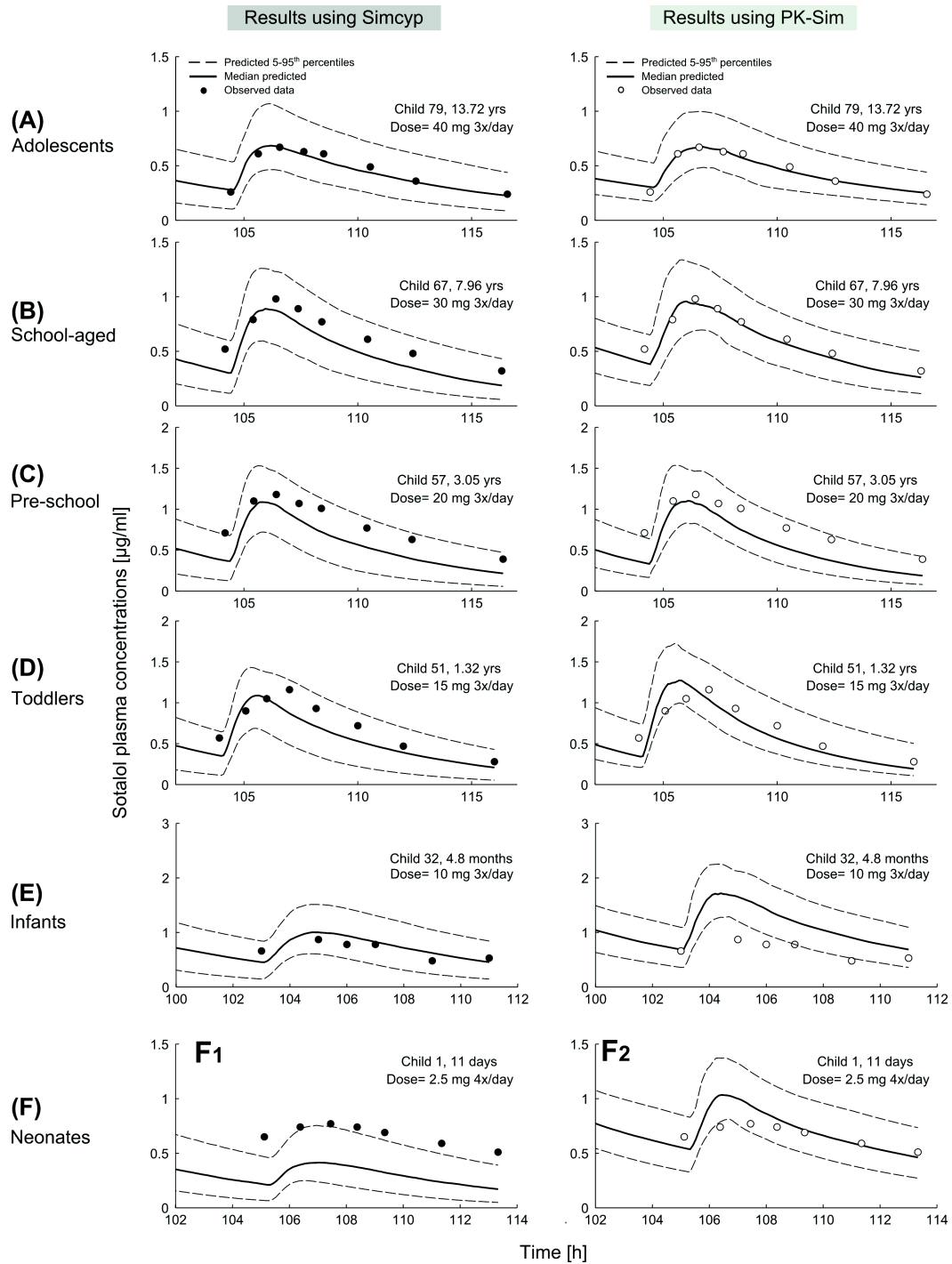


Figure 2-7. Comparison of predicted (lines; median, 5–95th percentile) vs individual observed (symbols) plasma concentrations in six representative pediatric patients from (a) adolescents to (f) neonates, after various doses of oral sotalol given 3-4 times daily. Predictions were made using software 1 (Simcyp®, left panel, filled circles) and software 2 (PK-Sim®, right panel, empty circles). All observed data are taken from Läer et al. 2005.

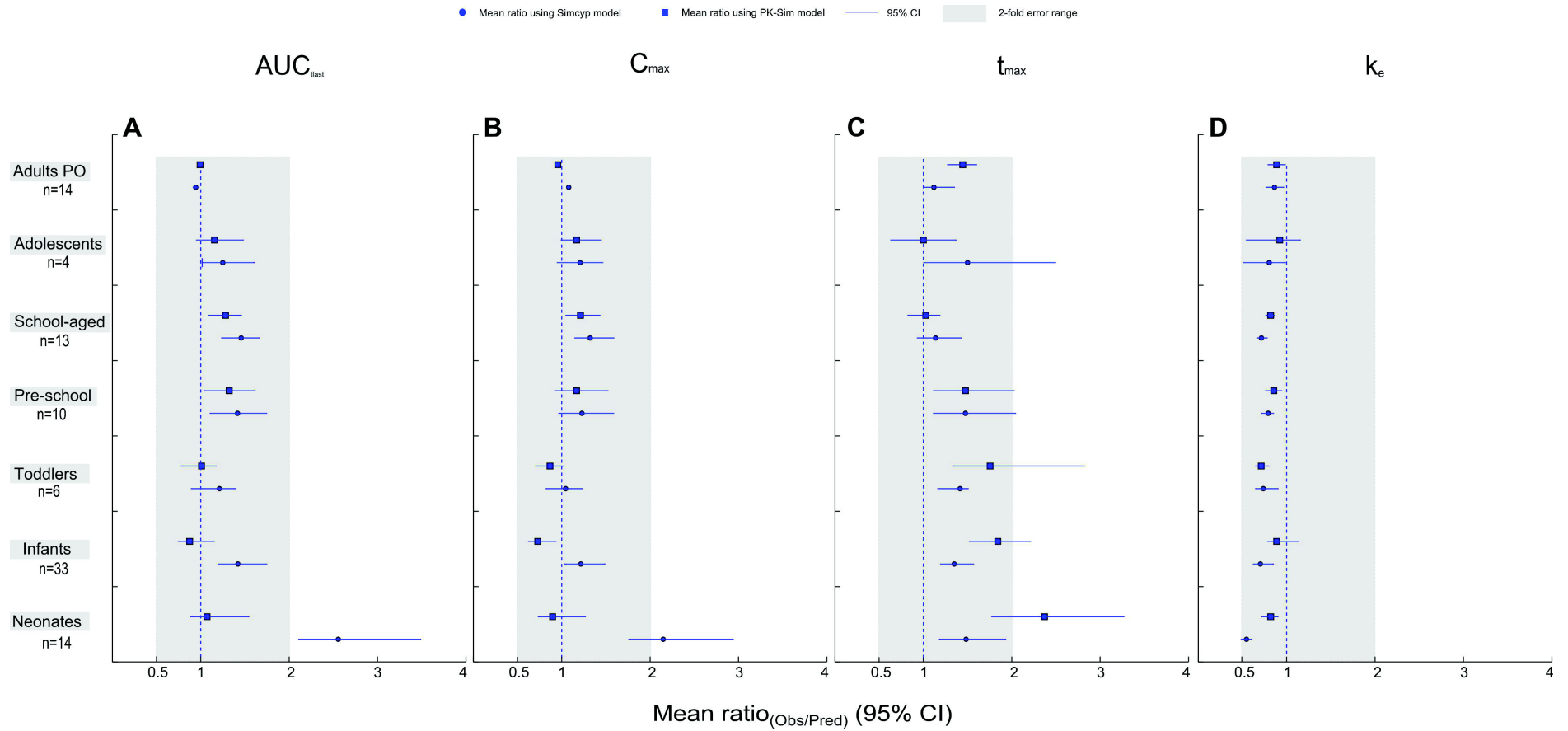


Figure 2-8. Comparison between the observed and predicted values of (A) the area under the plasma concentration-time curve (AUC_{last}), (B) maximum concentration (C_{max}), (C) time of the maximum concentration (t_{max}), and (D) the elimination rate constant (k_e) in adults oral studies and in children. Results are presented as mean ratios in each age group (symbols: circles for software 1 results, squares for software 2 results) with a 95% confidence interval (horizontal lines).

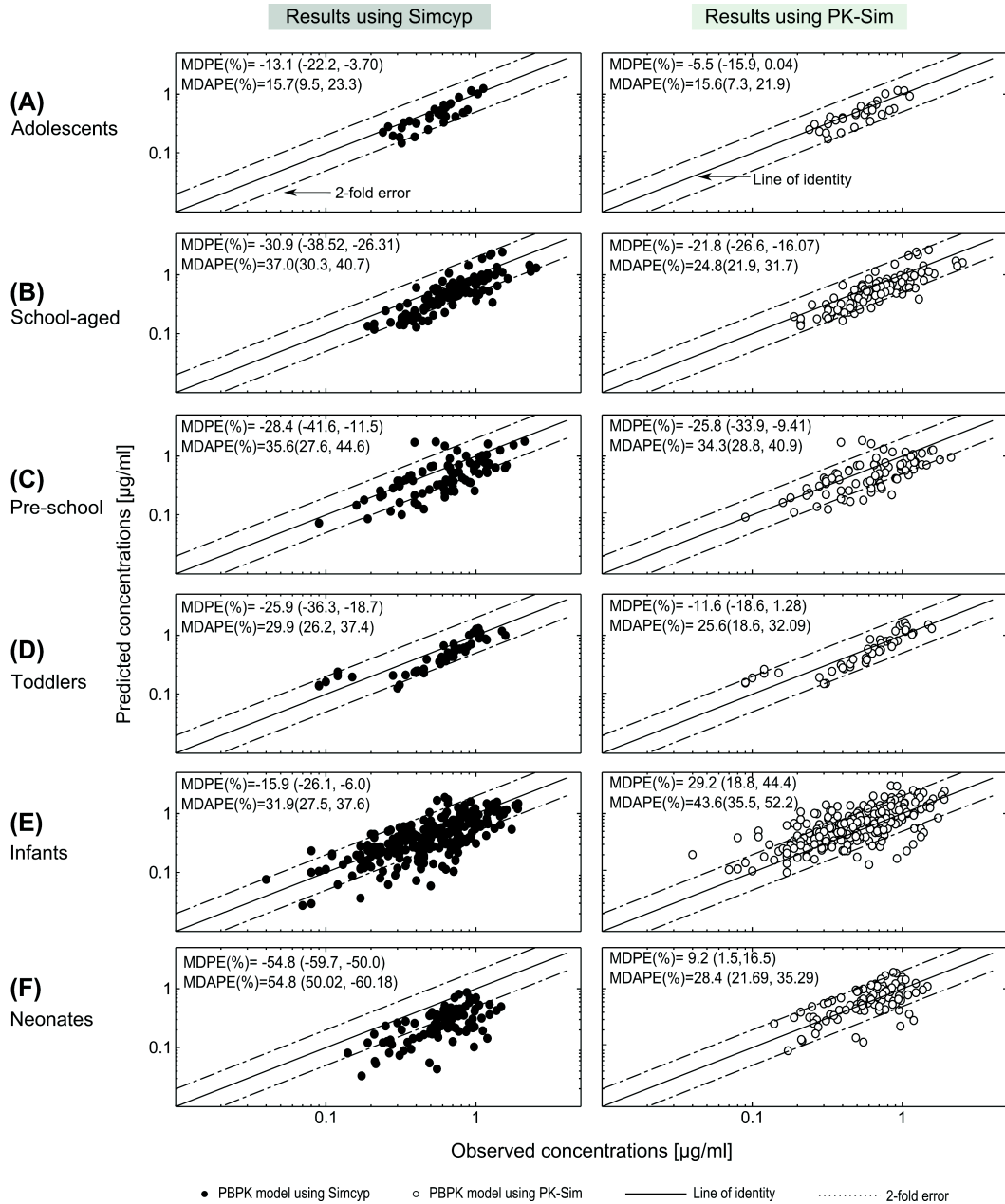


Figure 2-9. Median predicted vs individual observed concentration plots for 80 pediatric patients stratified in 6 pediatric age groups from (a) adolescents to (f) neonates. Results are obtained using software 1 (SIMCYP®, left column, filled circles) and software 2 (PK-Sim®, right column, empty circles). Line= Line of unity; dashed lines= two-fold error range; MDPE= median percentage error (95% confidence interval [CI]); MDAPE= median absolute percentage error (95% CI).

Table 2-8. Evaluation metrics and calculated observed to predicted ratios of AUC_{last}, C_{max}, t_{max}, and k_e of the entire pediatric collective using both models.

Patient Code	Age (year)	AUC _{last} ratio _{OBS/PRED}		C _{max} ratio _{OBS/PRED}		t _{max} ratio _{OBS/PRED}		k _e ratio _{OBS/PRED}		MDPE (%)		MDAPE (%)	
		Simcyp	PKSIM	Simcyp	PKSIM	Simcyp	PKSIM	Simcyp	PKSIM	Simcyp	PKSIM	Simcyp	PKSIM
1	0.030	2.205	0.922	1.892	0.747	1.000	1.947	-	-	-53.237	3.417	53.237	10.130
2	0.033	2.367	1.112	2.041	0.937	2.885	2.885	-	-	-64.545	-16.583	64.545	37.883
3	0.036	1.737	0.711	1.417	0.542	1.000	1.739	0.586	0.853	-40.500	31.848	40.500	31.848
4	0.036	2.420	0.934	2.182	0.916	1.000	1.000	-	-	-56.675	8.296	56.675	10.551
5	0.036	3.252	1.273	2.717	1.032	1.331	2.500	0.495	0.738	-69.854	-28.787	69.854	30.044
6	0.038	6.253	2.846	5.234	2.282	3.000	6.000	-	-	-85.202	-68.200	85.202	68.200
7	0.041	2.266	0.806	1.674	0.635	2.061	3.961	0.627	1.006	-57.095	16.730	57.095	16.730
8	0.049	1.337	0.549	1.395	0.556	0.502	1.000	0.560	0.900	-26.347	83.766	26.347	83.766
9	0.049	2.828	1.259	2.037	0.837	1.938	3.479	0.456	0.613	-63.937	-26.592	63.937	31.500
10	0.052	2.187	0.831	1.796	0.713	1.545	2.957	0.460	0.744	-55.149	11.181	55.149	11.181
11	0.058	3.569	1.407	3.377	1.434	1.000	1.000	-	-	-71.148	-29.672	71.148	29.672
12	0.060	2.116	0.876	1.611	0.647	1.500	2.727	0.383	0.598	-49.073	9.386	49.073	21.008
13	0.068	2.071	0.947	1.695	0.820	1.000	1.000	0.637	0.947	-47.788	6.504	47.788	6.504
14	0.071	1.173	0.517	1.005	0.459	1.000	1.000	0.707	0.973	-17.056	86.477	17.056	86.477
15	0.082	3.001	1.233	2.342	0.979	1.519	2.926	0.476	0.698	-65.726	-22.757	65.726	28.443
16	0.088	2.939	1.228	2.254	1.072	1.000	1.000	0.497	0.722	-63.729	-16.606	63.729	16.606
17	0.088	4.210	1.839	2.956	1.258	1.971	3.083	0.380	0.593	-74.800	-48.468	74.800	48.468
18	0.099	2.342	1.096	1.856	0.847	1.500	1.500	0.468	0.653	-58.710	-13.236	58.710	25.634
19	0.115	1.694	0.826	1.808	0.952	1.000	1.000	0.436	0.585	-44.684	12.938	44.684	12.938
20	0.126	0.554	0.261	0.578	0.262	1.000	1.738	1.006	1.428	84.501	268.778	84.501	268.778
21	0.126	0.999	0.477	0.911	0.432	1.500	3.000	1.847	2.693	2.842	91.721	16.325	91.721
22	0.129	0.926	0.421	1.133	0.561	1.000	1.000	-	-	4.420	143.397	13.302	143.397
23	0.167	1.230	0.521	0.814	0.471	3.000	1.500	0.574	0.916	-36.594	59.172	54.369	59.172
24	0.180	1.998	0.947	1.669	0.803	2.068	3.821	0.761	1.026	-57.167	-12.555	57.167	22.016
25	0.214	0.828	0.413	0.697	0.327	2.005	3.637	0.488	0.692	14.429	110.989	26.762	110.989
26	0.236	0.948	0.521	0.811	0.469	1.000	1.000	0.696	0.888	9.173	94.399	16.569	94.399

Table 2-8. continued

Patient Code	Age (year)	AUC _{last} ratio _{OBS/PRED}		C _{max} ratio _{OBS/PRED}		t _{max} ratio _{OBS/PRED}		k _e ratio _{OBS/PRED}		MDPE (%)		MDAPE (%)	
		Simcyp	PKSIM	Simcyp	PKSIM	Simcyp	PKSIM	Simcyp	PKSIM	Simcyp	PKSIM	Simcyp	PKSIM
27	0.238	1.316	0.719	0.995	0.523	1.333	1.333	0.516	0.662	-24.838	29.158	24.838	29.158
28	0.247	0.881	0.488	0.851	0.463	1.000	2.000	0.944	1.263	13.541	96.234	13.541	96.234
29	0.282	0.991	0.569	0.790	0.424	1.985	3.769	0.619	0.781	-1.580	55.162	26.846	55.162
30	0.304	0.389	0.560	0.344	0.471	1.500	3.000	-	-	166.767	74.530	166.767	74.530
31	0.370	1.393	3.389	1.067	2.483	1.505	1.505	0.717	0.889	-24.157	-72.069	24.157	72.069
32	0.395	0.926	0.608	0.868	0.526	1.000	1.000	-	-	10.443	68.348	17.744	68.348
33	0.400	1.473	0.712	1.097	0.552	2.713	2.713	-	-	-36.900	27.072	36.900	27.072
34	0.411	2.255	1.383	3.208	1.724	1.000	3.000	0.553	0.660	-52.579	-29.318	52.579	29.953
35	0.422	1.518	1.000	1.289	0.797	1.000	1.000	0.892	1.072	-37.263	-7.353	37.263	8.763
36	0.433	2.000	1.140	1.550	0.900	1.500	3.000	0.715	0.905	-50.375	-18.149	50.375	23.539
37	0.482	0.748	0.647	0.581	0.428	1.499	1.499	-	-	18.338	35.170	18.338	35.170
38	0.570	0.855	0.588	0.670	0.422	1.469	2.817	0.525	0.584	16.022	53.514	27.202	53.514
39	0.611	0.784	0.539	0.664	0.429	1.000	1.000	0.600	0.625	32.285	80.966	36.176	80.966
40	0.611	1.524	1.117	1.380	0.902	1.000	1.000	0.814	0.933	-35.605	-18.236	35.605	18.236
41	0.655	0.845	0.605	0.893	0.594	1.000	1.000	0.897	1.022	19.872	65.606	25.136	65.606
42	0.688	0.984	0.725	0.845	0.582	1.448	1.448	0.505	0.520	3.377	29.744	16.151	29.744
43	0.693	1.998	0.986	1.522	0.838	1.000	1.000	-	-	-43.723	9.389	43.723	20.497
44	0.696	1.148	0.872	1.027	0.704	1.000	1.000	0.876	0.915	-5.115	18.150	5.742	20.647
45	0.712	1.014	0.773	0.879	0.613	1.000	1.000	0.703	0.718	0.555	23.927	11.925	23.927
46	0.816	1.303	0.978	0.980	0.672	0.500	0.500	0.409	0.442	-26.069	-9.989	26.069	30.736
47	0.970	0.845	0.674	0.811	0.585	0.500	1.000	1.065	1.059	22.515	44.241	22.515	44.241
48	1.047	1.364	1.038	1.328	1.036	1.500	1.500	0.785	0.773	-32.584	-11.813	32.584	16.533
49	1.216	1.346	1.148	1.019	0.841	1.458	3.500	0.652	0.612	-29.442	-17.924	29.442	31.001
50	1.244	1.131	0.868	0.819	0.650	1.452	1.452	0.604	0.647	-20.562	5.093	26.952	24.410
51	1.318	1.204	1.088	1.104	0.940	1.500	1.500	0.984	0.860	-24.292	-14.499	24.292	19.607
52	1.584	1.601	1.362	1.367	1.169	1.000	1.000	0.654	0.671	-37.364	-25.905	37.364	25.905
53	1.693	0.621	0.547	0.627	0.567	1.579	1.579	-	-	60.052	83.160	60.052	83.160

54	2.093	0.881	0.804	0.805	0.766	1.000	1.000	-	-	11.690	22.720	11.690	22.720
55	2.901	2.232	1.315	2.308	1.260	1.000	1.000	0.774	0.813	-56.549	-20.813	56.549	20.813
56	2.940	2.050	1.825	1.808	1.683	1.500	1.500	0.881	0.946	-57.989	-51.611	57.989	51.611
57	3.049	1.367	1.376	1.124	1.104	1.000	1.000	0.759	0.672	-29.597	-28.934	29.597	28.934
58	3.156	1.453	1.329	1.056	1.011	3.125	3.125	0.725	0.805	-38.674	-33.215	38.674	38.517
59	3.321	1.169	2.180	1.184	2.213	1.000	1.000	0.579	0.602	-15.536	-54.811	18.558	54.811
60	3.636	1.984	1.742	1.479	1.359	2.041	2.041	0.688	0.811	-56.865	-49.984	56.865	49.984
61	3.850	1.450	1.171	1.133	0.970	1.660	1.660	0.929	1.034	-42.924	-27.376	42.924	29.025
62	4.077	0.541	0.519	0.429	0.409	1.938	1.938	0.885	0.920	35.659	39.010	35.659	39.010
63	4.236	1.032	0.953	0.960	0.902	0.495	0.495	0.900	1.085	-3.644	3.055	11.304	8.383
64	6.392	1.126	1.039	1.150	1.093	0.500	0.500	0.774	0.873	-12.236	-2.669	12.236	9.804
65	6.855	1.569	1.338	1.281	1.226	1.000	0.502	0.694	0.823	-34.631	-27.419	34.631	27.419
66	7.942	1.569	1.362	1.256	1.137	1.459	1.459	0.613	0.713	-37.418	-26.307	37.418	26.307
67	7.960	1.246	1.065	1.122	1.046	1.000	1.000	0.702	0.830	-20.841	-6.025	20.841	6.937
68	8.789	2.273	1.961	2.316	2.057	1.000	1.000	0.665	0.753	-56.497	-49.701	56.497	49.701
69	8.932	1.486	1.346	1.290	1.190	2.304	1.352	0.895	0.953	-34.525	-26.941	34.525	26.941
70	9.025	1.293	1.102	1.140	1.016	1.500	1.500	0.796	0.909	-25.435	-12.136	25.435	12.136
71	9.060	1.053	0.871	0.908	0.799	1.000	1.000	0.652	0.806	-4.429	15.204	8.861	16.590
72	9.249	0.607	0.565	0.619	0.569	1.000	1.000	0.921	0.966	61.482	72.711	61.482	72.711
73	9.279	1.878	1.561	1.730	1.477	1.500	1.500	0.573	0.616	-49.481	-37.703	49.481	37.703
74	11.293	1.425	1.234	1.232	1.140	1.000	1.000	0.555	0.755	-30.880	-21.590	30.880	21.590
75	11.578	1.762	1.624	1.786	1.681	0.539	0.539	0.735	0.825	-43.158	-37.822	43.158	37.822
76	11.737	1.661	1.569	1.357	1.325	1.000	1.000	-	-	-28.036	-24.586	28.036	24.586
77	13.014	1.712	1.610	1.613	1.550	1.000	1.000	0.792	0.931	-44.193	-40.479	44.193	40.479
78	13.129	0.936	0.877	0.898	0.968	1.000	0.500	0.954	1.144	3.201	15.348	7.935	17.370
79	13.718	1.042	1.016	0.992	0.997	1.000	1.000	1.058	1.207	-3.701	0.428	6.634	3.096
80	17.751	1.305	1.116	1.329	1.159	3.000	1.500	0.406	0.407	-21.664	-10.355	21.664	10.355

AUC_{0-t_{last}}= Area under the plasma concentration-time profile from time 0 to infinity. C_{max}= Maximum concentration in the plasma profile; t_{max}= time of the maximum concentration; k_e= elimination rate constant; MDPE= Median Percentage Error; MDAPE= Median Absolute Percentage Error; Simcyp= predicted value by Simcyp® software; PKSIM=predicted value by PKSIM® software. In 14 patients, k_e was not calculated due to a short sampling time

2.5. Discussion

2.5.1.1. Key findings

Whole-body PBPK models for sotalol, an orally given drug, were developed using 2 specialized modeling software packages. The presented models were able to successfully describe sotalol pharmacokinetics in adults and over a wide range of the pediatric age spectrum, except in neonates. The results obtained by both models were comparable and showed differences only in children under 1 year of age.

Following this methodological approach, PBPK models of sotalol were first developed and evaluated in adults. Both models were able to accurately and reliably predict sotalol exposure after a wide range of IV and oral dosing (**Figures 2-5, 2-6**), which indicates that they adequately captured the major processes driving sotalol pharmacokinetics. The initial development and validation of the model in adults presents a modeling strategy that forms a solid basis for age extrapolation to increase the accuracy of the pediatric model predictions. Such a strategy is common in the development of pediatric models and has already been used by other researchers (Edginton et al. 2006a; Kersting et al. 2012; Parrott et al. 2011).

In adolescents down to infants, the pediatric models seemed to properly reflect the age-related changes in sotalol pharmacokinetics, as indicated by the adequate description of the experimental plasma profiles, which was further supported by the numerical metrics and a good prediction of $AUC_{t_{last}}$, C_{max} , t_{max} , and k_e indicated by a mean ratio_(Obs/Pred) within a two-fold error range (**Figures 2-7, 2-8, 2-9**). The only exception was for t_{max} , where the calculated 95% CI exceeded the two-fold error range in some age groups; however, this could be explained, except for infants, by the relatively low number of included children. Our results are similar to those reported by Parrot et al., whose pediatric model for orally administered oseltamivir and its metabolite revealed a predicted AUC in infants that was within a two-fold range of the observed value (Parrott et al. 2011).

In neonates, no model was able to predict a mean ratio_(Obs/Pred) for all reported PK parameters (AUC_{last} , C_{max} , t_{max} , and k_e) within the predefined two-fold error range, as a result of which the results were judged as inadequate (**Figure 2-8**). The noticed deviation was seen for parameters reflecting the extent and rate of drug absorption (AUC_{last} , C_{max} , or t_{max}) rather than drug disposition (k_e). In the previously mentioned model developed by Parrot et al., a difference of more than two-fold was obtained upon AUC prediction of oseltamivir and its metabolite in neonates, which is similar to our findings (Parrott et al. 2011). A mean ratio_(Obs/Pred) higher than 2 for any PK parameter—as in our results—implies that the model predicts a value that is, on average, less than half of the experimentally observed one. Nevertheless, the clinical relevance of such results should be eventually judged after also taking into consideration the intended use of the generated data, and the allowable error for that particular drug (e.g., low for drugs with narrow therapeutic window). For example, this deviation seen in neonates would be of more clinical relevance if the model is intended to be used to make dose recommendations than to suggest sampling times. In the former case, any recommendations in neonates based on such low predicted AUC, in comparison to the observed AUC, could lead to recommending higher therapeutic doses than necessary, with potential toxicity (e.g., torsades de pointes with sotalol) as a clinical consequence.

Both of the presented models performed similarly in adults and in almost all pediatric age groups with the only discrepancy seen in children less than 1 year of age. First, whereas the software 1 model tended to under-predict plasma concentrations in all age groups, including infants and neonates (negative MDPE), the software 2 model under-predicted plasma concentrations only in children over 1 year of age. Finally, in neonates, the software 1 model was unable to accurately predict the extent of drug absorption as indicated by a mean ratio_(Obs/Pred) exceeding 2 for AUC_{last} and C_{max} , whereas the software 2 model did not adequately predict the rate of drug absorption (t_{max}) in the same age group.

We suggest that the inaccuracy of the predictions seen in neonates is attributed to the absorption rather than elimination or distribution processes. This

is because the major factors that influence sotalol disposition (e.g., maturation of the renal function, the age-related differences in body composition, tissue volumes, and blood flows) are well characterized over the entire pediatric age range and are successfully implemented in the used modeling tools, which should make the scaled information (e.g., clearance) a good estimate. In this exercise, both models were able to acceptably predict the elimination rate constant in all pediatric age groups (**Figure 2-8**). However, the marginally accepted low mean $\text{ratio}_{(\text{Obs}/\text{Pred})}$ for k_e in neonates obtained using software package 1 indicate relatively high predicted values that are most probably attributed to high predicted clearance in this age group. As a result, the potential influence of any inaccuracy in clearance scaling on the obtained results in neonates should not be completely excluded.

In contrast, the absorption process is more complex and involves many factors apart from the pharmaceutical formulation of the drug. The first set of factors are anatomical and physiological, such as gastrointestinal organ volume and blood flow, radius, length and effective surface area, pH, GET, SITT, metabolizing enzymes, transporters, and fluid secretion. Influenced, in part, by difficulties in obtaining age-specific information in the literature, an age specific value is not incorporated for all of these factors in the pediatric absorption models integrated within the used modeling tools, which makes them an area in need of improvement (**Table 2-9**). For instance, the ADAM model used by software 1 to predict the oral drug absorption is under further improvement to fill such gaps with age-specific values (e.g., for metabolizing enzymes, transporter, pH profile, and volume of secreted fluids). As sotalol is not metabolized or actively transported throughout the gastrointestinal tract and is highly soluble, an age-related change in the pH profile could be the sole possible factor from this list to influence its extent of absorption.

The second set of parameters is drug dependent, such as solubility, pK_a , volume/size of the molecule, and its intestinal permeability. Concerning the latter, Yang et al. suggested that paracellular transport plays a major role in sotalol permeability (Yang et al. 2007). Dahan et al. stated that, in adults, sotalol shows a

unique permeability pattern as a combination of a basic moiety with pK_a and $\log P$ values within a critical range, and that sotalol permeability in the distal small intestine is high and compensates for its low permeability in the proximal segments (Dahan et al. 2010). This explains the low in vitro measured jejunal permeability of sotalol, a BCS class I drug. In recognition of this information, the predictions of software 1 model in neonates would have been improved if a higher permeability of sotalol is assumed and incorporated into the model, as it has already been reported that paracellular transport is higher in neonates than in adults due to wider tight junctions (Edginton and Fotaki 2010). On the other hand, the findings of Dahan et al. highlight the role of higher pH values in sotalol absorption, and points to a rationale for incorporation of different values of permeability throughout the intestinal segments, which could improve software 2 model predictions. Running simulation scenarios using the presented PBPK pediatric models would clarify, reject, or confirm these assumptions and would help in detecting the most influential factor on sotalol absorption.

Table 2-9. List of the anatomical, physiological, and drug-specific parameters that are involved in the drug absorption with the availability of corresponding age-specific values, as default, in the used pediatric absorption models

	Software 1 (Simcyp®)	Software 2 (PK-Sim®)
I. Anatomical and physiological parameters		
GIT organs volumes	Scaled with age specific data	Scaled with age specific data
GIT organs blood flows	Scaled with age specific data	Scaled with age specific data
Radius of the intestinal segments	Scaled with age specific data	Scaled with age specific data
Length of the intestinal segments	Scaled with age specific data	Scaled with age specific data
Effective surface area of intestinal segments	Scaled with age specific data	Scaled with age specific data
Gastric pH	Not scaled (adult values) ^{a,b}	Not scaled (adult values) ^a
Intestinal pH	Not scaled (adult values) ^a	Not scaled (adult values) ^a
Gastric emptying time (GET)	Not scaled (adult values) ^a	Not scaled (adult values) ^a
Small intestinal transit time (SITT)	Not scaled (adult values) ^a	Not scaled (adult values) ^a
Intestinal enzyme ontogeny	Scaled for CYP3A4 and UGT	Scaled for CYP3A4 and UGT
Intestinal enzyme abundance	Not scaled (adult values) ^c	Not scaled (adult values) ^c
Intestinal Transporter ontogeny	Not scaled (adult values) ^c	Not scaled (adult values) ^c
Intestinal Transporter abundance	Not scaled (adult values) ^c	Not scaled (adult values) ^c
Fluid secretion volume	Not scaled yet ^b	Volumes are scaled according to length and radius of intestinal segments
II. Drug specific parameters		
Molecular weight of the molecule	Unchanged	Unchanged
pKa value	Unchanged	Unchanged
Lipophilicity	Unchanged	Unchanged
Solubility	Unchanged	Unchanged
Permeability coefficient in the gut wall	Unchanged	Unchanged

This list does not include factors related to the pharmaceutical formulation

^a Values and variability ranges could be manually assigned. In software 2, various distribution types of the variability could be assigned during the simulations of virtual populations

^b To be incorporated in the upcoming versions

^c No sufficient literature of specific pediatric data

2.5.2. Limitations

The two presented models were not completely identical in their input parameters (**Table 2-1**); however, the different input values of B:P ratio and intestinal permeability measures resulted eventually in similar V_{ss} and bioavailability values and are therefore not likely to be responsible for any major finding. Second, although the work presented here would contribute to a better understanding, and thus to a more correct use of the PBPK model-generated data in the pediatric population, sotalol is a drug with a relatively simple PK profile (i.e., renally excreted, not metabolized, unbound to plasma proteins, and has no known active transporters [Hanyok 1993; Tjandramaga 1980]); therefore, the used software tools may not necessarily do as well with predictions for drugs with more complex PK characteristics. In addition to that, sotalol is a BCS class I drug with a high solubility and permeability profile, which means that this exercise will give no information on the accuracy of the drug absorption in the lower intestinal segments and its age dependence. As a result, further examples with drugs that possess different PK profiles (e.g., hepatic elimination with first-pass effect or with involvement of transporters) and physicochemical properties (e.g., belonging to different BCS groups) are still needed.

2.5.3. Implications and generalizations

This work was not designed to investigate new insights into the pharmacokinetics of sotalol, as this has already been extensively studied in both adults and children (Hanyok 1993; Tjandramaga 1980; Anttila et al. 1976; Salazar et al. 1997; Uematsu et al. 1994; Somberg et al. 2010; Rehm et al. 1987; Poirier et al. 1990; Kimura et al. 1996; Kahela et al. 1979; Ochs et al. 1985; Läer et al. 1997; Liebau 1999; Läer et al. 2005). However, the current work is planned to support a future pediatric clinical trial, which will aim to develop a safe IV dosing regimen as a substitute for oral sotalol in children with supraventricular tachycardia by providing the necessary sampling times for an optimal PK analysis. Additionally, such validated models could play a role in supporting clinical decision making in individual patients, for example, with reduced renal function.

The obtained results in infants through adolescents indicate good model predictability and thus substantiate the use of PBPK models to generate data a priori for this age group, saving time, effort, and resources. This could probably be generalized to other orally administered drugs that share a similar PK profile as sotalol. On the other hand, the lower model predictability of sotalol pharmacokinetics seen in neonates indicates the need for a more cautious use of model-generated data in this age group, acknowledging that the final judgment depends on the purpose of the model and the properties of the modeled drug.

2.6. Conclusion

In summary, the PBPK models presented in this study have shown good predictability of observed data in adults and in almost all pediatric age groups, except in neonates where a lower predictive performance was seen, which suggests a more cautious use of model-generated data in this age group. These results encourage the use of PBPK models, especially when adult data are available to validate the basic model, to predict oral drug exposure in a wide range of pediatric ages, which can aid in supporting pediatric clinical trials and, potentially, clinical decision making for individual children.

Chapter 3:

A Pediatric PBPK model to predict amiodarone intravenous exposure in severely ill pediatric patients

3.1. Introduction and rationale for this project

Amiodarone is an effective antiarrhythmic drug used in the treatment of multiple forms of heart dysrhythmias refractory to, or in patients intolerant of, other antiarrhythmic agents. Amiodarone is used “off-label” in children where very little is known about the pharmacokinetics of this drug in this vulnerable population. The lack of pediatric PK data, the potential side effects of amiodarone therapy, as well as its complex PK profile hinder its optimal use in routine pediatric clinical practice and complicate the conduct of any informative pediatric PK studies. A safety and observational PK study was recently published (Ramusovic et al. 2013). Although the previous study was not able to conduct an informative PK analysis, its reported PK data can be used to evaluate a pediatric PBPK model for amiodarone. Developing such a PBPK model for amiodarone could help optimize its use in pediatric drug therapy by exploring the impact of age-dependent changes in the body composition and organ functions on its systemic exposure. Furthermore, an evaluated model, if proven able to adequately reflect amiodarone pharmacokinetics in children, could be used to support physician decisions in treating individual pediatric patients by providing information about the expected drug exposure in advance.

3.2. Objectives of this project

The main objective of this project was to develop a pediatric PBPK model for amiodarone and then to evaluate its ability to predict amiodarone concentrations in a pediatric population in order to use the model in the future to explore the impact of age-related physiological changes on amiodarone pharmacokinetics from birth to adolescence.

3.3. Methods

3.3.1. Literature search - the modeled drug

3.3.1.1. Basic physicochemical properties of amiodarone

Amiodarone is a basic drug with a molecular weight of 645.31 g/mol (PubChem Compound CID= 2157) and reported pKa values ranging from 6.56 to 9.12 (Bonati et al. 1984; Chatelain and Laruel 1985). Amiodarone is very lipophilic, and high LogP values were reported in the literature: 6.66 (Chatelain and Laruel 1985), 7.6 (PubChem Compound CID= 2157), 7.8 (Ruell et al. 2004), 7.9 (Wang), and 8.8 (Zhi et al. 2003).

3.3.1.2. Amiodarone disposition

Amiodarone is extensively metabolized in the liver by various CYP isoenzymes. It has been reported that CYP3A4, CYP2C8, CYP1A2, CYP2D6, and CYP2C19 are involved in catalyzing the N-deethylation of amiodarone (Ohyama et al. 2000). Although the relative contribution of these enzymes to amiodarone metabolism remains to be determined, CYP3A4 is considered the major enzyme responsible for it; CYP2C8, especially at low amiodarone concentrations, is also reported to be significantly involved (Ohyama et al. 2000). Multiple PK studies have reported the total plasma clearance of amiodarone to be 1.9 mL/min/kg (Holt et al. 1986), 2.63 mL/min/kg (Vadiei et al. 1997), 229 mL/min (~ 3.27 mL/min/kg), 3.33 mL/min/kg (Shiga et al. 2011), and 3.67 mL/min/kg (Bradley et al. 1996). Due to the highly lipophilic nature of amiodarone, its volume of distribution is high and was reported to be 45 L/kg (Shiga et al. 2011), 57 L/kg (Vadiei et al. 1997), or 65.8 L/kg (Holt et al. 1986), with a terminal elimination half-life in adults of 40-55 days (range 26-107 days) [DI]. The therapeutic concentration range of amiodarone is reported to be 0.55–2.5 mg/L (Drug Information Handbook 2013).

3.3.1.3. Amiodarone binding to plasma proteins

Amiodarone binds extensively to plasma proteins. Lalloz et al. stated that both albumin and lipoproteins are the main binding proteins (Lalloz et al. 1984).

The in vitro estimation of the extent of amiodarone binding to plasma proteins was performed by various researchers who reported it to be <0.1 (Paixao et al. 2010), <0.001 (Austin et al. 2002), or 0.0002 (Veronese et al. 1988). The differences seen in these reported values are attributed to differences in the used methods and experimental conditions; however, all of them indicate a very small fraction of unbound amiodarone concentrations in the systemic circulation.

Moreover, the study conducted by Venerose et al. showed that the free fraction of amiodarone was independent of the total drug concentration, and of the albumin level (Veronese et al. 1988). The latter finding can be explained by the non-specific binding of amiodarone to plasma proteins other than albumin (e.g., lipoproteins).

3.3.2. Used modeling software and model parameterization

All simulations were carried out using Simcyp® simulator (v.12.2 [academic license]; Simcyp Ltd, Sheffield, UK) for adults and pediatrics (Simcyp) that provided the basic model structure and a large database of anatomical and physiological parameters with their age dependencies as required for the pediatric simulations.

A comprehensive literature search was conducted to collect the additionally needed physicochemical properties and other model input data for the description of the substance distribution and clearance (see overview of the modeled drug). **Table 3-1** summarizes the final model input parameters. The used fraction unbound (f_u) was 0.00015, which is in good agreement with the reported value by Venerose et al. (Veronese et al. 1988). The clearance was described over the enzyme kinetics with CL_{int} values of the involved enzymes obtained via the retrograde model by using an in vivo IV clearance of 14 L/h and a percentage contribution of 65%, 25%, 6%, 2%, and 2% for CYP3A4, CYP2C8, CYP1A2, CYP2D6, and CYP2C19, respectively (see ***Retrograde model for amiodarone clearance description*** for more information about the model). The previously mentioned input of the IV in vivo clearance is consistent with the reported values in the literature (Shiga et al. 2011), whereas the assigned percentage contribution for the sub-enzymes was guided by reports of CYP3A4 being the main contributing

enzyme in amiodarone metabolism, followed by CYP2C8, and finally CYP1A2, CYP2D6, and CYP2C19 playing a minor role.

Table 3-1. Input parameters for the basic amiodarone PBPK model

Parameter	Unit	Model input value	Reference value	Reference
Physicochemical properties				
Molecular weight	g/mol	645.31	645.31	PubChem 2157
Molecular type	-	Monoprotic Base	Monoprotic Base	Holt 1983
logP	log unit	7.6	7.6, 7.8	PubChem 2157, Ruell 2004
pKa	-	8.47	-	ADMET predictor
f _u	-	0.00015	0.0002, <0.001	Venerose 1988, Austin 2002
Clearance				
CL _{IV}	L/h	14	13.74, 13.9	Pollak 2000, Shiga 2010
Clearance pathway	-	Hepatic metabolism via CYP enzymes	-	-
Renal elimination	-	None	None	Paixao 2012
CL proportion (via CYP3A4)	%	65	-	-
CL proportion (via CYP 2C8)	%	25	-	-
CL proportion (via CYP1A2)	%	6	-	-
CL proportion (via CYP2D6)	%	2	-	-
CL proportion (via CYP2C19)	%	2	-	-
Distribution				
Used distribution model	-	Rodgers and Rowland	-	-
Blood: plasma concentration ratio	-	0.56	0.73	Holt 1983
Volume of distribution in steady state	L/kg	45.6	45	Shiga 2010

LogP= octanol-water partition coefficient; pK_a= acid dissociation constant; f_u= fraction unbound; CL_{IV, total}= total intravenous clearance.

3.3.3. Specific features of the adopted modeling strategy

The modeling strategy is similar to that reported previously for sotalol, with initial model development and evaluation in adults before scaling to children, and the use of population simulation as the main model results. However, this model restricted itself for the IV drug application, and therefore, no evaluation with oral data was performed. In addition, two unique aspects of the amiodarone model are mentioned in the next two sections.

3.3.3.1. Retrograde model for amiodarone clearance description

The retrograde model is one of the models incorporated in Simcyp®, and allows for the calculation of intrinsic clearance values of the involved metabolizing enzymes from an in vivo measured clearance. In order to do that, the retrograde model utilizes in the first step: 1) an in vivo measured value of the adult IV or oral clearance including fractions of hepatic, renal, or any additional clearance, 2) drug fraction unbound (f_u), 3) B:P ratio, and 4) the liver blood flow to calculate the hepatic intrinsic clearance as given in the equation of the well-stirred liver model:

$$CL_{int} = \frac{Q_H \times CL_H}{f_{u_b} \times (Q_H - CL_H)} \quad \text{Equation (3-1)}$$

In a second step, this hepatic CL_{int} value is divided between the involved hepatic elimination pathways (i.e., the different CYP enzymes) using input information about the percentage contribution of these metabolizing enzymes in the drug clearance.

3.3.3.2. Model adjustment for protein binding

As amiodarone is a drug highly bound in plasma, the age-related changes in the levels of the binding proteins will influence its unbound fraction, and thus, its disposition within the body.

By default in the pediatric simulator in the used modeling software tool, the drug fraction unbound (f_u) is scaled down to children by utilizing: 1) the average concentration of the binding protein in the pediatric age, 2) the average

concentrations of the binding protein in adult, and 3) the model input value of the unbound fraction in adults as described by Johnson et al. (Johnson et al. 2006):

$$f_{u\text{ Pediatric}} = \frac{1}{1 + \frac{(1 - f_{u\text{ Adult}}) \times [P]_{\text{Pediatric}}}{[P]_{\text{Adult}} \times f_{u\text{ Adult}}}} \quad \text{Equation (3-2)}$$

Where [P] is the concentration of the plasma protein in adults or children and $f_{u\text{ Adult}}$ is the unbound fraction of the drug in adults.

However, for a group of patients who have low total protein levels (n= 11), the use of the average values of the binding proteins, instead of the individual ones, may not be appropriate and could lead to a lower predicted fraction unbound than in patients and thus to a lower volume of distribution. Therefore, this predicted pediatric unbound fraction was adjusted by using the measured median values of the total protein levels instead of the normal average pediatric levels. This modification has led to a slightly higher pediatric f_u in this patient collective, and to a slight improvement of the model predictions compared with the standard model results.

3.3.4. Amiodarone pharmacokinetic and clinical data in adults

Data from three different PK studies of IV amiodarone in adults were used for basic amiodarone model development and evaluation (Shiga et al. 2011; Cushing et al. 2009; Pourbaix et al. 1985). All the subjects enrolled in these studies were healthy and received a single IV dose of amiodarone. The original data of one study was provided by the author (Shiga et al. 2011), including individual plasma concentration-time profiles after 3 different IV doses, whereas the mean plasma concentrations of the other two studies (Cushing et al. 2009; Pourbaix et al. 1985) were scanned from the publications figures. **Table 3-2** gives an overview of the populations and the administered dosing in the used adult studies.

3.3.5. Amiodarone pharmacokinetic and clinical data in children

The original PK and anthropometric data of 20 pediatric patients that were reported in a published pediatric observational safety study were kindly provided

by the author (Ramusovic et al. 2013) and were used as part of model evaluation data.

In addition to the previously mentioned pediatric data, amiodarone concentrations were investigated in 7 pediatric patients and are presented here for the first time. The newly investigated patients received amiodarone during their hospitalization in the intensive care unit, mostly due to post-operative supraventricular arrhythmias. The age of these patients ranged from 14 days to 10.68 years, with an average of 2.91 years. The weight and height ranged from 3.97 to 18 kg and from 49 to 115 cm, respectively. The amiodarone treatment consisted of an initial loading IV bolus of 5 mg/kg over 30 minutes, followed by an infusion of 10 mg/kg/day, with potential additional bolus doses of 5 mg/kg if indicated by the clinical condition. As a result, the total given dose of amiodarone differed among the patients and ranged from 235.94 mg to 2012.50 mg.

As a result, data from a total collective of 27 pediatric patients were used for the pediatric model evaluation. The demographics, dosing, and laboratory findings of this cohort are summarized and presented in **Tables 3-3 and 3-4**.

Table 3-2. Summary of the characteristics of the used PK studies for the development of the amiodarone adult model

Reference study	Pourbaix et al., 1984	Cushing et al., 2009	Shiga et al., 2010	Shiga et al., 2010	Shiga et al., 2010
No. of Subjects	12	78	6 †	10 †	10 †
Applied dose [mg or mg/kg]	5 mg/kg	150 mg	1.25 mg/kg	2.5 mg/kg	5 mg/kg
Application type	IV Infusion over 20 min.	IV Infusion over 10 min.	IV Infusion over 15 min.	IV Infusion over 15 min.	IV Infusion over 15 min.
Gender [% male]	75%	~65%	100%	100%	100%
Age [years] mean± SD (range)	23± 2	37.4 ± 11.9 (18–59)	(20–32)*	(20–32)*	(20–32)*
Height [cm] mean± SD (range)	180 ± 8	NR	NR	NR	NR
Weight [kg] mean± SD (range)	73 ± 12	NR	50.9–69.5*	50.9–69.5*	50.9–69.5*
Last measured conc. [h]	72	72	240	336	1848
Analytical method	HPLC-UV	LC/MS/MS	HPLC-UV	HPLC-UV	HPLC-UV
LOQ [ng/mL]	5 ng/mL	NR	NR	NR	NR
LOD [ng/mL]	< 1 ng/mL	10 ng/mL	5 ng/mL	5 ng/mL	5 ng/mL

All these studies were single dose IV studies conducted in healthy individuals.

IV= Intravenous; NR=not reported; LOQ= Limit of quantification of the used analytical method; LOD= Limit of detection of the used analytical method.

† Japanese population.

* The reported range for age and weight is for the entire study population.

Table 3-3. Demographics and dosing information of the entire pediatric cohort used for the amiodarone model evaluation

Patient Code	Age in [years]	Gender	Weight	BSA (m ²)	BMI [kg/m ²]	Given dose [mg]	Number of given boluses
1	5.62	♂	16	0.683	14.51	235.00	1
2	0.49	♂	4.44	0.277	11.55	66.56	1
3	0.33	♀	4.7	0.280	13.06	74.48	1
4	0.21	♂	4.3	0.259	13.71	216.42	4
5	15.03	♂	22	0.989	8.59	575.69	3
6	0.04	♂	4	0.243	14.24	297.71	1
7	0.40	♂	6.1	0.329	14.89	245.83	3
8	0.11	♀	4.7	0.268	15.54	88.06	3
9	0.28	♀	3.75	0.242	11.96	62.50	2
10	0.02	♀	2.77	0.194	11.54	144.62	3
11	0.08	♂	3.88	0.248	11.94	382.78	3
12	0.24	♀	4	0.240	14.79	394.94	4
13	2.08	♂	12.6	0.574	14.26	201.25	1
14	0.05	♀	2.77	0.196	11.08	280.00	3
15	0.34	♂	6	0.329	14.20	371.25	2
16	0.04	♂	4.43	0.265	13.63	162.63	1
17	0.02	♀	2.5	0.173	13.52	159.72	3
18	0.02	♀	3.89	0.235	14.96	203.13	1
19	3.74	♂	18	0.728	16.02	975.00	2
20	0.17	♂	3.44	0.225	12.25	138.77	1
21	0.04	♂	3.97	0.242	14.13	373.06	3
22	0.66	♀	6	0.329	14.20	357.19	2
23	10.68	♂	18	0.758	13.61	2102.50	3
24	4.97	♀	17	0.714	14.57	377.19	1
25	0.04	♂	2.66	0.190	11.08	235.94	4
26	0.80	♂	9.8	0.437	20.00	399.31	1
27	3.19	♀	17.2	0.705	15.90	915.52	2

♀: female; ♂: male

BMI= Body-Mass Index; BSA= Body surface area.

Table 3-4. Laboratory findings of the entire pediatric cohort used for the amiodarone model evaluation

Patient Code	BSA	CREAT (mg/dL)	Protein (g/dL)	Albumin (g/dL)	AST (U/L)	ALT (U/L)	γ -GT (U/L)	CRP (mg/L)
1	0.68	0.37	6.40	3.95	41	16.5	38	4.6
2	0.28	0.44	6.24	2.92	35	16	50	19.4
3	0.28	0.29	4.97	3.13	17	10.5	38	91.7
4	0.26	0.64	4.70	2.81	185.5	34.5	17.5	15.3
5	0.99	0.10	6.00	2.90	93.5	24.5	55	56
6	0.24	1.59	5.32	3.57	41	24	24	19.1
7	0.33	0.29	4.92	3.32	73	39	16.5	39.9
8	0.27	0.89	5.20	3.30	126	70	34	75.3
9	0.24	0.31	5.63	3.58	419	51	39	29.85
10	0.19	0.56	4.68	2.98	16	11	22	17.1
11	0.25	0.34	4.60	2.95	40	25	53	15.7
12	0.24	0.37	4.47	2.81	153	53	14	43.6
13	0.57	0.23	5.45	3.65	39	18	8	2.65
14	0.20	0.34	5.29	3.20	23.5	36	39.5	1
15	0.33	0.25	6.30	3.52	32	27	69	2.7
16	0.26	0.34	4.85	2.88	154	28.5	14.5	46.25
17	0.17	0.68	4.30	2.87	36	66	46	24.9
18	0.23	1.66	4.15	2.48	114	26	21	20
19	0.73	0.28	5.50	3.45	23	14	18	22.6
20	0.23	0.56	4.45	3.07	382	80	61	38.5
21	0.24	1.82	6.10	3.63	29	10	21.5	39.55
22	0.33	0.34	5.04	3.38	45	16	9	52.7
23	0.76	0.54	5.64	2.62	92	29	71	29.6
24	0.71	0.73	6.13	3.83	413	43	24	98.8
25	0.19	0.59	3.74	2.41	101	21.5	61	42.25
26	0.44	0.37	5.63	3.20	158	19	21	44.4
27	0.70	0.60	4.76	3.00	204.5	35	15.5	85.35

CREA= serum creatinine levels; AST= Aspartate Aminotransferase; ALT= Alanine transaminase; γ -GT= Gamma glutamyl transpeptidase; CRP= C-reactive protein.

3.3.5.1. Sample collection and amiodarone assay

Serum concentrations of amiodarone and its metabolite, desethylamiodarone (DEA), were measured using a HPLC-UV standard kit (RECIPE Chemicals & Instruments GmbH, München, Germany). The lower limit of quantification (LLOQ) of the assay is 0.1 µg/mL for both analytes, with an intra-assay precision of 2.1% and 2.5% and an inter-assay precision of 4.0 and 4.2% for amiodarone and DEA, respectively. Finally, the accuracy of the assay is 95-105%. The measured plasma concentration-time profiles are presented in **Figure 3-1**.

3.3.6. Evaluation of model performance

Model evaluation was based on simulations. Visual predictive checks were performed with superimposed simulated and observed concentration-time profiles. The area under the concentration-time curve from 0 to last (AUC_{last}) was calculated via the trapezoidal rule for both the observed and simulated data and an observed-to-predicted ratio was then reported. Percentage errors for model predictions of individual concentration points were calculated as the difference between the predicted and observed values. Mean prediction error was then reported as a measure of the model accuracy, whereas mean absolute prediction error was reported as a measure of the model precision. These metrics were discussed in more detail in **Chapter 2**.

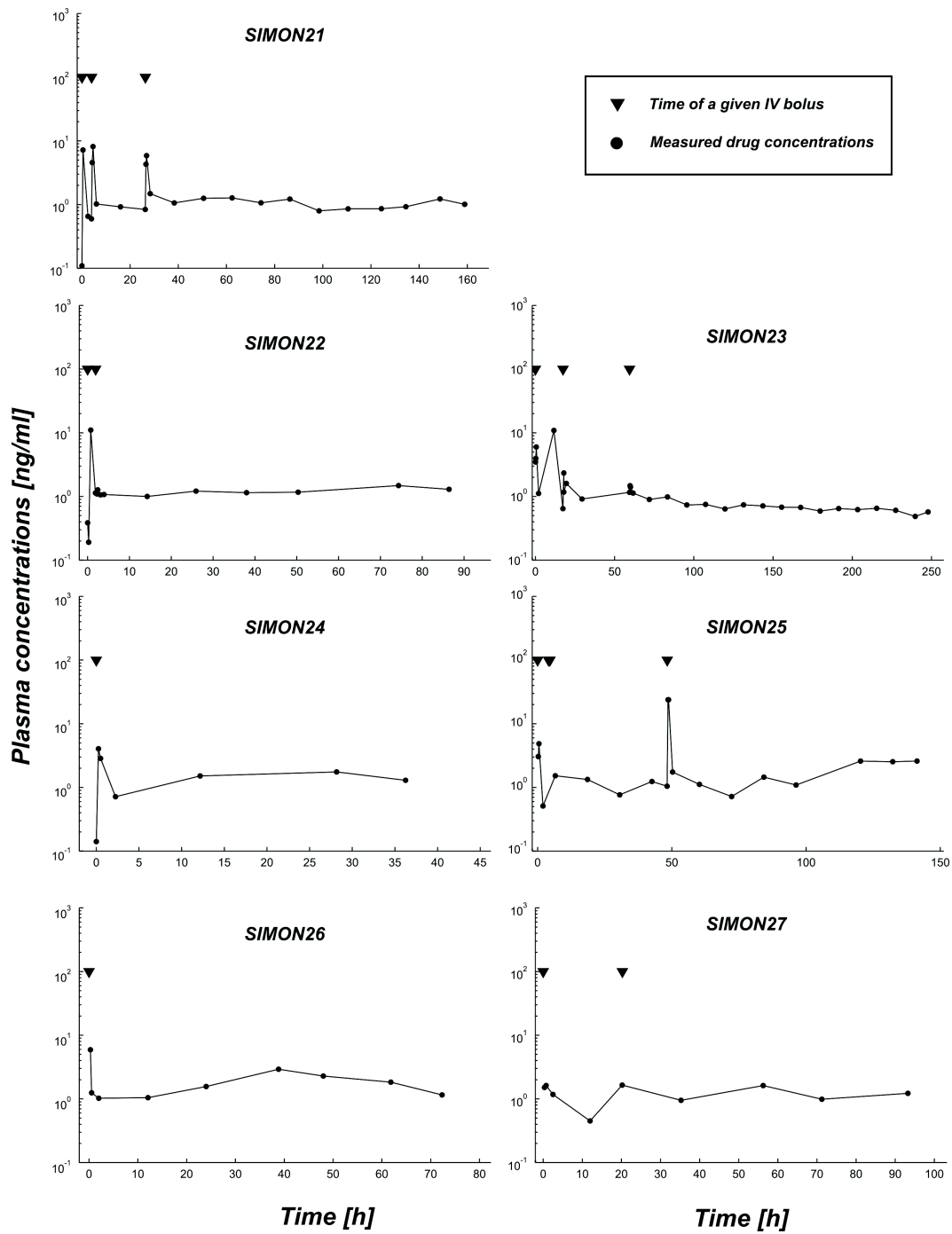


Figure 3-1. The measured plasma concentration-time profiles (dots and lines) of amiodarone in the 7 newly investigated pediatric patients. Triangles represent an administration of an IV bolus.

3.4. Results

3.4.1. Model simulation results in adults

The obtained model results were in very good agreement with the observed data, indicating that the presented model is able to adequately describe amiodarone exposure in adults, thus permitting an age extrapolation to children. The adult model evaluation metrics are contained in **Table 3-5**. A visual predictive check of observed and simulated data for five different amiodarone dosing regimens in 3 published PK studies is shown in **Figure 3-2**. The measured amiodarone profile differed in the length of blood sampling, and amiodarone was measured in one group (Shiga et al. 5 mg/kg) over 1848 h (i.e., 77 days) with mean values only available over the first 1008 hours of observation. The only deviation seen between the model predictions and the observed concentrations was for those measured after 700 hours of the dose application. This was the case only in the previously mentioned group in the Shiga study (Shiga et al. 2010). However, as the observed data clearly show, the measured concentrations were almost equal to the reported lower limit of detection (LOD= 5 ng/mL; concentrations ranged from 6.9 to 11 ng/mL), and were almost constant from over a period from 30 to 77 days. For this reason, the accuracy of these measured concentrations is doubtful and this deviation was judged not to indicate a shortcoming in the present model.

Table 3-5. Model simulation results of IV amiodarone application in adults

Study	Dose	AUC _{0-tlast}			MPE (%)	MAPE (%)
		OBS	PRED	Ratio		
Shiga 2010	1.25 mg/kg	4.429	5.573	0.795	9.543	29.012
Shiga 2010	2.5 mg/kg	9.823	12.102	0.812	7.727	35.551
Shiga 2010	5 mg/kg	26.582	28.759	0.924	-4.669	35.970
Cushing 2009	150 mg	8.114	6.517	1.245	-17.908	20.939
Pourbaix 1984	5 mg/kg	15.240	15.788	0.965	14.185	26.330

AUC_{0-tlast}= Area under the plasma concentration time profile from 0 to the last measured concentration point; OBS=Observed; PRED=Predicted; Ratio=Observed to predicted ratio; MPE= mean percentage error; MAPE= mean absolute percentage error.

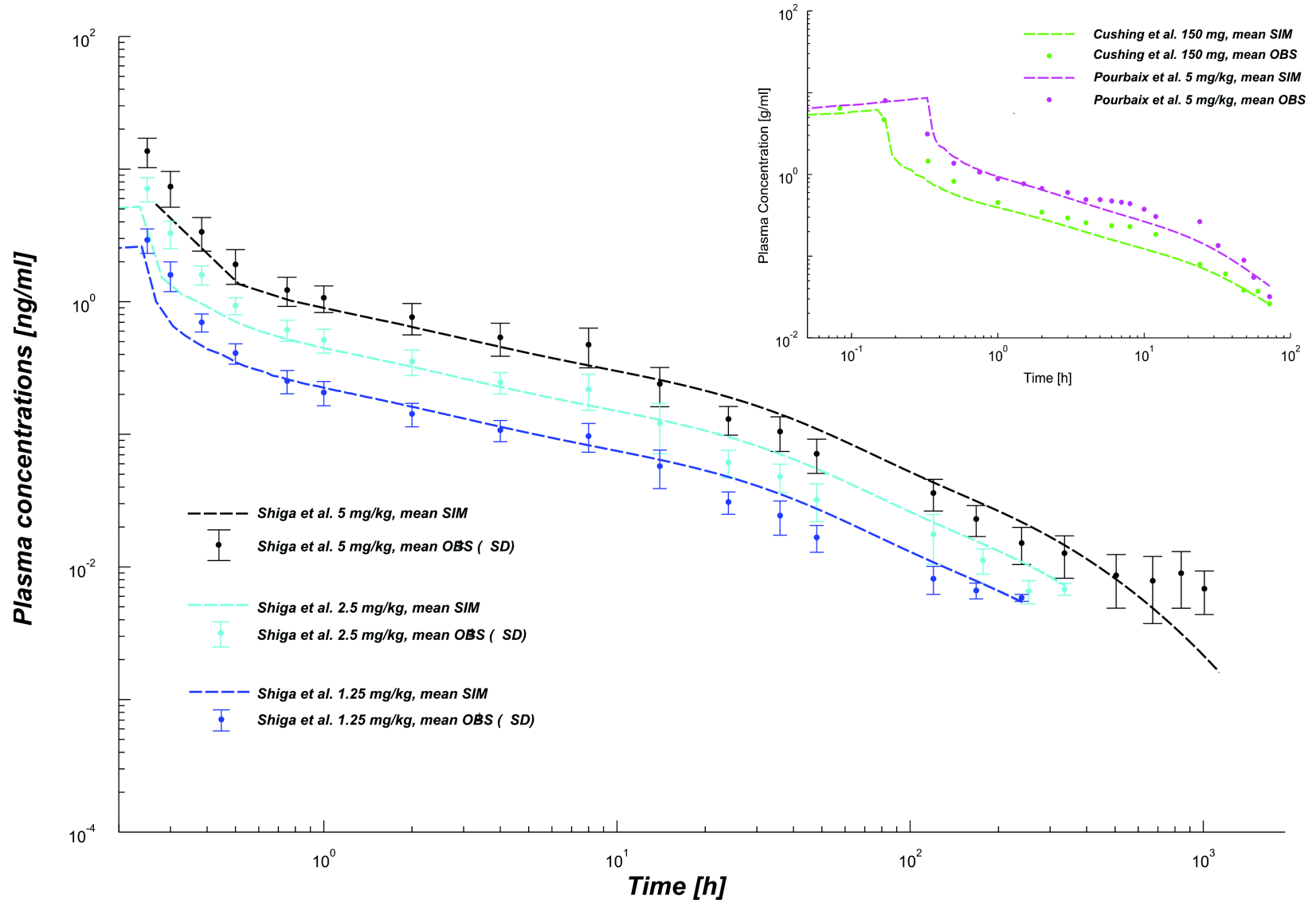


Figure 3-2. The simulated systemic concentrations (dashed line) of intravenously administered amiodarone in comparison to observed (dots) values in adult. Data are presented on a double-logarithmic scale.

3.4.2. Model simulation results in pediatrics

The previously developed and evaluated adult model formed the basis for the amiodarone pediatric model, which was used to predict amiodarone exposure in a total collective of 27 pediatric patients. The pediatric cohort consisted of 9 neonates, 11 infants, 5 preschool-aged children, 1 school-aged child, 1 adolescent, and no toddlers. This skewed distribution of the children between the different age groups made it difficult to compare the accuracy of the model predictions across the pediatric age groups, and was one reason for a different data analysis than that established and presented in the previous chapter.

First, a comparison of model predictions of amiodarone concentrations superimposed with the experimentally measured values is presented in **Figures 3-3 to 3-5** for a visual predictive check. It can be seen that the presented pediatric model is able to reasonably predict amiodarone concentrations in the majority of the patients ($n=22$, 81.48%) despite some shortcomings in hitting the initial concentration points shortly after the given bolus. On the other hand, the model seems to fail in accurately describing the measured amiodarone exposure in 5 patients (ID= 1, 4, 5, 16, and 18; i.e., in 18.5% of the entire collective). The calculated prediction errors for each concentration point that were plotted for each patient and ordered in an ascending rank based on MPE enabled the confirmation of the previous finding regarding the 5 patients, for whom the concentrations were not accurately predicted as seen by a median calculated prediction error exceeding the acceptable 2-fold error range (**Figure 3-6**). In addition, sorting the prediction errors according to age showed that the model's prediction accuracy is mostly independent of the age of the patient as the deviant predictions were distributed across the age spectrum (**Figure 3-6**).

However, for the majority of the deviant data (i.e., in 4 of the 5 patients), there were some suspected reasons. For example, in one patient who suffered from a severe muscular dystrophy and weighed only 22 kg at the age of 15.03 years (0.1 percentile weight for his age), it might be the case that a smaller distribution volume of amiodarone is responsible for the high measured

amiodarone plasma concentrations in this patient, suggesting that incorporating this physiological change may lead to improvement of the model predictions. The PBPK models are mechanistic and data independent, which encourages the use of these models to explore such “what-if” scenarios and investigate the influence of each suspected reason for deviation from the norm on systemic exposure of amiodarone. Therefore, all of these suspected scenarios were incorporated into subsequent simulations and their impact on model predictions was quantified. The suspected reasons as well as the change in model evaluation metrics are both given in **Table 3-6**.

Table 3-6. List of the suspected reasons of the deviations in 4 pediatric patients together with their impact on the calculated model evaluation metrics

Patient ID	Observed deviation	Standard		Suspected reason for this deviation	Scenario	
		AUC ratio	MPE (%)		AUC ratio	MPE (%)
4	Higher observed concentrations	4.271	-61.284	Double dose was given to the patient	2.560	-21.275
4	Higher observed concentrations	4.271	-61.284	existent polymorphism of CYP 2C8	3.468	-54.614
5	Higher observed concentrations	6.991	-70.876	Impact of Duchenne muscular dystrophy	3.616	-27.541
16	Low observed concentrations in maintenance phase	0.392	187.862	IV infusion stopped after 24 h	0.720	55.373
18	Low observed concentrations in maintenance phase	0.351	230.929	Infusion was not started until day 2	0.836	55.296

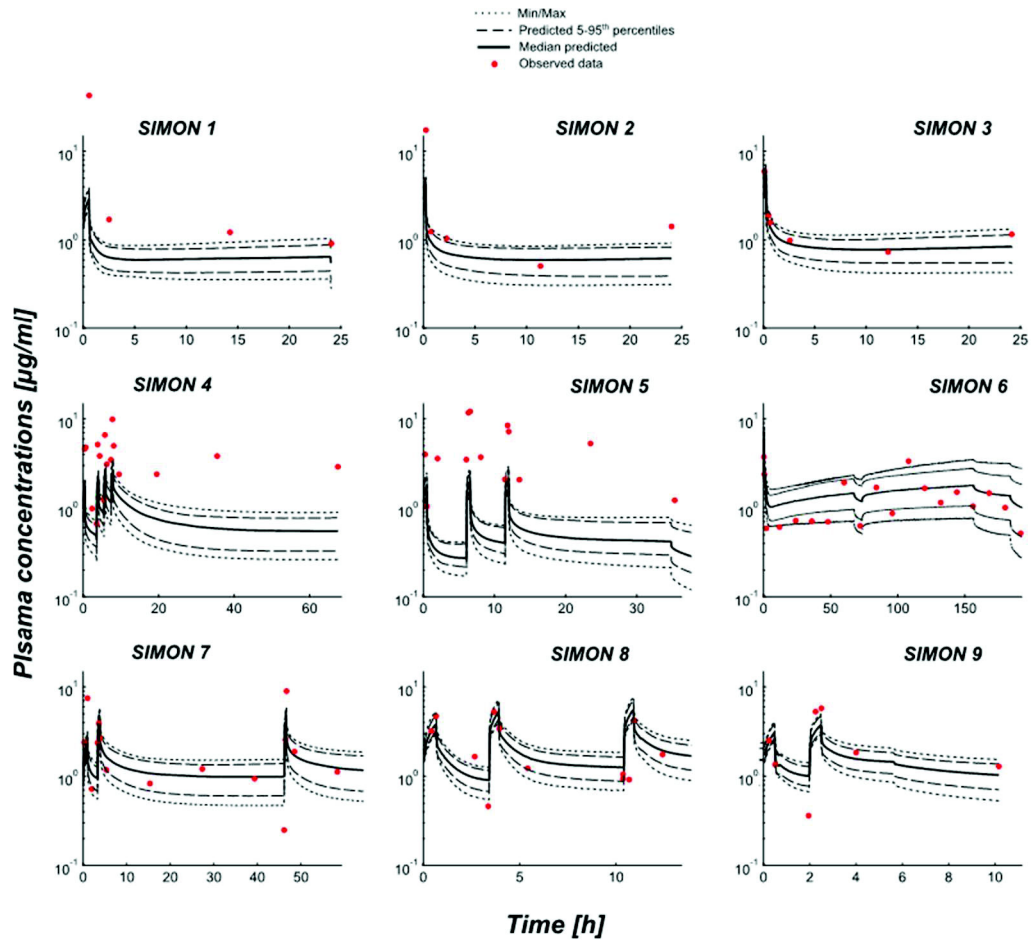


Figure 3-3. Results of simulations using the pediatric amiodarone model (patients 1-9).

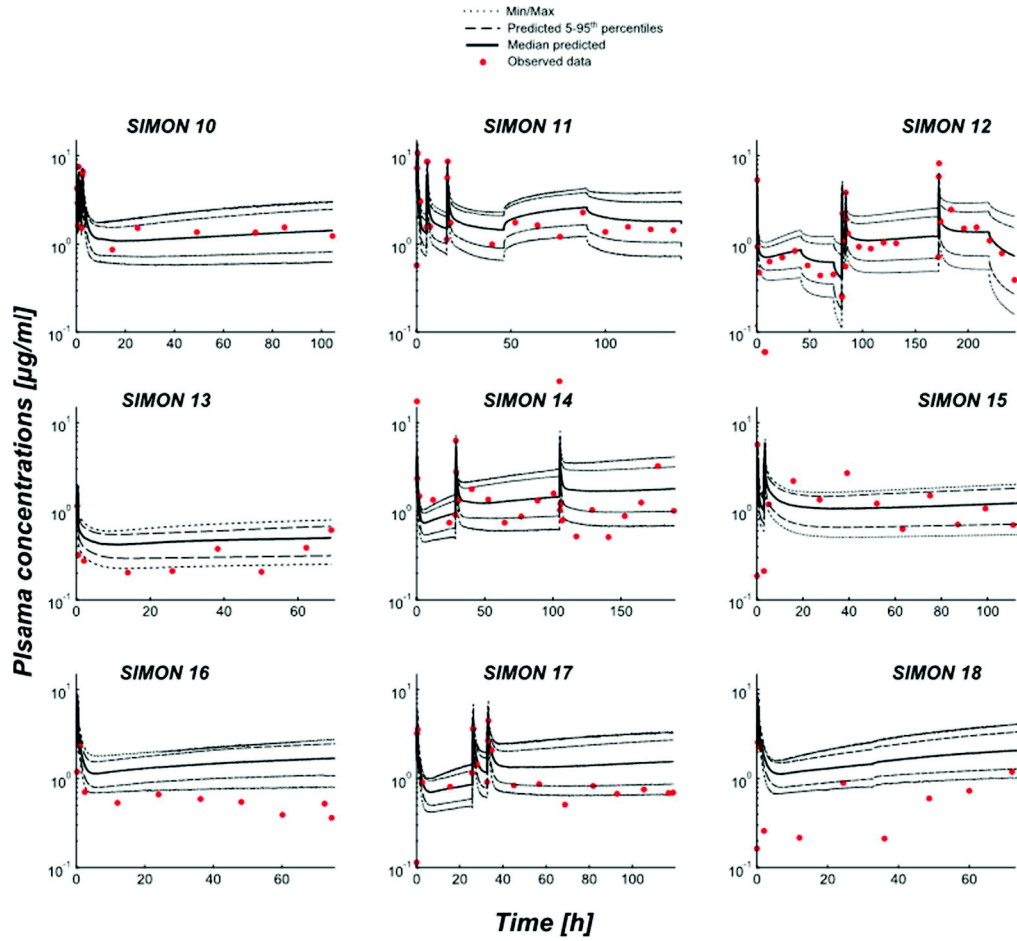


Figure 3-4. Results of simulations using the pediatric amiodarone model (patients 10-16).

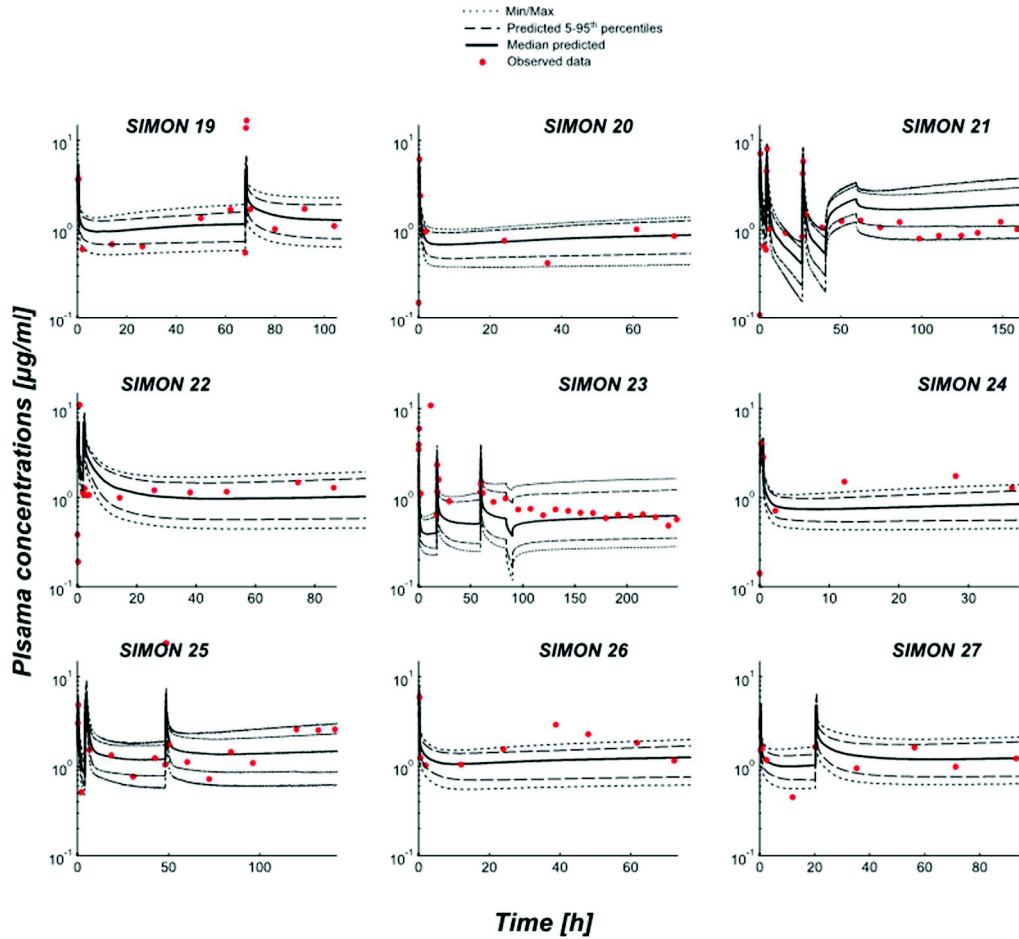


Figure 3-5. Results of simulations using the pediatric amiodarone model (patients 19-27).

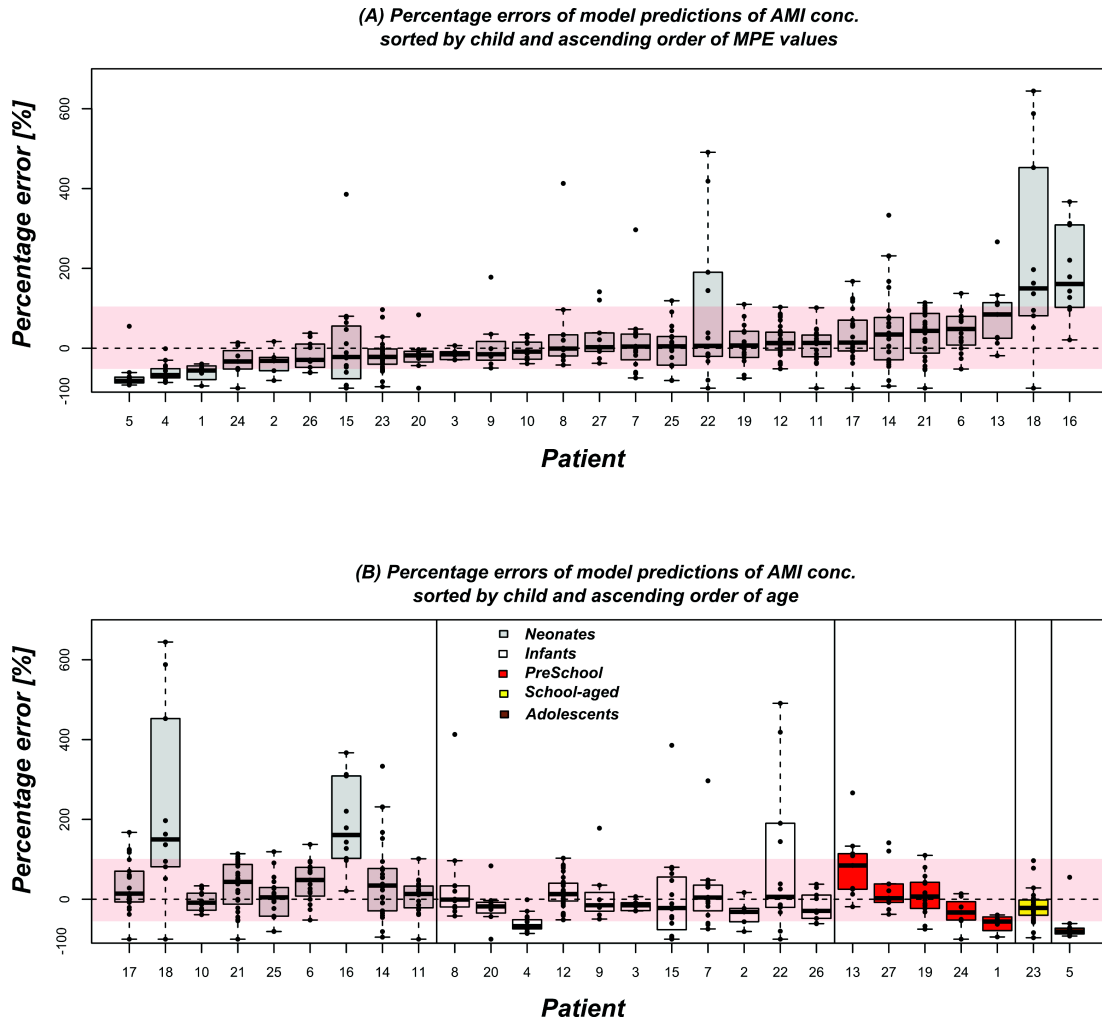


Figure 3-6. Boxplots of percentage errors of model predictions of amiodarone (AMI) concentrations in each individual pediatric patient sorted by: a) ascending value of the mean percentage error (MPE) and b) ascending age with the corresponding age group. The numbers on the x-axis indicate the patient code in the study. The shadowed area indicates the acceptable 2-fold error range between -50 and +100.

The numerical model evaluation of the pediatric model for each individual child is given in **Table 3-7**.

Table 3-7. Model evaluation metrics of pediatric simulation of intravenous amiodarone in 27 children

Child Code	Gender	Age (year)	Age group	AUC _{OBS/PRED}	MRE (%)	MARE (%)
1	♂	5.62	Preschool	4.359	-61.4	61.4
2	♂	0.49	Infant	1.603	-35	41.7
3	♀	0.33	Infant	1.125	-15	17.2
4	♂	0.21	Infant	4.271	-61.3	61.3
5	♂	15.03	Adolescent	6.991	-70.9	79.3
6	♂	0.04	Neonate	0.849	44.8	54.5
7	♂	0.40	Infant	1.078	15.4	51.5
8	♀	0.11	Infant	1.006	40	59.5
9	♀	0.28	Infant	1.260	12.5	48.4
10	♀	0.02	Neonate	1.149	-3	22.2
11	♂	0.08	Neonate	0.812	7.4	33.9
12	♀	0.24	Infant	0.935	51.5	67.1
13	♂	2.08	Preschool	0.607	83.7	87.9
14	♀	0.05	Neonate	1.053	50.6	79.2
15	♂	0.34	Infant	2.866	4.8	78.4
16	♂	0.04	Neonate	0.392	187.9	187.9
17	♀	0.02	Neonate	0.690	35.1	54.4
18	♀	0.02	Neonate	0.351	230.9	250.9
19	♂	3.74	Preschool	1.012	9.7	42
20	♂	0.17	Infant	1.015	-17.1	38
21	♂	0.04	Neonate	0.716	32	58.6
22	♀	0.66	Infant	1.060	239.2	278.9
23	♂	10.68	School-aged	1.837	-18.1	32.6
24	♀	4.97	Preschool	1.706	-33.6	39.7
25	♂	0.04	Neonate	1.150	4.4	41.1
26	♂	0.80	Infant	1.524	-17	34.5
27	♀	3.19	Preschool	0.991	27.9	44.3

AUC_{OBS/PRED}= Ratio of observed to predicted area under the concentration-time profile from 0 to the last measured concentration; MPE= mean percentage error as a metric for model accuracy; MAPE= mean absolute percentage error as a metric for model precision.

3.4.3. Results of the pediatric model modified for low protein levels

In the used pediatric collective, only 11 children had total protein levels that were not within the normal reference range (as reported by the laboratory) and where the low protein levels persisted for more than one day (see **Table 3-4**). Low protein levels could lead to an increase in the drug unbound fraction and thus an increase in its volume of distribution and elimination from the body, which is observed as a decrease in amiodarone plasma concentrations. The model was therefore adjusted for this factor. **Figure 3-7** shows a comparison between the calculated prediction errors between the results of the standard model (without adjustment for low/high total protein levels) and the final adjusted model. Incorporating these individual total protein levels led to a slight improvement in model predictions, and although both the MPE and MAPE of the whole collective remained almost constant, the mean $AUC_{OBS/PRED}$ ratio dropped from 1.67 to 1.57 in the adjusted model.

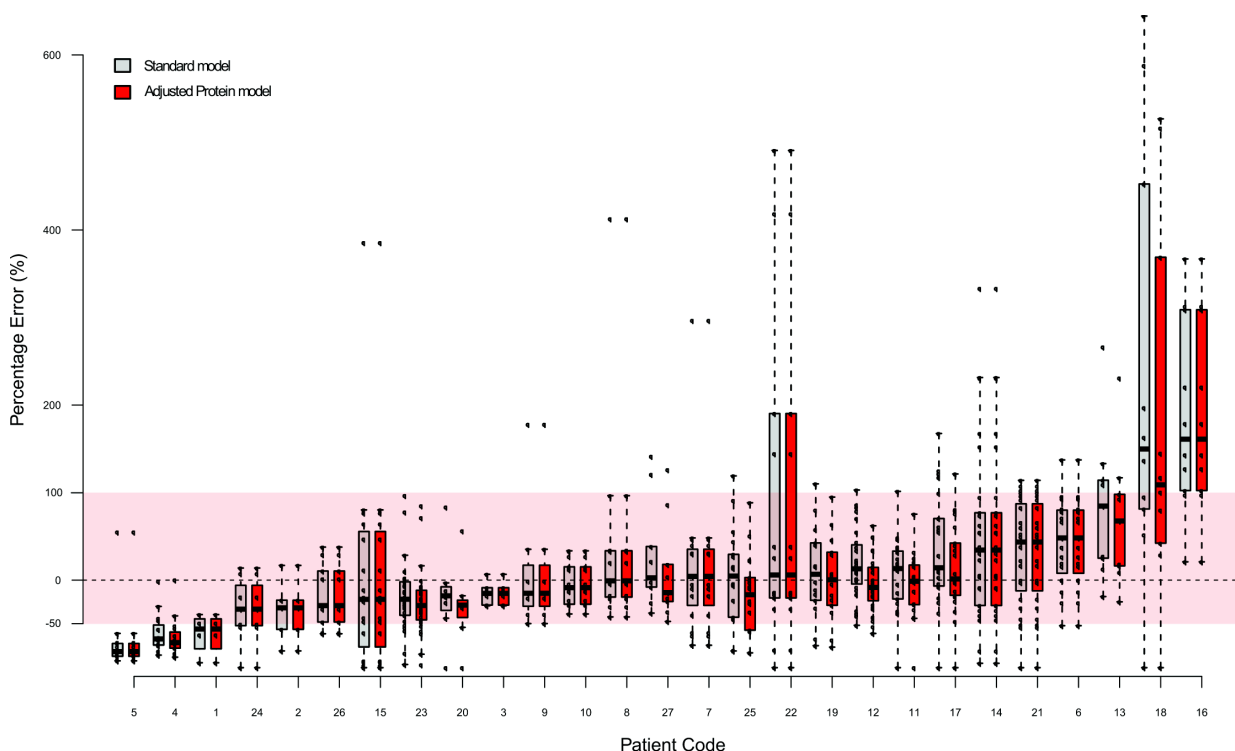


Figure 3-7. Comparison between the standard and the protein-adjusted model of IV amiodarone prediction errors presented as boxplots

3.5. Discussion

A PBPK model for amiodarone that is able to adequately reflect its PK behavior in humans was developed and evaluated with available adult and pediatric PK data. This model will be the tool to explore the age-related PK changes of amiodarone across the entire pediatric developmental continuum, in order to provide additional insights into the pharmacokinetics of a substance for which few pediatric PK data are available, and for which the conduct of pediatric clinical trials is complicated by an unfavorable PK and safety profile.

In adults, the model was shown to adequately predict the measured amiodarone profiles reported in 3 different publications as shown by the visual predictive checks and the comparison of calculated observed and predicted $AUC_{OBS/PRED}$ (**Figure 3-2, Table 3-5**). This is the first reported physiologically based model for amiodarone. The model showed that despite its high binding to plasma proteins, amiodarone possess a large volume of distribution of about 45 L/kg, which is a result of its high lipophilicity and high affinity to bind to tissue proteins and adipose tissues. This adult model formed the basis for an age-extrapolated pediatric model.

After extrapolation to children, the model was shown to adequately predict amiodarone exposure in 81.48% of the pediatric population that received IV doses for the treatment of post-surgical supraventricular and ventricular tachycardia in the intensive care unit. This finding was supported by visual predictive checks of the plasma concentration-time profiles, and the calculated $AUC_{OBS/PRED}$ ratios and the MPE and MAPE values (**Table 3-7**). A comparison between the model predictions across the different age groups was possible, as the available pediatric data was not large enough to cover each pediatric age group with adequate number of children. However, it seems that the accuracy of model predictions is independent of the age of the child (**Figure 3-6**). To put these results in other words, for 4 out of every 5 pediatric patients to be treated, this model is able to a priori and adequately explore the resulting exposure after any given IV dosing regimen within an acceptable error margin of maximal 2-fold error,

regardless of the age of the child. This ability enables the model to support the clinical decision of the treating physician by providing a valuable insight into the expected drug exposure in advance, thus enhancing the efficiency of the drug therapy.

On the other hand, in 5 of the 27 enrolled patients (18.5%), the physiologically based model seemed unable to adequately predict their amiodarone exposure at first glance; however, such results should be judged keeping in mind the nature of this pediatric cohort that have multiple pathophysiological factors that could influence amiodarone fate in the body, as well as the fact that sudden modifications in the administered drug therapy frequently occur, guided by the patients' clinical condition, safety concerns, and the pharmacological response. The latter necessitate an increased accuracy in documenting any changes in drug administration. Nevertheless, there were potential suspected reasons for this observed deviation in 4 of these 5 patients (**Table 3-6**). PBPK models are mechanistic and data independent, which encourages the use of these models to explore such "what-if" scenarios and investigate the influence of each suspected reason on amiodarone systemic exposure.

The impact of the patient's clinical condition on amiodarone disposition was suspected to be large enough to make the initial model predictions inadequate in one child (patient ID= 5). The patient was suffering from Duchenne muscular dystrophy, a progressive neuromuscular disorder characterized by muscle weakness associated with muscle wasting and therefore weighed only 22 kg at the age of 15 years. This abnormally low weight is associated with reduced muscle mass and altered body composition (i.e., water, fat and muscle proportions). These physiological changes were implemented in the model and the simulations were run again to investigate the impact of the reduced muscle mass on amiodarone concentrations in this patient. Incorporating these changes led to improvement in predictions as a result of a lower volume of distribution and an increase in drug plasma concentrations (**Figure 3-8**). However, this seems to only explain a part of the observed deviation.

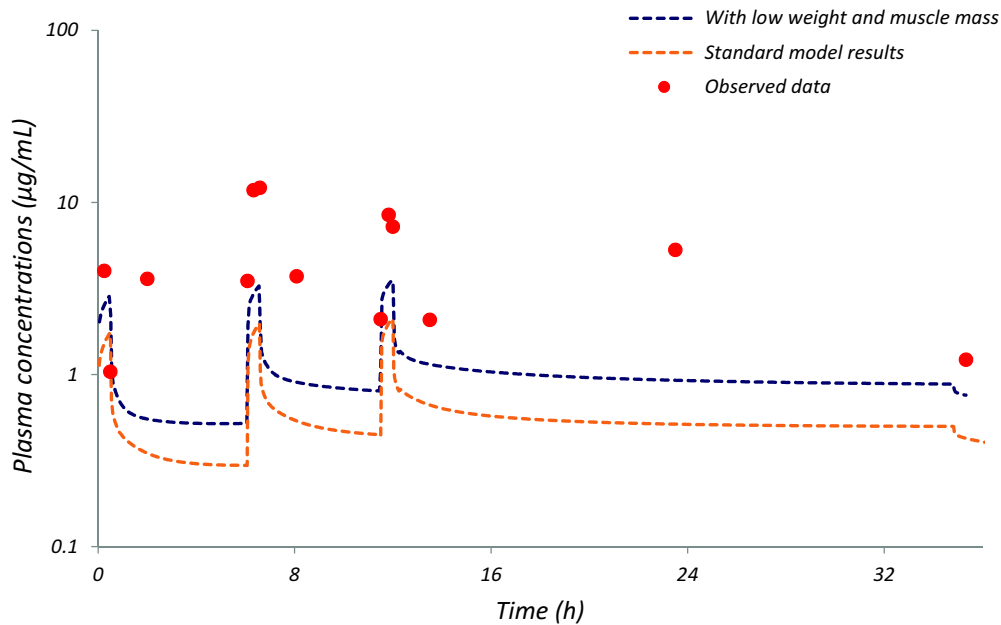


Figure 3-8. The impact of abnormally low body weight and decreased muscle mass on amiodarone systemic concentrations as simulated by the PBPK model.

It is also known that all members of the CYP2C gene subfamily, namely CYP2C8, CYP2C9, CYP2C18, and CYP2C19 are polymorphic, and that 4 mutations are already known for CYP2C8 with a reported frequency of 30% among Caucasians (Martinez et al. 2005). These mutations are reported to be associated with impaired drug metabolism as seen with paclitaxel or ibuprofen (Martinez et al. 2005). In the present model, 25% of drug clearance was attributed to degradation by CYP2C8. Therefore the low predicted concentrations could be, at least theoretically, attributed to CYP2C8 polymorphisms, although there is no information on the genotype of these patients. As a result, the possible impact of the existence of such mutations on amiodarone disposition in the 2 patients who expressed much higher concentrations than expected (i.e., patients with ID numbers 4 and 5), was investigated with additional virtual simulations. These simulations showed clearly that there is no impact of such polymorphisms, even if they existed, on the predicted drug exposure in these 2 patients. This could be explained by the fact that distribution, rather than elimination, is the main driving process for amiodarone disposition during this relatively short duration of drug

level monitoring. These results did not change even if the proportion of amiodarone metabolised by CYP2C8 was further increased to more than 50%. Nevertheless, this may make clear to researchers the importance of considering genetic factors when investigating drugs with unclear or complicated metabolism profiles and alert them to the potential impact of polymorphic enzymes. For instance, they could consider drawing an extra blood/saliva sample to perform genotyping and screen for enzyme polymorphisms from the very beginning.

An undocumented deviation from the study protocol dosing is suspected in 3 of these 5 patients (ID= 4, 16, 18). For most of the patients, the medication administration records of the pediatric ward were checked, when available, against the reported study dosing documentations in order to increase confidence in the dosing information of each child. This check-up revealed some deviations (e.g., infusion rate reduction or infusion stoppage) which were not correctly reported in the standard documentations of the study dosing. However, for some patients (e.g., patients with ID numbers 4, 16, and 18), these medication administration records were not available during the entire duration of amiodarone therapy. Therefore, the accuracy of the study dosing documentation was relied on, with the possibility of undocumented protocol deviations being very real.

In the patient with ID number 4, the suspicion was that a double bolus dose (i.e., 10 mg/kg instead of the planned 5 mg/kg bodyweight) could have been administered to the patient, as the observed plasma concentrations were much higher than the simulated ones. In contrast, in patients with ID numbers 16 and 18, the suspicion was that amiodarone infusion could have been stopped completely or temporarily during the drug therapy, as indicated by the changes in the observed heart rate profile as well as the shape of the measured concentration-time profile. The new simulations, which incorporate the suspected dosing changes, showed a significant improvement in the description of the measured concentrations, the $AUC_{OBS/PRED}$ ratios and the calculated MPE (**Table 3-6**). These assumptions remain hypothetical despite some indications that they may be plausible; however, they highlight the importance of a careful and

accurate documentation of any changes undertaken from the intended study protocol in order to avoid misinterpretations of the effects of these deviations. Therefore, proper training and education of the medical staff responsible for the administration, sampling, and documentation of the study drug therapy and any unplanned changes should not be ignored and should be an integral part of any future clinical trials in order to maximize their accuracy and benefit.

The present model incorporates age-related changes in the levels of binding proteins and the consequent age-related changes in the fraction unbound (f_u), a main driving parameter for the drug distribution in the body. However, this does not reflect abnormal protein levels for the different age groups. In the pediatric cohort that was used to evaluate the model, 11 patients had total protein levels that were, in median, abnormally low for their age during the duration of amiodarone treatment. The model was therefore further adjusted in order to reflect the low protein levels in these individual patients. Modifying the model to individual protein levels in these patients did not seem to have a major impact on the results (**Figure 3-7**). However, the model predictions were slightly improved, as seen by the model evaluation parameters (the mean $AUC_{OBS/PRED}$ ratio dropped from 1.67 to 1.57). The absence of a large impact of modification of the model is mostly explained by the fact that the decrease in total protein levels in these patients in the collective was marginal (on average 9.5% less than the lower normal level), with all but 1 patient having levels within 15% of normal.

In this study, a pediatric PBPK model of amiodarone was developed and validated with pediatric data. The model can now be used to construct as many PK pediatric virtual studies as desired in order to report detailed information about the age-related changes of amiodarone distribution and elimination in children. Moreover, the present model could potentially be extended for oral drug application, and could be used to form the basis for a subsequent coupled PBPK/PD model of amiodarone and/or a coupled PBPK model of substrate-metabolite.

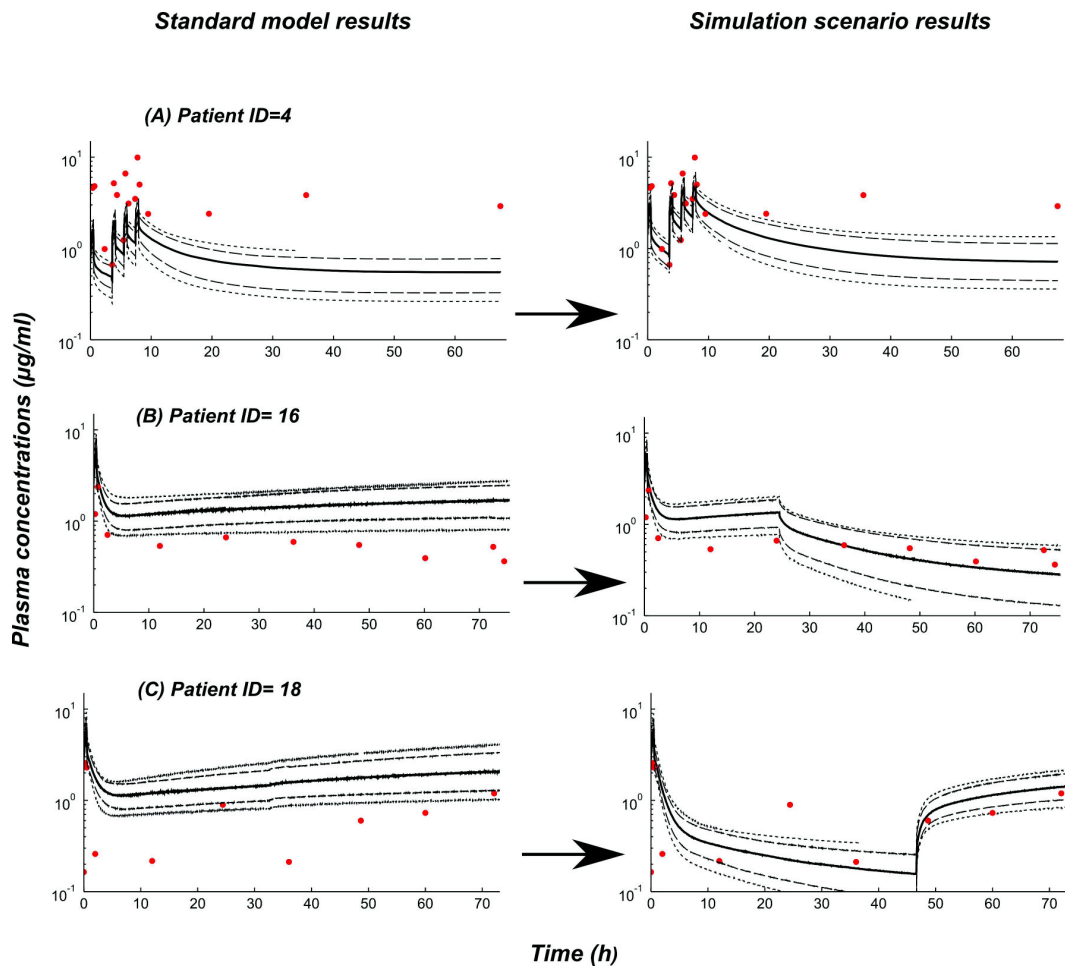


Figure 3-9. A comparison between simulated (dashed line) and observed (dots and line) concentrations of IV amiodarone in 3 pediatric patients, and the impact of suspected undocumented protocol deviations on model results. The left panel depicts simulation results of the patients following the default study dosing protocol for each patient. The right panel depicts the simulation results if the suspected protocol deviation scenario is applied: A) Patient with a suspicion of having received double the dose; B) Patient with a suspicion of infusion stoppage after 24 hours; and C) Patient with a suspected start delay. The simulation results are shown on a semilogarithmic scale.

3.6. Conclusions

Development of a PBPK model for amiodarone, a very effective drug in the treatment of cardiac dysrhythmia, was described in this chapter. The importance of such a model lies in its ability to take advantage of the few available PK data of amiodarone, a substance that possesses an unfavorable PK and safety profile that complicates the conduct of pediatric clinical trials, to further explore its age-related PK changes. The developed model was able to adequately describe amiodarone systemic exposure in adults and in 4 out of 5 pediatric patients irrespective of their age, which is a success keeping in mind the nature of this pediatric cohort that has multiple pathophysiological factors that could influence amiodarone fate in the body and in view of the fact that sudden modifications in the administered drug therapy frequently occur based on the patients' clinical condition, safety concerns, and the pharmacological response, with the resulting likelihood of undocumented dosing changes. The "what-if" scenarios modeled in this study investigated the impact of plausible reasons for prediction deviations in 5 patients for whom the model was unable to adequately predict amiodarone concentrations. These included undocumented changes in amiodarone dosing, CYP2C8 polymorphism, and reduced muscle mass due to Duchenne muscular dystrophy. The impact of possible CYP2C8 polymorphism, for instance, was seen to be negligible. Moreover, some valuable learning experiences were presented by the findings of this study. For example, undocumented violation of the study protocol is an important aspect to consider during conduct of such studies. It is therefore advisable to minimize the likelihood of violation of study protocols in advance by training and educating the nursing and medical staff involved in drug administration, dosing documentation, and sample collection in future trials. Moreover, it is also suggested, when performing PK trials for drugs that are extensively metabolized, that an extra sample (e.g., blood or saliva) be withdrawn for genotyping, as polymorphisms in the metabolizing enzyme could influence the drug disposition.

Chapter 4:

Ivabradine dose selection in “first-in-children” trials: an application of a pediatric PBPK model to support the clinical drug development process

4.1. Introduction

Ivabradine is a pure heart rate-lowering agent that acts by inhibiting I_f , an important ionic current involved in the pacemaker activity in the cells of the sinoatrial node and in the physiological regulation of heart rate (Tardif et al. 2009). Ivabradine does not show negative inotropic activity or depress intracardiac conduction (Camm and Lau 2003) and has only minor effects on blood pressure, which makes it a promising therapeutic option in the pharmacotherapy of cardiovascular diseases. Ivabradine has been recommended for the medical management of patients with stable angina pectoris who are intolerant of beta-blockers, or in whom these agents are contraindicated (Smith, JR et al. 2006). Another indication for ivabradine is in the pharmacotherapy of heart failure (HF). A recent randomized controlled clinical trial showed that heart rate reduction with ivabradine can be important for improving clinical outcomes in HF, and that it is associated with a pronounced reduction in the risk of repeated hospitalizations for worsening heart failure (Borer et al. 2012). Although pediatric patients may also benefit from such a drug, for example, in the treatment of supraventricular tachycardia (SVT), pediatric clinical trials must be first performed in order to license ivabradine for this indication.

The technique of PBPK modeling, with its ability to take into consideration information about the maturation, growth, and age dependence of anatomical and physiological processes, can facilitate extrapolation of information on drug pharmacokinetics from adults to children. In doing so, PBPK modeling can help explore age-related changes in drug pharmacokinetics. Valuable PK information gained through such modeling can then be used to support future pediatric clinical trials and potentially reduce costs and the required number of enrolled children. For example, information about drug exposure generated a priori by such a

modeling exercise can help establish a rational dosing scheme in children of different ages.

4.2. Objective of this project

The aim of this project was to predict hypothetical IV ivabradine exposure from birth to adolescence in order to guide dose selection of future “first-in-children” trials to be performed by the pharmaceutical industry.

4.3. Methods

4.3.1. Adult clinical data

Original data on the demographics, dosing information, and observed PK profiles following IV administration of ivabradine to a patient collective were provided by a pharmaceutical company. The doses given to the patients in this collective ranged from 6.3 to 15.4 mg in total. The most frequently given dose was 10 mg of ivabradine administered as a 5 mg IV bolus followed by a 5 mg IV infusion over 8 hours (i.e., 480 minutes), with 25 patients receiving this dosing regimen. **Table 4-1** shows the general characteristics of this collective. This data set was divided into 2, with one-half being used for model development and internal validation and the other half being kept for later external validation of the developed model.

Table 4-1. General characteristics of the patient collective receiving IV ivabradine (n = 48)

Number of patients who received Ivabradine	n = 48
Age (years)	41–81
Gender	Male and female (39 M, 9 F)
Height (cm)	155–189
Weight (kg)	47–100
Given dose (mg)	6.3–15.4
Application type	Combination of IV bolus and infusion

4.3.2. Model parameterization and characterization

The modeling software used (PK-Sim® version 4.2 [commercial license]; Bayer Technology Services GmbH, Leverkusen, Germany) provides the user with the general structure of a PBPK model as well as its necessary physiological and anatomical parameters (PK-Sim; Willmann S et al. 2003). However, in order to complete the parameterization of an ivabradine PBPK model, physicochemical

properties of ivabradine along with other drug-specific information (e.g., clearance and blood:plasma ratio) are needed. Such information was either provided with the original data or was obtained from the literature.

Ivabradine is a weak base with a molecular weight of 468.58 g/mol [PubChem Compound CID = 132999] and a pK_a value of 8.59 (Baruscotti et al. 2005). Ivabradine lipophilicity has been reported as a $\text{Log}P$ value of 2.4 [PubChem Compound CID = 132999] or 2.25 (provided with the original data). There was no significant difference seen with the use of either value during drug development. Ivabradine is approximately 70% plasma protein bound (EMA 2013), which is in good agreement with the fraction unbound (f_u) value of 0.37 provided with the original data and which was used in our model. The partition coefficients in the tissues were calculated using the Rodgers and Rowland distribution model (Rodgers and Rowland 2007; Rodgers et al. 2005). The B:P ratio used was 0.78, which was between the value of 0.693 provided with the original data and the value of 1.08 calculated by PK-Sim[®] based on the physicochemical properties of ivabradine.

Drug clearance can be described using either an in vivo plasma or blood clearance value or in vitro values for K_m and V_{max} of the metabolizing enzymes. Ivabradine is extensively metabolized (80-82.5%) by oxidation through cytochrome P450 3A4, and its renal clearance constitutes about 17.5-20% of the total clearance (EMA 2013; Portoles et al. 2006), which is reported to be 400 mL/min (EMA 2013). Two modeling studies have estimated the total clearance to be 616 mL/min (after a 10 mg IV bolus) and 27.4 L/h (or 457 mL/min) (Duffull et al. 2000; Ragueneau et al. 1998). Therefore, the total clearance value of ivabradine is expected to range between 400-616 mL/min. During the development of our model, the initial value assigned for total clearance was 400 mL/min (EMA 2013). However, a satisfactory visual representation of the mean data (see step 1 of the model development strategy, section 4.3) was reached at a value of 405 mL/min taking into consideration the percentages of hepatic and renal clearances reported in the literature. The final set of input parameters used in our model is summarized in **Table 4-2**.

Table 4-2. Input parameters for the ivabradine PBPK model developed using PK-Sim®

Parameter	Model input	Reference value	Reference
Molecular weight (g/mol)	468.58	468.58	PubChem 132999
LogP_(o/w)	2.40	2.40	Baruscotti 2005
Ionization constant (pK_a)	8.59†	8.59†	Company data
Fraction unbound (f_u)	0.37	0.3–0.37	EMA 2013, Company data
Blood: plasma conc. ratio	0.78	0.68	Company data
CL_{total}	6 mL/min/kg (~420mL/min)	400-616 mL/min	EMA 2013, Duffull et al. 2000, Ragueneau et al. 1998
Percentage of CL_H (%)	80	80–82.5%	EMA 2013, Portoles 2006
Percentage of CL_R (%)	20	17.5–20%	EMA 2013, Portoles 2006
Distribution model	Rodgers	-	-

†As base; CL_H =Hepatic clearance; CL_R = renal clearance

4.3.3. Model development strategy

An adult model of IV ivabradine was first developed and validated before extrapolation to children. The workflow for the development of the model resembles the one presented previously in **Chapter 2**, with the exception that this model was only developed for the IV application.

The first step in the development of the adult model was the choice of the best set of model input parameters. However, for some parameters (e.g., $\text{Log}P$), two or more reference values were available. In this case, and in order to choose a single input value, the mean observed concentration-time profile of members of the patient collective who received 10 mg ivabradine ($n = 25$) was used to choose the reference value that gave the best visual fit.

The developed model with its final set of input parameters—i.e., without changing any of the basic input parameters—was then used to simulate individual plasma concentration profiles using individual data on dosing, age, height, weight, and gender. This was first done for all the patients who received 10 mg total ivabradine ($n = 25$) and then for the remaining patients who received doses other than 10 mg ($n = 23$). The simulated results in both cases were compared with the observed individual data, followed by a graphical and statistical analysis. Because the mean values of the former group in the collective—i.e., those who received 10 mg ivabradine in total—was used in the first step of model development and parameterization, this set of individual data was considered to form the internal validation set. Consequently, data from the latter group—i.e., those who received doses other than 10 mg—had not been previously used in any step of model development and was therefore considered as an external validation set.

4.3.4. Model evaluation

The evaluation of the model was performed using a combination of graphical and statistical analyses, and resembles the one already established and presented in detail in **Chapter 2**. However, we additionally reported 2 metrics on general model predictability: Root Mean Square Error (RMSE) and the Mean Relative Deviation

(MRD). RMSE was calculated as the square root of the average of calculated squared errors, whereas MRD was calculated as follows: $MRD = 10x$, where $x =$ square root of the average of the logarithm of all square errors.

All of the metrics listed above were calculated separately for a) the internal validation set, which includes all the patients who received 10 mg total of ivabradine ($n = 25$), b) the external validation set, which includes all the patients who received doses of ivabradine other than 10 mg ($n = 23$), and c) for all adult patients who received ivabradine ($n = 48$).

The PK parameters were calculated via a non-compartmental analysis. The elimination rate constant (k_e) was calculated as the slope of the logarithm of the last 3 concentrations in the terminal phase. Half-life ($t_{1/2}$) was then calculated as $t_{1/2} = \ln 2/k_e$. The area under the plasma concentration-time curve to the last concentration point (AUC_{last}) was first calculated via the trapezoidal rule and then extrapolated to infinity (AUC_{0-inf}) by adding the terminal area (C_{last}/k_e). Using the total dose (IV bolus plus infusion) as the applied dose, further calculations were performed and reported as clearance ($CL = \text{Dose}/AUC$), and volume of distribution ($V_d = CL/k_e$).

4.3.5. Investigating age-related differences in ivabradine exposure

After establishing and evaluating an adult model that is capable of describing ivabradine pharmacokinetics in adults, the adult clearance was scaled to the pediatric population using the clearance-scaling module that is integrated within PK-Sim[®]. The resulting pediatric clearance—along with other age-specific anatomical and physiological parameters (e.g., tissue volumes and blood flows) already incorporated into the model—enabled us to explore the hypothetical pediatric exposure of IV ivabradine across the entire pediatric age spectrum. This was performed by simulating the administration of a uniform weight-normalized adult dose to a virtual pediatric population comprised of hypothetical patients of different ages. The population simulations for each pediatric age group consisted of 1000 virtual children of the same age and incorporated inter-individual variability ranges for renal and hepatic clearances. The main outputs of these

pediatric simulations are plasma concentration-time profiles. As a result, a range of total drug exposure (AUC_{0-inf}) values (minimum, median, and maximum, as well as the 5th, 25th, 75th, and 95th percentiles) was calculated and then compared with the reference adult values. This enabled us to detect any age-specific differences in systemic exposure of ivabradine. Based on that, a preliminary recommendation for an age-specific dose adaptation was suggested. The simulations were then repeated after incorporation of these dose adaptations.

4.4. Results

4.4.1. Predictability of IV ivabradine pharmacokinetics by the basic adult model

The first simulations of ivabradine basic model for the IV application involved the use of the mean values (age, weight, height, and plasma concentrations) of the internal validation set (i.e., the 25 individuals who received a total of 10 mg ivabradine). In this section, the ability of the basic model to reflect ivabradine fate in the body was examined by comparing the resulted mean values of various PK parameters predicted by the basic adult model to the mean calculated observed values of the real adult population.

As previously mentioned, the PK parameters were calculated via a non-compartmental analysis in which the total dose (IV bolus plus infusion) were used to estimate a value for CL and V_d . The latter calculations may not be completely accurate for a physiological interpretation. However, as these calculations were performed identically for both observed and simulated data, they were deemed to be suitable for a comparison between the two sets. The results of this comparison are shown in **Table 4-3**.

Table 4-3. Comparison between the PK parameters of simulated plasma concentration-time data (by PK-Sim[®]) and mean values of the observed data (n = 25) after the administration of a 10 mg total dose of ivabradine^a

PK Parameter	Mean observed	Mean simulated
AUC _{0-inf} (mg.h/L)	0.473	0.43
k_e (h ⁻¹)	0.164	0.183
$t_{1/2}$ (h)	4.23	3.78
CL _{total} (L/h)	21.14	23.25
CL _{total} (mL/min)	352.33	387.5
V_d (L)	129.22	127.08

^aThe total dose was given as a 5 mg IV bolus followed by an IV infusion of 5 mg over 480 minutes.

4.4.1.1. Simulation results in individual patients (n = 25, internal validation)

Based on the developed IV model, plasma concentration-time profiles of ivabradine were individually simulated for patients who received 10 mg total ivabradine (internal validation set, n = 25) by entering the individual dosing, gender, age, height, and weight for each patient. The resulting simulated plasma concentration-time curve for each individual was compared with the corresponding observed data for that individual (**Figure 4-1**).

As can be seen by visual inspection of these results, the model was able to adequately simulate the individual observed concentrations in a majority of patients in this collective. However, in some patients (e.g., patients 27 and 72), the observed concentration-time course does not correlate with the expected time course after administration of an IV bolus followed by infusion and shows obvious deviation from the results obtained for the rest of the patients. This could indicate errors in analytical determination or a protocol deviation, and might explain the deviation of the model results from the expected predicted values. Examples of deviations are given in **Section 4.4.1.6**.

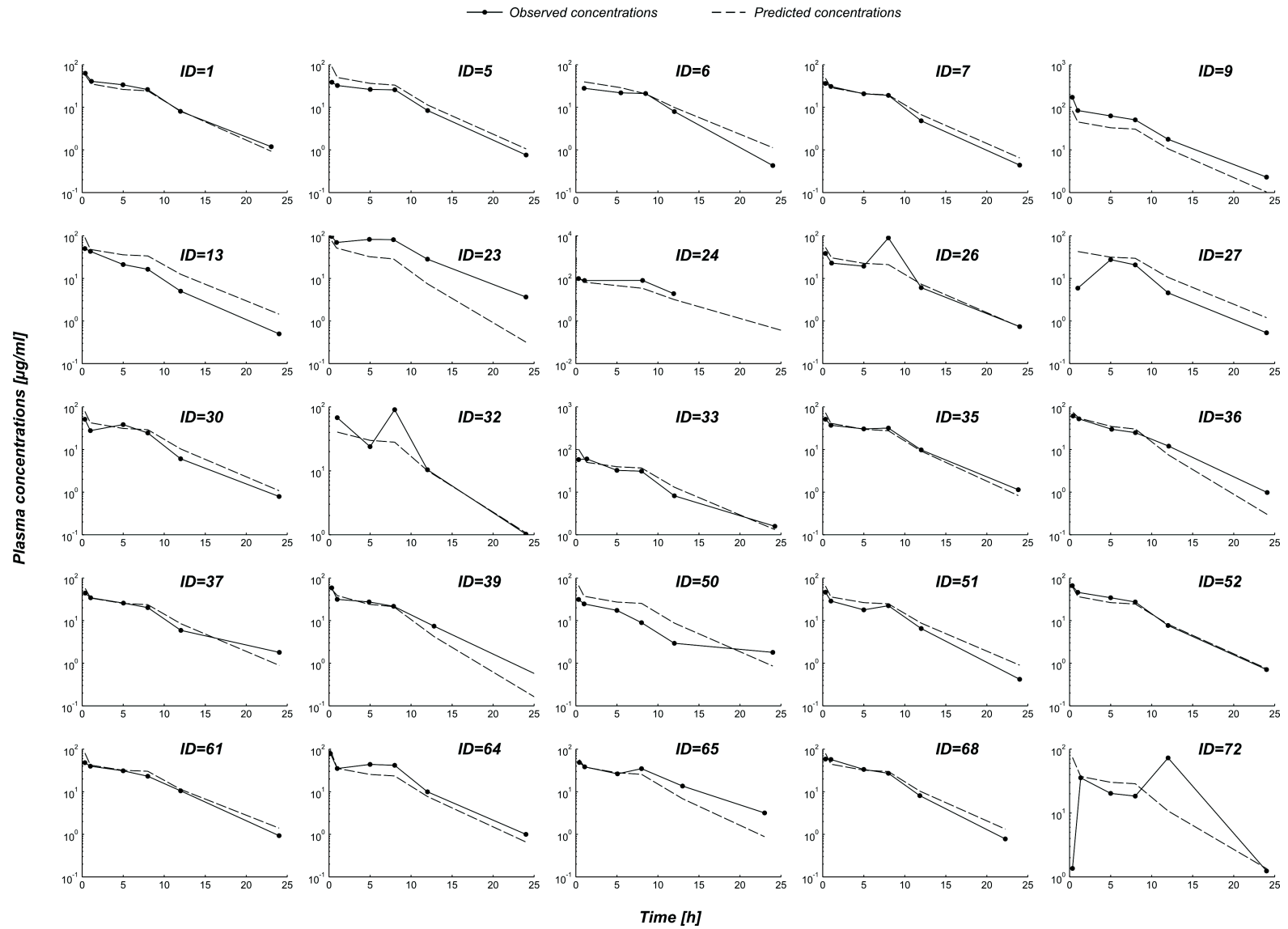


Figure 4-1. Comparison of individual observed (solid line) and predicted (dashed line) plasma concentration-time profiles of ivabradine in adults (internal validation set). Data are shown on a semilogarithmic scale.

4.4.1.2. Simulation results in individual patients (n = 23, external validation)

For the external validation, plasma concentration-time profiles were simulated in all patients who received doses other than 10 mg total ivabradine (n=23) by entering the individual dosing, gender, age, height, and weight for each patient. The resulting simulated plasma concentration-time curve was compared with the observed data for each individual (**Figure 4-2**).

The results show that the predictions by the PBPK model presented here were in good agreement with the individual observed concentrations for the majority of the individual patients in the external validation set despite some deviations seen in patients 29, 34, 46, 47, and 67. Apart from the quality of the model, a few additional factors could potentially be responsible for these deviations. For example, inter-individual variations in both hepatic and renal clearance were not included in these individual predictions since the basic model utilized a unique clearance value that was weight-normalized in mL/min/kg in all of these simulations. Other potential reasons for the observed variations include errors in the analytical determination of the observed concentration, protocol deviations, and unknown factors.

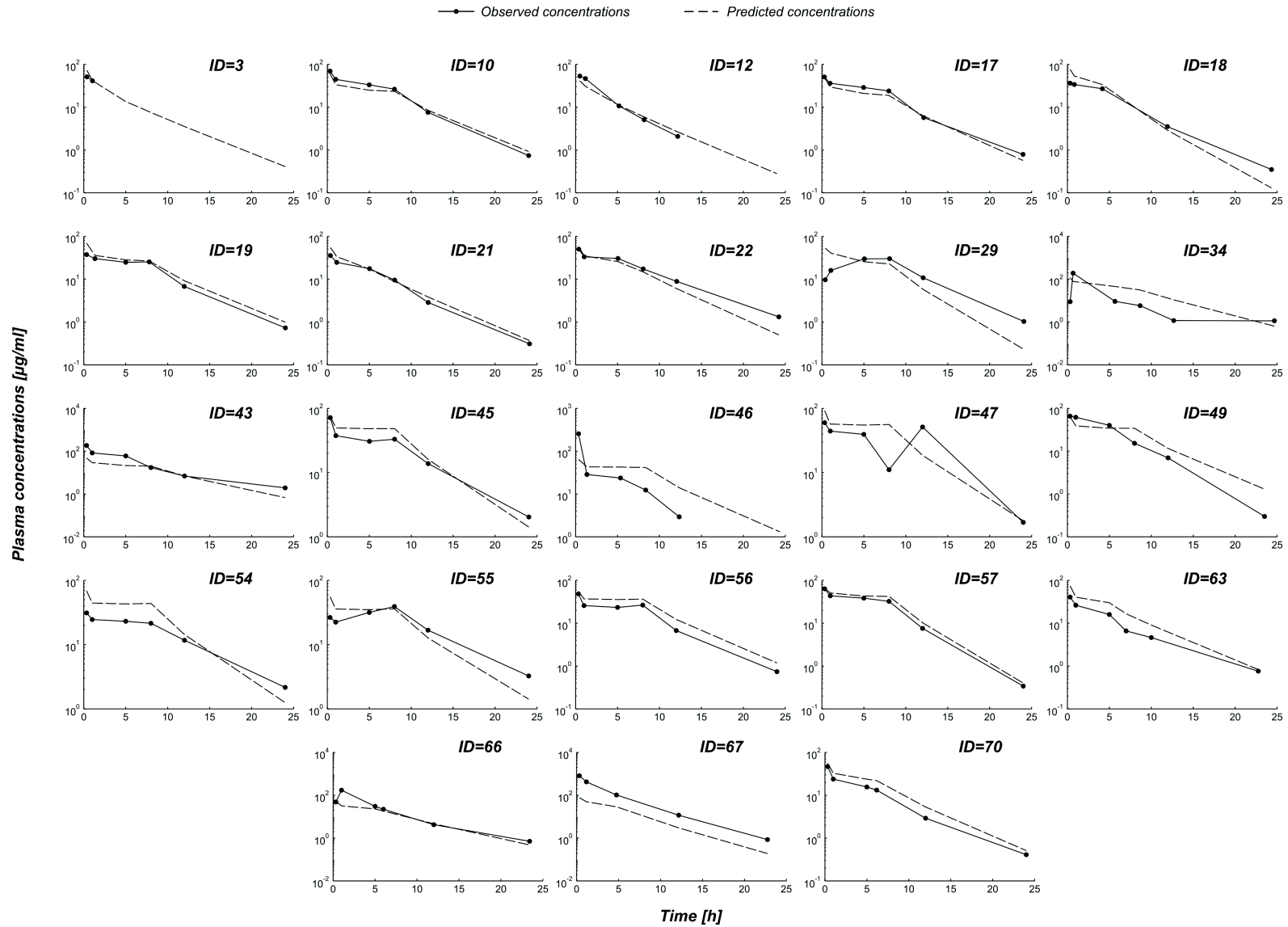


Figure 4-2. Comparison of individual observed (solid line) and predicted (dashed line) plasma concentration-time profiles of ivabradine in adults (internal validation set). Data are shown on a semilogarithmic scale.

Parameters that were individualized and those that form a probable reason for the deviation of simulated data from the observed data are summarized in **Table 4-4**. To investigate the effect of incorporating the inter-individual variability in hepatic and renal clearance into the model, a population simulation in adults in the internal validation group (n = 25)—used because they had received the same dose—was performed and compared with the observed data in the section titled ‘*Population simulation of ivabradine in adults.*’ To investigate the impact of any undocumented protocol deviations, four examples of presumptive protocol violation scenarios are shown in the section titled ‘*Possible protocol violation scenarios.*’

Table 4-4. List of individualized and fixed input value parameters with possible sources of variation/deviation

Parameter	Individualized input value	Fixed input value (weight-normalized)	Possible source of variation
Age	✓		
Gender	✓		
Height	✓		
Weight	✓		
Applied dose	✓		
Dosing/application type	✓		
Hepatic clearance		✓	✓
Renal clearance		✓	✓
Undocumented protocol deviation			✓
Analytical assay			✓
Unknown (others)			✓

4.4.1.3. Results of model graphical analyses

Individual predicted vs observed plots for the plasma concentrations allow us to assess the goodness of fit of our model (**Figure 4-3, panels A1-A3**). The line

of identity indicates an ideal model with perfect prediction of the data. Dashed lines on either side of the line of identity indicate a 2-fold error range. Therefore, the model is ideal when all the points fall either on the line of identity or very close to it.

The ‘residuals vs predicted concentrations’ and ‘residuals vs time’ plots for all data reveal 7 clear outliers out of the total number of points ($n = 275$) for which the calculated residual was >100 ng/mL (**Figure 4-3, panels B1-B3 and C1-C3**). The last 2 outliers of the observed data (concentrations of 814 and 422 ng/mL, respectively) are for the same individual (ID No. 67). We have no clear explanation for the exceptionally high-observed data seen at all time-points for this particular individual. As for the remaining outliers (5 points, each from a different individual), they are concentrations measured within the first 20 or 40 minutes of drug administration (4 points at 20 minutes and 1 point at 40 minutes). The low predicted value vis-à-vis the observed value might be attributable to an undocumented delay in the administration of the bolus dose.

As can be seen from **Figure 4-3**, the majority of the calculated weighted residuals are contained within a range of 0.5 to 2 (dashed lines), which indicates a 2-fold error range in the predictions. However, based on this weighted residual analysis, 7 outliers out of a total of 275 data points (2.5%) with a weighted residual >4 can be detected. These outliers are best seen in the last two figures (**Figure 4-3, panels D1-D3 and E1-E3**). Three out of these 7 outliers belong to the same patient (ID No. 34), while an additional 3 outliers were for concentrations measured during the first hour of drug administration.

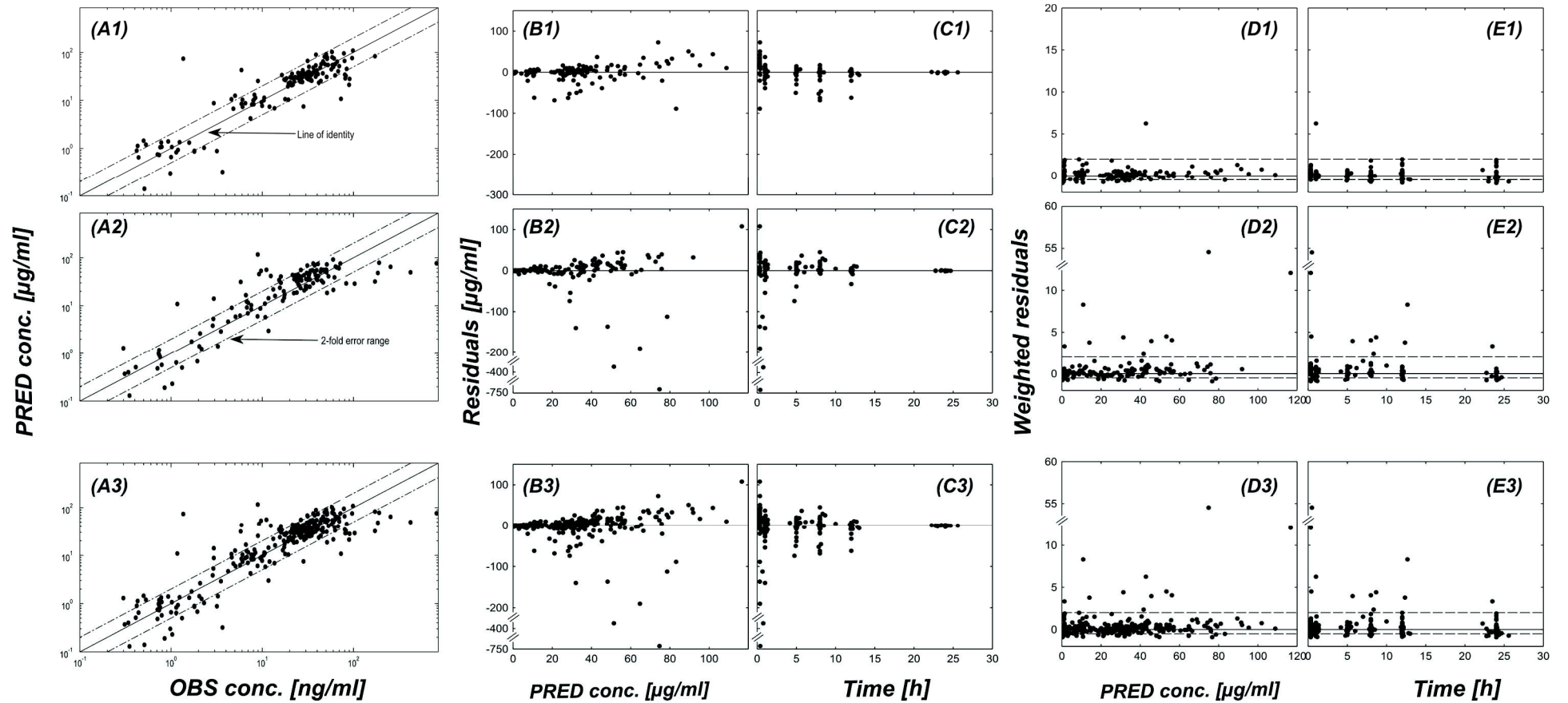


Figure 4-3. Summary of the goodness of fit plots: A) Predicted [PRED] vs Observed [OBS] plots, B) Residuals vs Predicted plots, C) Residuals vs Time plots, D) Weighted Residuals vs Predicted plots, and E) Weighted residuals vs Time plots. The first row presents data for the internal validation set, the second row presents data for the external validation set, and the third row presents all data together.

4.4.1.4. Results of model statistical analyses

The obtained residuals and weighted residuals for every predicted concentration point after the IV ivabradine exposure in the adult patient collective were used as the basis to calculate various metrics for a numerical evaluation of the model accuracy, precision, and general predictive performance of the model. **Table 4-5** presents the results of the statistical analyses of the ivabradine model.

Table 4-5. Ivabradine model evaluation metrics

	Metrics of Accuracy			Metrics of Precision			Additional Metrics	
	ME [ng/mL]	MPE [%]	MDPE [%]	MAE [ng/mL]	MAPE [%]	MDAPE [%]	RMSE	MRD
All data concentration points included in the evaluation								
Internal set	0.08	53.97	8.19	11.15	80.50	32.10	19.58	1.95
External set	-8.04	46.38	14.53	23.72	75.47	35.98	79.17	2.15
All	-3.76	50.38	10.58	17.09	78.12	34.22	56.26	2.04
Excluding outliers (n=13 out of 275 concentration points [4.7 %])								
Internal set	-0.68	12.93	6.63	10.54	39.84	30.78	18.50	1.75
External set	3.47	26.54	14.98	9.77	50.50	32.34	15.64	1.70
All	1.20	19.11	10.53	10.19	44.70	32.17	17.26	1.76

ME = Mean Error, MPE = Mean Percentage Error, MDPE = Median Percentage Error, MAE = Mean Absolute Error, MAPE = Mean Absolute Percentage Error, MDAPE = Median Absolute Percentage Error, RMSE = Root Mean Square Error, MRD = Mean Relative Error. An outlier was defined when either the calculated absolute residual of a concentration prediction is > 100 ng/mL, or the calculated weighted residual of a concentration prediction is > 4 fold.

As can be seen in the table, the model shows on average a slight bias towards an under-prediction of the observed concentrations (as indicated by a

mean error [ME] of -3.76 ng/mL) and tends to predict every concentration with an average error of 50% (as indicated by a mean percentage error [MPE] of 50.38%) if all the data points are included in the statistical analysis. However, the median values of percentage and absolute percentage errors could be better predictors for model accuracy and precision than the mean values, as some obvious outliers do exist (also detected by the graphical residual analysis) and can greatly influence the previously reported average values. The median percentage error (MDPE) for the complete data set is 10.58% and the median absolute percentage error (MDAPE) is 35.98%, both of which indicate good accuracy and precision for a predictive model. Nevertheless, and in order to further investigate the effect of these outliers on the numerical metrics set, the statistical analysis was repeated after exclusion of these outliers ($n=13$, 4.7%). Results of this repeat analysis are reported in the same table.

4.4.1.5. Population simulation of ivabradine in adults

As was earlier discussed in **Section 4.4.1.2**, inter-individual variability was not incorporated into the previously reported individual predictions. A population simulation for patients who received 10 mg ivabradine ($n = 25$) was therefore performed. The population module (“PK-Pop”) is an extension of the PBPK software, PK-Sim®. Its goal is to describe the PK behavior of a chemical substance in a physiologically diverse set of individuals. Information about the dependence of the physiological parameters relevant for PK-Sim® (e.g., organ weights, blood flow rates, and tissue composition) on age, gender, body weight, and body mass index have been collected through a comprehensive literature search and are included in the population parameters database of the software (PK-Sim). Population simulations in adults facilitate the inclusion of inter-individual variations in many physiological parameters including hepatic and renal clearance into modeling studies. For this reason, a virtual group of patients ($n=1000$) with the same characteristics as the real patients who received a 10 mg ivabradine dose ($n = 25$) was created, and a 30% inter-individual variation in the clearance (inserted into the model as 1.3 log-normal deviations around the mean) was assigned. The results of the population simulation were then compared with the observed data

to see if the model is capable of accurately describing the PK behavior of IV ivabradine following incorporation of inter-individual variations in physiological parameters. Characteristics of both the virtually simulated and real populations are summarized in **Table 4-6**. The results of the simulation are depicted in **Figure 4-4**.

Table 4-6. Characteristics of the virtual population created via PK-Sim® (n = 1000) and the real population (n = 25) from which the observed data were obtained

Parameter	Simulated Population	Observed Population
Number of individuals	1000 virtual individuals	25 real individuals
Race	European	---
Gender	Male (84%), female (16%)	Male (84%), female (16%)
Age (years)	41-80 ^a	41-81
Height (cm)	155-185	155-185
Weight (kg)	52-100	52-100
Dose (mg)	5 mg IV bolus followed by 5 mg IV infusion over 8 hours	5 mg IV bolus followed by 5 mg IV infusion over 8 hours

An inter-individual variation (log-normal distribution, 1.3 deviations around the mean) was assigned for both renal and hepatic clearance in this virtual population.

^a80 years is the upper limit for age input in PK-Sim®.

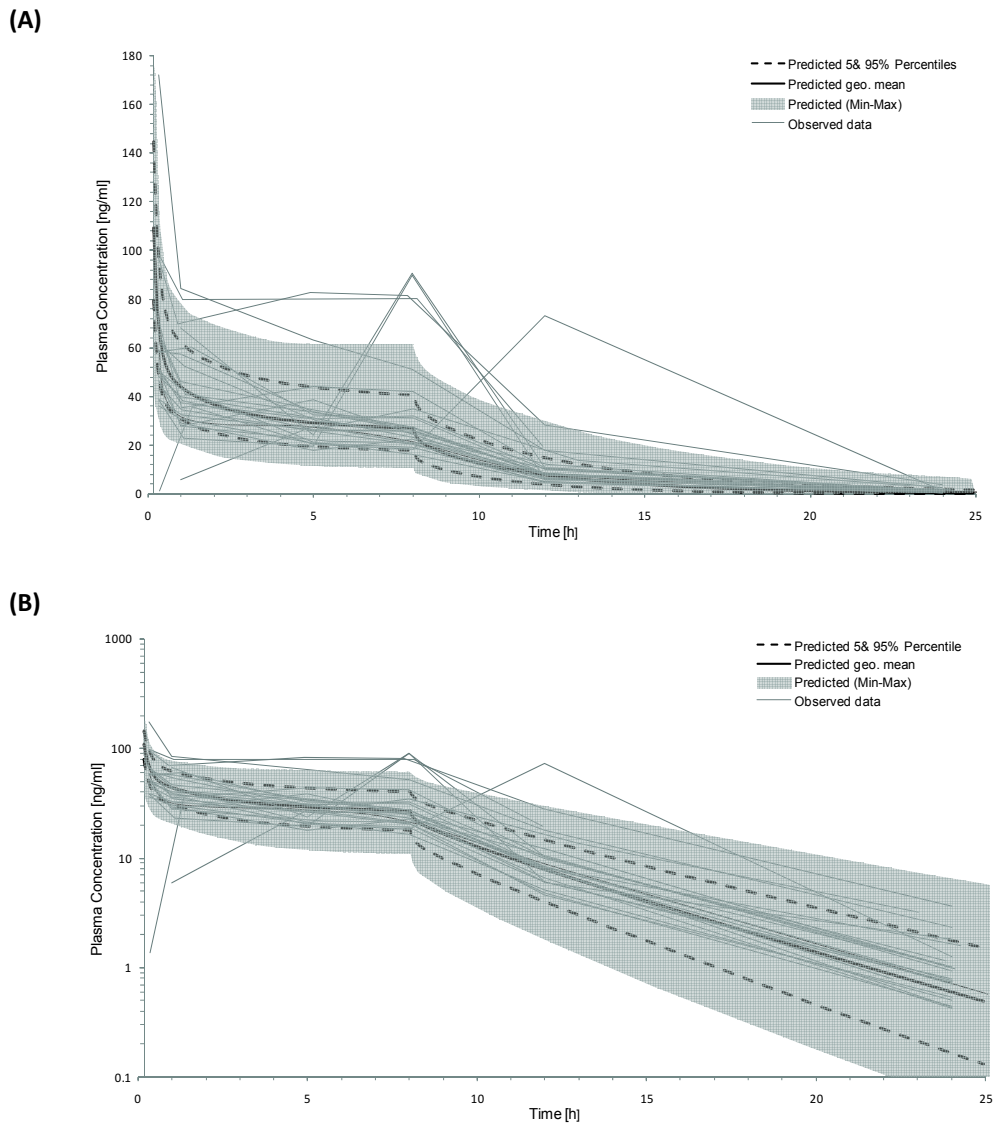


Figure 4-4. Comparison of simulated population (geometric mean [thick solid line], Min/Max [shaded area] and 5-95% Percentile [dashed lines]) and experimentally obtained (thin solid lines, individual data) plasma concentration-time profiles of ivabradine after administration of 5 mg IV bolus followed by 5 mg IV infusion over 8 hours. (A) linear concentration scale and (B) logarithmic concentration scale.

4.4.1.6. Possible protocol violation scenarios

Despite the ability of the model to make good predictions for a majority of the patients, there were still some deviations from the observed data. These deviations could be, in part, due to potential errors in the analytical determination assay of drug concentrations, or result from undocumented deviations from the study protocol (e.g., study dosing). The latter assumption is supported by the fact that in some patients (n=4), the shape of the observed plasma concentration-time course curve of ivabradine either did not correspond to the distinct shape resulting after the administration of a combined IV bolus and infusion regimen, or differed clearly from the rest of the observed data set. In silico simulations performed using the developed PBPK model can investigate the potential effect of such factors. In **Figure 4-5**, we present possible protocol violation scenarios of 4 different patients in whom we suspect different dosing conditions from those documented in the study protocol. These examples demonstrate the utility of a PBPK model in highlighting and simulating the effect of factors that could account for discrepancies between the drug exposure predicted by in silico simulations and the actually observed exposures.

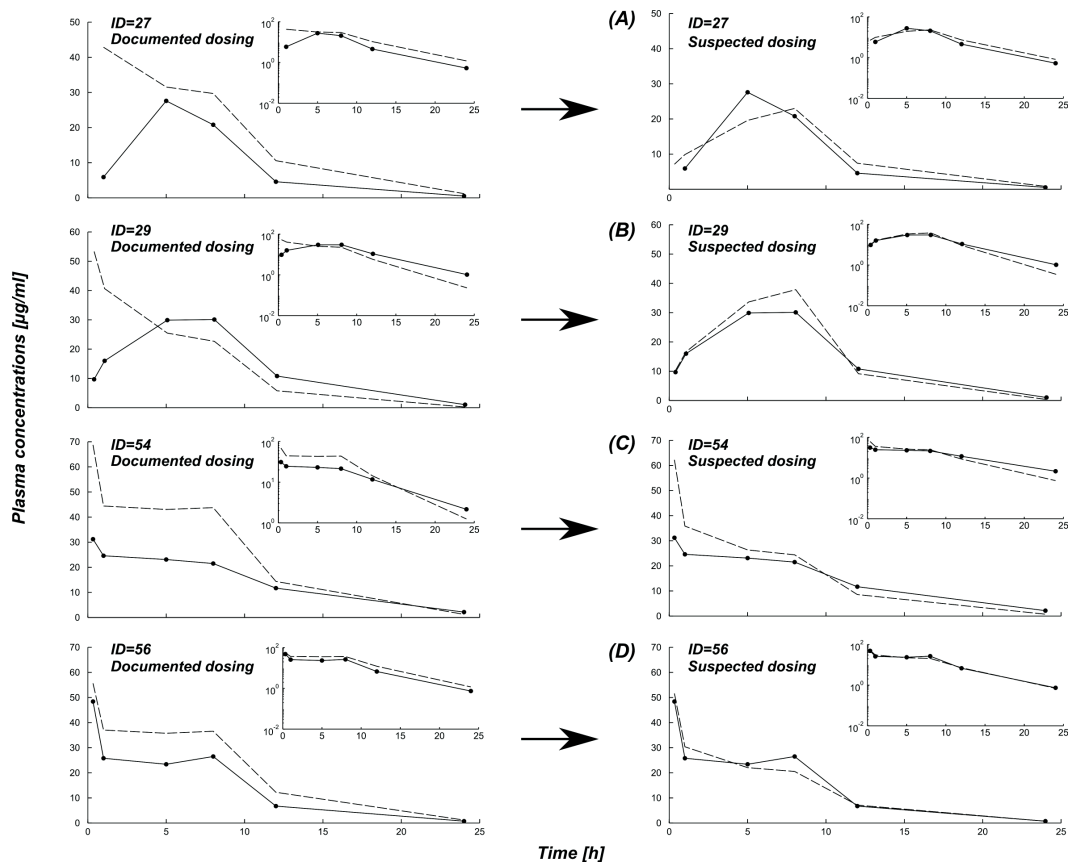


Figure 4-5. A comparison between simulated (dashed line) and observed (dots and solid line) concentrations of IV ivabradine in 4 adult patients, and the effect of suspected undocumented protocol deviations on model results. The left panel depicts simulation results of the patients following the default study dosing protocol of ivabradine, which is the administration of a fixed loading dose of 5 mg IV bolus followed by another dose as an IV infusion over 8 hours (5 mg: patient A; 5.10 mg : patient B; or 10 mg: patients C and D). The right panel depicts the simulation results if the suspected protocol deviation scenario is applied: A) Patient with a suspicion of a missed bolus dose (i.e., only a dose of 5 mg IV infusion is given); B) Patient with a suspicion of having been administered the total amount as infusion only instead of a combination of bolus and infusion; C) and D) Patients with a suspicion of belonging to a group which received a 5 mg IV infusion instead of the supposed 10 mg as listed in the patient information. The simulation results are shown on a linear scale. Inlay graphs show the same results on a semilogarithmic scale.

4.4.2. Ivabradine clearance scaling to children

The clearance scaling module that is integrated into PK-Sim®, the modeling software package used in this study, combines integrated information about ontogeny and maturation of eliminating organs and clearance pathways with information on age-specific differences in organ blood flows and protein binding in order to scale down drug clearance from adults to any pediatric age of interest. In this instance, the clearance scaling was carried out on the previously developed IV adult PBPK model, assuming the hepatic in vivo clearance to be fully attributable to CYP3A4. **Figure 4-6** illustrates the modeled time course of both renal and hepatic clearance of ivabradine across the entire pediatric age spectrum.

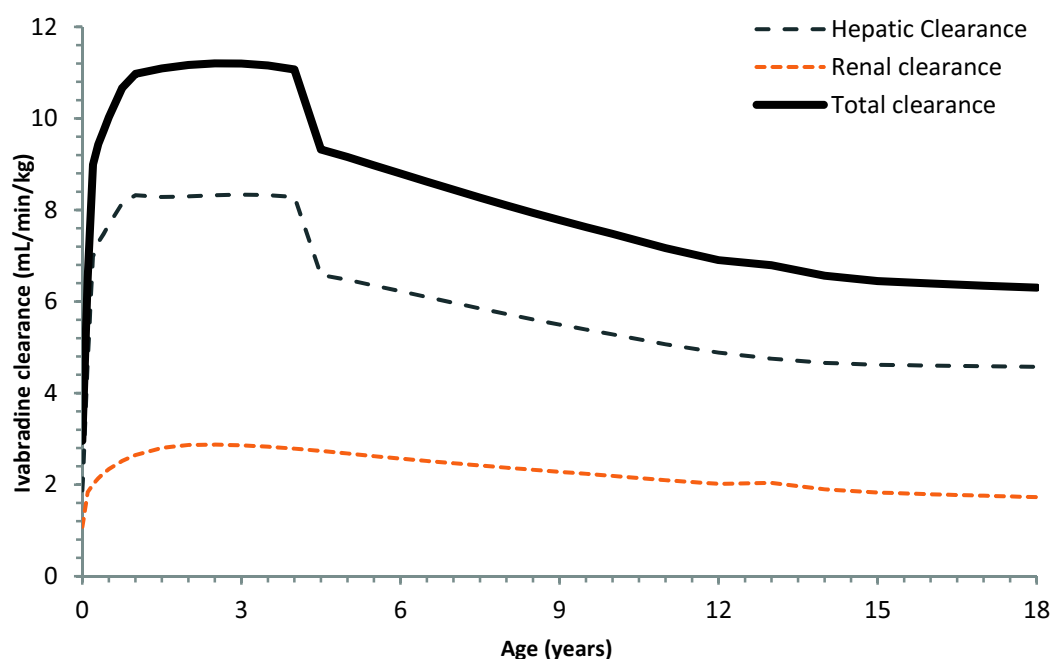


Figure 4-6 Time course of ivabradine clearance through all pediatric age groups: total (bold line), hepatic (dashed gray line) and renal clearance (bottom orange line).

4.4.3. Hypothetical ivabradine exposure in children

Multiple simulations of ivabradine administration to virtual pediatric populations of different age groups were performed using the scaled pediatric model. As previously mentioned, these simulations permit the examination of any age-related differences in ivabradine exposure and disposition between adults and children, and enable the detection and recommendation of any necessary adjustments to the dosing regimens in children, which are usually chosen to be weight-normalized to the same adult dose.

As a result, 32 different population simulations were performed for the following ages:

- 0, 1, 2, 3, 7, and 14 days
- 1, 3, 4, 4.5, 5, 6, and 9 months
- 1, 1.5, 2, 3, 4, 5, 6, 7, 8, 9, 10, 11, 12, 13, 14, 15, 16, 17, and 18 years

Each age group-specific simulation included 1000 virtual children of both genders (50% male, 50% female) who received the same adult weight-normalized dose. This dose was chosen to be 0.14 mg/kg, derived from the most common adult total dose of ivabradine (10 mg) and the mean weight (72.2 kg) of the individuals who received this dose in the original input data. The ivabradine was also administered, as in the adult population, as a combination of an initial bolus of 0.07 mg/kg followed by an IV infusion of 0.07 mg/kg that began 1 minute later and continued for 8 hours. No specific weight or height boundaries were assigned to these virtual populations. To account for inter-individual variations in renal and hepatic clearance, a value of 1.3 log-normal deviations around the mean age-specific clearance was assigned. Results of these simulations are shown in **Table 4-7** and depicted in **Figure 4-7**.

Table 4-7. Predicted Ivabradine Exposure (in Terms of AUC_{0-inf}) Across the Pediatric Age Range

Age	AUC _{0-inf} (mg.h/L)								
	Average	Geo. Mean	Min.	Max.	5 th Prct	25 th Prct	50 th Prct	75 th Prct	95 th Prct
0 d	0.97	0.96	0.54	1.84	0.71	0.84	0.96	1.08	1.3
1 d	0.8	0.79	0.46	1.27	0.59	0.71	0.8	0.89	1.04
2 d	0.7	0.69	0.41	1.33	0.51	0.61	0.69	0.77	0.91
3 d	0.65	0.64	0.4	0.99	0.48	0.57	0.63	0.72	0.84
7 d	0.61	0.6	0.37	1.03	0.46	0.54	0.6	0.67	0.8
14 d	0.53	0.52	0.29	0.89	0.39	0.47	0.52	0.59	0.69
1 m	0.39	0.38	0.23	0.67	0.28	0.34	0.38	0.43	0.52
3 m	0.32	0.31	0.19	0.55	0.24	0.28	0.31	0.35	0.42
4 m	0.19	0.19	0.12	0.31	0.14	0.17	0.19	0.21	0.25
5 m	0.2	0.2	0.12	0.33	0.15	0.18	0.2	0.23	0.27
6 m	0.18	0.18	0.12	0.29	0.14	0.16	0.18	0.2	0.23
9 m	0.18	0.18	0.12	0.31	0.14	0.16	0.18	0.2	0.23
1 y	0.21	0.21	0.13	0.35	0.16	0.19	0.21	0.23	0.27
1.5 y	0.21	0.2	0.12	0.34	0.16	0.18	0.2	0.23	0.26
2 y	0.21	0.21	0.13	0.32	0.16	0.19	0.21	0.23	0.27
3 y	0.2	0.2	0.12	0.32	0.15	0.18	0.2	0.22	0.26
4 y	0.17	0.17	0.1	0.3	0.13	0.15	0.17	0.19	0.23
4,5 y	0.24	0.24	0.15	0.41	0.18	0.22	0.24	0.27	0.32
5 y	0.29	0.29	0.17	0.47	0.22	0.26	0.29	0.33	0.39
6 y	0.35	0.35	0.23	0.58	0.26	0.31	0.35	0.39	0.46
7 y	0.28	0.28	0.18	0.47	0.22	0.25	0.28	0.32	0.36
8 y	0.33	0.32	0.19	0.61	0.25	0.29	0.32	0.36	0.42
9 y	0.27	0.26	0.19	0.43	0.2	0.24	0.26	0.3	0.35
10 y	0.32	0.32	0.2	0.55	0.24	0.28	0.32	0.36	0.42
11 y	0.35	0.35	0.21	0.61	0.26	0.31	0.34	0.39	0.47
12 y	0.38	0.37	0.21	0.64	0.28	0.33	0.37	0.42	0.48
13 y	0.33	0.32	0.2	0.55	0.25	0.29	0.32	0.36	0.43
14 y	0.38	0.38	0.22	0.63	0.29	0.34	0.38	0.42	0.49
15 y	0.37	0.36	0.21	0.68	0.28	0.33	0.36	0.4	0.48
16 y	0.43	0.42	0.26	0.68	0.32	0.38	0.42	0.47	0.56
17 y	0.44	0.43	0.26	0.76	0.33	0.38	0.43	0.48	0.57
18 y	0.45	0.45	0.28	0.71	0.35	0.4	0.45	0.5	0.59
Adults	0.41	0.4	0.19	0.78	0.27	0.34	0.4	0.47	0.59

The administered dose was a unique total dose of 0.14 mg/kg given as an IV bolus injection (0.07 mg/kg) followed by an IV infusion (0.07 mg/kg) over 8 hours (extrapolated from the adult total dose of 10 mg). Results obtained from paediatric population simulations. The reference adult group is of 41-80 years, which is the age range of the observed adult population.

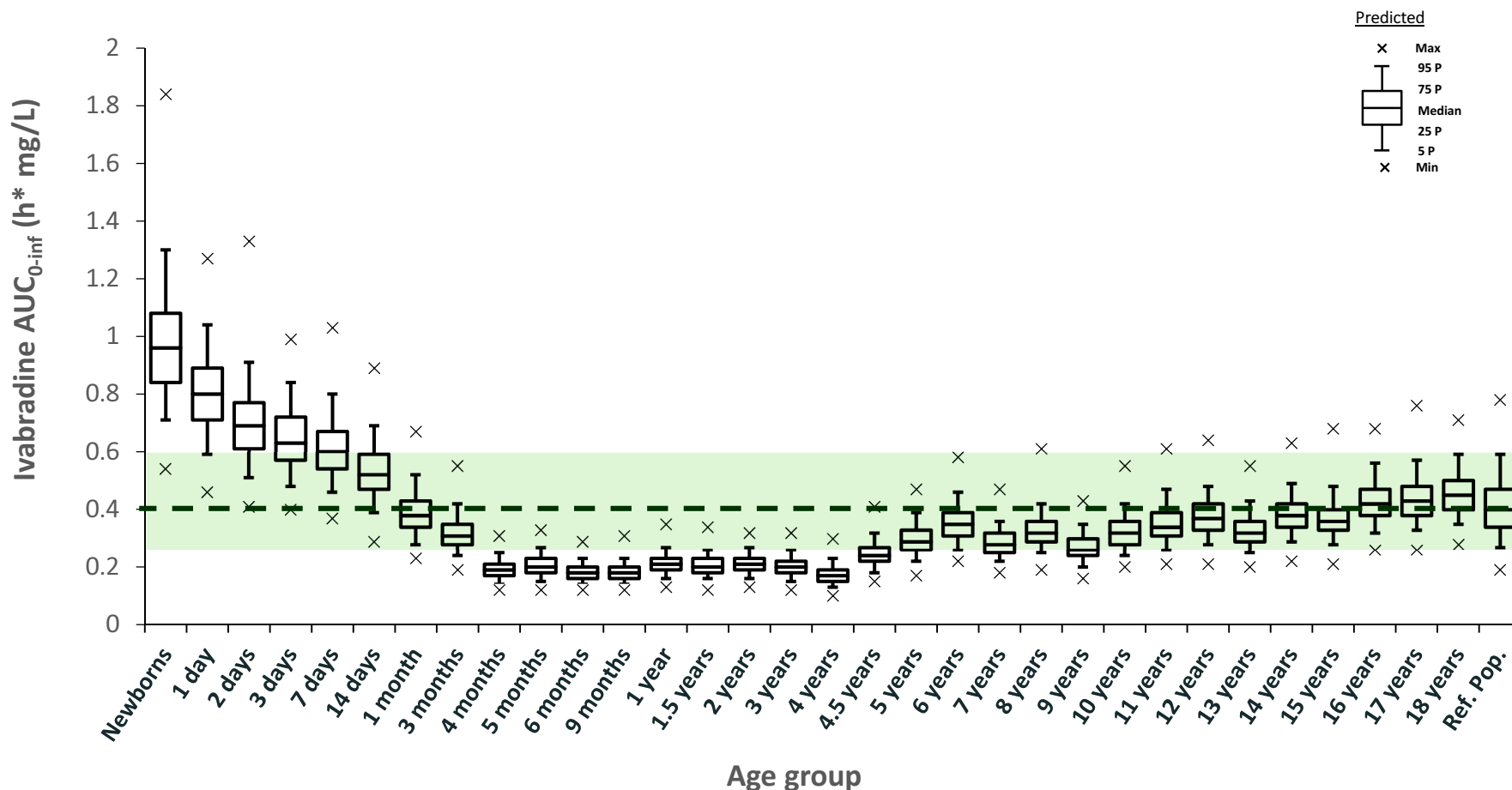


Figure 4-7 Comparison of ivabradine exposure (AUC_{0-inf}) in different pediatric age groups after the administration of a unique total dose of 0.14 mg/kg. The dose was extrapolated from the adult total dose of 10 mg and given as a 0.07 mg/kg IV bolus injection followed by a 0.07 mg/kg IV infusion over 8 hours; n = 1000 virtual children; 50:50 M:F. Inter-individual variation for renal and hepatic clearance were assigned (log-normal distribution, 1.3 deviations around the mean). Reference population age is 41-80 years, which is the age range of the observed adult population. The bold dashed line indicates the average exposure in the reference adult population. The shadowed area indicates the the range between the 5th and 95th percentiles of the exposure in the reference adult population.

As can be seen, the administration of the same weight-normalized adult dose to children without any age adaptation results in variable ivabradine exposures (from -57.5% to +140% of the corresponding adult exposure) with a clear pattern. In comparison to the adults, ivabradine exposure was higher in newborns especially during the first 2 weeks, but much lower in children aged 4 months through 4 years. A higher exposure can be associated with drug toxicity, whereas a lower exposure can be associated with sub-therapeutic concentrations and consequent failure of therapy. These differences in the degree of drug exposure are mainly due to different weight-normalized clearance values across the pediatric age spectrum. For example, children between the ages of 4 months and 4 years show higher weight-normalized clearance values in comparison with adults. Therefore, 95% of the simulated profiles in children within this age range showed an AUC_{0-inf} which was under the 5th percentile of the adult AUC_{0-inf} , indicating the need for a higher weight-normalized dose than in adults.

4.4.4. Recommendations for age-specific dose adaptation in children

The previously presented results of the simulations in the pediatric population show that an age-specific dose adaptation is necessary to achieve a relatively constant drug exposure across the pediatric age spectrum similar to that seen in adults. Therefore, preliminary recommendations on age-specific dose adaptation have been given guided by the previous findings, and doses recommended for pediatric administration in order to achieve the same exposure as in the case of adults are listed in **Table 4-8**.

Table 4-8. Model-predicted pediatric doses needed to achieve the same IV ivabradine exposure as in adults

Pediatric Age	Recommended dose to be given
First 2 weeks of life	0.07 mg/kg BW ^a
Neonates aged 14 days-infants aged 3 months	0.14 mg/kg BW
Infants aged 4 months-children aged 4 years	0.28 mg/kg BW
Children aged 5 through 14 years	0.18 mg/kg BW
Adolescents aged 15 through 18 years	0.14 mg/kg BW or an absolute dose of 10 mg total IV ivabradine

^aBW = Body weight. These doses are recommended to achieve a similar exposure to that achieved by a reference adult dose of 10 mg intravenous ivabradine (~0.14 mg/kg IV). The recommended doses are the total doses for a combined IV bolus and an IV infusion.

To investigate whether these dose adaptations could lead to a more constant exposure in the pediatric population resembling that obtained in adults, the entire set of simulations was repeated using the dose adaptations suggested above. The results showed a significant reduction in the variability of pediatric drug exposure when compared to that of adults (without dose adaptations variations of -57.5% to +140%, with dose adaptations variations of -30% to +30%). The results of representative groups are shown in **Figure 4-8**.

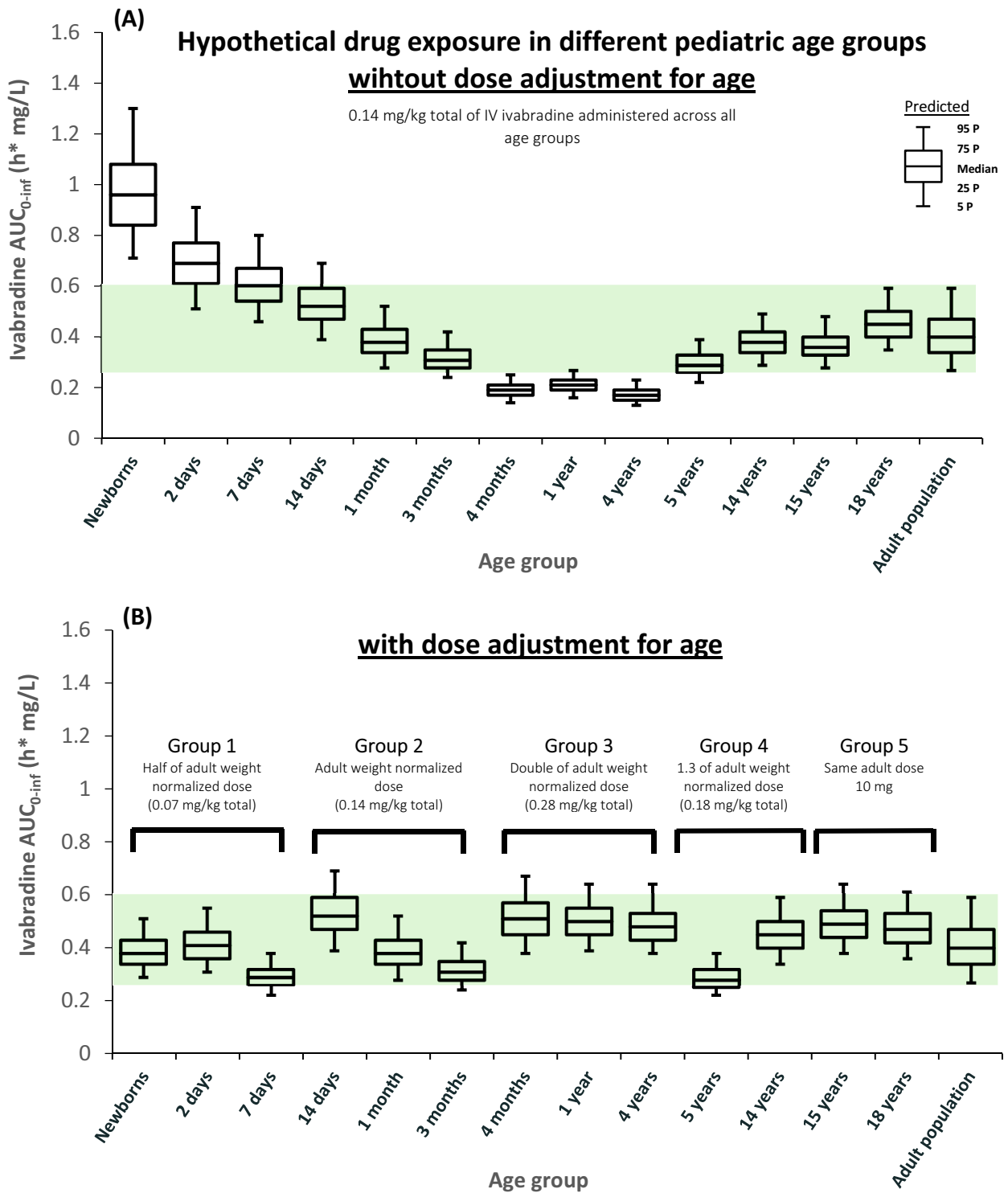


Figure 4-8. Comparison of hypothetical ivabradine exposure **(A)** after administration of the same adult “weight-normalized” dose to all age groups, and **(B)** after administering age-adjusted doses for the different age groups. Ivabradine was administered as a combined IV bolus and infusion just as in the case of adults. Newborns represent neonates on the day of birth. The shadowed area indicates the the range between the 5th and 95th percentiles of the exposure in the reference adult population.

4.5. Conclusion

The final chapter of this thesis presented a physiologically based PK model for the heart-rate lowering drug ivabradine, a drug that could be used in the treatment of SVT in children. A PBPK model for this drug was first developed and validated in adults and then extrapolated to children. The adult model described the observed data in 48 adult patients with adequate accuracy and precision, as indicated by visual inspection of the predicted and observed plasma profiles and by the calculated numerical model metrics. This model was then scaled to children to explore the hypothetical ivabradine exposure from birth to adolescence after IV administration of the drug. The model simulations showed that administering the same weight-normalized adult dose to children resulted in variable ivabradine exposures across the pediatric age spectrum, reflecting age-related PK changes and indicating the need for an age-specific dose adaptation. For example, newborns needed lower weight-normalized doses whereas children aged 4 months to 4 years old needed higher weight-normalized doses compared to adults in order to achieve the same exposure seen in adults. As a result, a dosing scheme of ivabradine was recommended in order to achieve a similar adult drug exposure obtained by the commonly given dose of 10 mg total IV ivabradine. This information will not only guide dosing in children, but will also help future PK trials to be confirmatory rather than exploratory, thus reducing both the costs and the total number of children to be enrolled.

X. Final summary of the thesis and perspectives

This thesis presents a comprehensive overview of the concept, structure, and applications of PBPK modeling and describes a systematic methodology for PBPK model development and validation that could help guide similar efforts in the future, particularly when extrapolating findings to pediatric applications. It also introduces newly evaluated pediatric PBPK models for 3 cardiovascular drugs. These models were developed to address the limitations of currently available models, to improve clinical drug therapy and knowledge of age-related drug PK changes, or to support the drug development process and clinical trials in the field of pediatric cardiology.

In the first part of the thesis, a PBPK model of sotalol was developed and evaluated for accuracy of prediction of the drug exposure in both adults and pediatric patients over the entire pediatric age range using observed PK data from a large patient collective. Neonates were identified as the age group in which the predictions of drug pharmacokinetics were least accurate using models developed with 2 leading PBPK modeling software packages. The findings indicated the need for additional caution while using prediction results from neonates for clinical purposes; however, the final decision should take into consideration both the purpose of the modeling practice as well as the drug safety profile. On the other hand, the good predictions obtained for the remaining pediatric age groups (i.e., children over one year of age), encourage a wider and more confident use of such models to support pediatric clinical trials by running ‘what if’ scenarios and exploring age-related differences in drug absorption and disposition. However, these results may not yet be able to be generalized to all drugs, as this work should be complemented by PBPK models of other drugs of different physicochemical and PK properties and with involvement of different metabolizing enzymes and transporters. Finally, it was seen that the absorption models incorporated into the available modeling software packages still lack age-specific data for some of their anatomical and physiological parameters, which indicates that more focus should be placed on improving them in the future, especially in view of the fact that oral route is the most frequently used route of drug administration.

In the second part, a pediatric PBPK model for amiodarone was developed and shown to be able to capture the complex pharmacokinetics of amiodarone and adequately predict its exposure after IV administration in adults and in 4 out of every 5 pediatric patients regardless of their age. This is a success keeping in mind the nature of this pediatric cohort whose constituents have multiple pathophysiological factors that could influence amiodarone fate in the body and in view of the fact that sudden modifications to the administered drug therapy frequently occur due to the patients' clinical condition, safety concerns, or the pharmacological response, with a resulting possibility of undocumented dosing changes. The "what-if" scenarios performed to explain the deviations observed in 18.45% of the children showed that possible undocumented deviations from study dosing protocol could have occurred. It is therefore recommended that such undocumented deviations be minimized as much as possible, for example, by training and educating the nursing and medical staff responsible for drug administration, by comprehensive documentation of dosing, and by improving sample collection (including collection of additional samples to prevent sample loss) in future trials. In addition, these "what-if" scenarios showed that the potential impact of CYP2C8 polymorphisms, if they exist, is negligible and does not influence the observed amiodarone plasma-concentration-time profile, as distribution processes rather than elimination drive amiodarone plasma concentration-time profiles during the first few days of therapy. Nevertheless, it may be advisable to consider obtaining an extra sample (e.g., blood or saliva) for genotyping to factor in the potential role played by enzyme polymorphisms when performing PK trials of drugs that are metabolized primarily by polymorphic enzymes, since any such polymorphisms could influence the drug disposition and since the availability of such information in advance will enable a more accurate and informative PK analysis. The potential influence of the pathophysiological changes associated with Duchenne muscular dystrophy on amiodarone exposure were also investigated in 1 patient, with the results showing that these changes do influence amiodarone disposition, thus partly explaining the observed deviation. This model can not only be used to support the rationale for adjustment of therapy for individual patients by exploring the dose-exposure relationship in

advance, but could also be extended to a coupled PBPK/PD model to maximize the clinical benefit of such modeling efforts.

In the third part, recommendations on dose selection for “first in children” trials of the heart-rate lowering drug ivabradine were proposed as a complete dosing schema from birth to adolescence. It was shown, using a validated PBPK model, that age-dependent changes in body composition and in organ functions do influence ivabradine disposition, and that dose adaptation must be undertaken for children of different ages in order to obtain a relatively constant drug exposure. As a result, children between 4 months to 4 years of age required double the adult weight-normalized dose to achieve the desired therapeutic concentrations, whereas children in the first few weeks of life did not need more than half the adult weight-normalized dose. These age-appropriate dose recommendations could be incorporated as part of the pediatric investigation plan to be submitted to the regulatory authorities to license ivabradine for use in children.

As has been seen, all of the findings discussed in this thesis, together with the presented examples and applications, point to the same conclusion: the capacity of the PBPK modeling approach to help increase the efficiency of pediatric clinical drug research and development in this vulnerable patient population is significant, which should encourage its utilization on a larger scale taking into consideration the knowledge of its current shortcomings and strengths. It would not be surprising if we soon witness a scenario in which every planned pediatric PK clinical trial is first simulated using the technique of PBPK modeling in order to optimize its design and outcomes, thus saving time, effort, and the need for a large number of trial participants. Moreover, validated PBPK models, especially for drugs with a narrow therapeutic window, could find their way into being integral components of clinical decision support systems for physicians in pediatric wards. Although implementation of the latter possibility may seem to be ambitious at this time, health care providers should not neglect any promising approach that could enhance therapeutic outcomes in routine clinical practice, especially given that many of these models could be, after

validation, extended to a coupled PBPK/PD model that will further encourage their implementation in routine clinical practice.

XI. References

Alt A, Potthast H, Moessinger J, Sickmuller B, Oeser H. Biopharmaceutical characterization of sotalol-containing oral immediate release drug products. *Eur J Pharm Biopharm* 2004;58(1):145–150.

Andrew MA, Hebert MF, Vicini P. Physiologically based pharmacokinetic model of midazolam disposition during pregnancy. *Conf Proc IEEE Eng Med Biol Soc* 2008;2008:5454–5457.

Antonaccio MJ, Gomoll A. Pharmacology, pharmacodynamics and pharmacokinetics of sotalol. *Am J Cardiol* 1990;65(2):12A-21A; discussion 35A-36A.

Anttila M, Arstila M, Pfeffer M, Tikkanen R, Vallinkoski V, Sundquist H. Human pharmacokinetics of sotalol. *Acta Pharmacol Toxicol (Copenh)* 1976;39(1):118–128.

Austin RP, Barton P, Cockcroft SL, Wenlock MC, Riley RJ. The influence of nonspecific microsomal binding on apparent intrinsic clearance, and its prediction from physicochemical properties. *Drug Metab Dispos* 2002;30(12):1497–1503.

Barbosa L, Vera H, Moran S, Del Prado M, Lopez-Alarcon M. Reproducibility and reliability of the ¹³C-acetate breath test to measure gastric emptying of liquid meal in infants. *Nutrition* 2005;21(3):289–294.

Barnett C, Snel A, Omari T, Davidson G, Haslam R, Butler R. Reproducibility of the ¹³C-octanoic acid breath test for assessment of gastric emptying in healthy preterm infants. *J Pediatr Gastroenterol Nutr* 1999;29(1):26–30.

Barrett JS, Della Casa Alberighi O, Laer S, Meibohm B. Physiologically based pharmacokinetic (PBPK) modeling in children. *Clin Pharmacol Ther* 2012;92(1):40–49.

Baruscotti M, Bucchi A, Difrancesco D. Physiology and pharmacology of the cardiac pacemaker ("funny") current. *Pharmacol Ther* 2005;107(1):59–79.

Bellanti F, Della Pasqua O. Modelling and simulation as research tools in paediatric drug development. *Eur J Clin Pharmacol* 2011;67 Suppl 1:75–86.

Bischoff KB. Some fundamental considerations of the applications of pharmacokinetics to cancer chemotherapy. *Cancer Chemother Rep* 1975;59(4):777–793.

Bjorkman S. Prediction of drug disposition in infants and children by means of physiologically based pharmacokinetic (PBPK) modelling: theophylline and midazolam as model drugs. *Br J Clin Pharmacol* 2005;59(6):691–704.

Bjorkman S, Wada DR, Berling BM, Benoni G. Prediction of the disposition of midazolam in surgical patients by a physiologically based pharmacokinetic model. *J Pharm Sci* 2001;90(9):1226–1241.

Bonati M, Gaspari F, D'Aranno V, Benfenati E, Neyroz P, Galletti F et al. Physicochemical and analytical characteristics of amiodarone. *J Pharm Sci* 1984;73(6):829–831.

Borer JS, Bohm M, Ford I, Komajda M, Tavazzi L, Sendon JL et al. Effect of ivabradine on recurrent hospitalization for worsening heart failure in patients with chronic systolic heart failure: the SHIFT Study. *Eur Heart J* 2012;33(22):2813–2820.

Bouzom F, Walther B. Pharmacokinetic predictions in children by using the physiologically based pharmacokinetic modelling. *Fundam Clin Pharmacol* 2008;22(6):579–587. doi:10.1111/j.1472-8206.2008.00648.x.

Brochot C, Toth J, Bois FY. Lumping in pharmacokinetics. *J Pharmacokinet Pharmacodyn* 2005;32(5-6):719–736. doi:10.1007/s10928-005-0054-y.

Brown RP, Delp MD, Lindstedt SL, Rhomberg LR, Beliles RP. Physiological parameter values for physiologically based pharmacokinetic models. *Toxicol Ind Health* 1997;13(4):407–484.

Buck SS de, Mackie CE. Physiologically based approaches towards the prediction of pharmacokinetics: in vitro-in vivo extrapolation. *Expert Opin Drug Metab Toxicol* 2007;3(6):865–878.

Camm AJ, Lau C. Electrophysiological effects of a single intravenous administration of ivabradine (S 16257) in adult patients with normal baseline electrophysiology. *Drugs R D* 2003;4(2):83–89.

Carr RA, Foster RT, Lewanczuk RZ, Hamilton PG. Pharmacokinetics of sotalol enantiomers in humans. *J Clin Pharmacol* 1992;32(12):1105–1109.

Chatelain P, Laruel R. Amiodarone partitioning with phospholipid bilayers and erythrocyte membranes. *J Pharm Sci* 1985;74(7):783–784.

Cheymol G, Poirier JM, Carrupt PA, Testa B, Weissenburger J, Levron JC et al. Pharmacokinetics of beta-adrenoceptor blockers in obese and normal volunteers. *Br J Clin Pharmacol* 1997;43(6):563–570.

Clewell H3, Gentry PR, Covington TR, Gearhart JM. Development of a physiologically based pharmacokinetic model of trichloroethylene and its metabolites for use in risk assessment. *Environ Health Perspect* 2000;108 Suppl 2:283–305.

Clewell H3, Gentry PR, Gearhart JM, Covington TR, Banton MI, Andersen ME. Development of a physiologically based pharmacokinetic model of isopropanol and its metabolite acetone. *Toxicol Sci* 2001;63(2):160–172.

Clewell HJ, Gentry PR, Covington TR, Sarangapani R, Teeguarden JG. Evaluation of the potential impact of age- and gender-specific pharmacokinetic. *Toxicol Sci* 2004;79(2):381–393. doi:10.1093/toxsci/kfh109.

Commission of the European Communities. Regulation (EC) No 1901/2006 on medicinal products for paediatric use and amending Regulation (EC) No 1768/92, Directive 2001/20/EC, Directive 2001/83/EC and Regulation (EC) No 726/2004. *Official Journal of the European Communities* L378 27/12/, 2006:1–19.

Cushing DJ, Adams MP, Cooper WD, Zhang B, Lipicky RJ, Kowey PR. Evaluation of the effects of PM101, a cyclodextrin-based formulation of intravenous amiodarone, on blood pressure in healthy humans. *Am J Cardiol* 2009;104(8):1152–1157.

Dahan A, Miller JM, Hilfinger JM, Yamashita S, Yu LX, Lennernas H et al. High-permeability criterion for BCS classification: segmental/pH dependent permeability considerations. *Mol Pharm* 2010;7(5):1827–1834.

Dennison JE, Bigelow PL, Mumtaz MM, Andersen ME, Dobrev ID, Yang RSH. Evaluation of potential toxicity from co-exposure to three CNS depressants (toluene, ethylbenzene, and xylene) under resting and working conditions using PBPK modeling. *J Occup Environ Hyg* 2005;2(3):127–135.

Duffull SB, Chabaud S, Nony P, Laveille C, Girard P, Aarons L. A pharmacokinetic simulation model for ivabradine in healthy volunteers. *Eur J Pharm Sci* 2000;10(4):285–294.

Dumont C, Mentre F, Gaynor C, Brendel K, Gesson C, Chenel M. Optimal sampling times for a drug and its metabolite using SIMCYP(R) simulations as prior information. *Clin Pharmacokinet* 2013;52(1):43–57.

Edginton AN, FOTAKI N. Oral drug absorption in pediatric populations. In: *Oral Drug Absorption: Prediction and Assessment*, 2nd edn.: New York, NY: Informa Healthcare, 2010, S. 108-126.

Edginton AN, Ritter L. Predicting plasma concentrations of bisphenol A in children younger than 2 years of age after typical feeding schedules, using a physiologically based toxicokinetic model. *Environ Health Perspect* 2009;117(4):645–652.

Edginton AN, Schmitt W, Voith B, Willmann S. A mechanistic approach for the scaling of clearance in children. *Clin Pharmacokinet* 2006;45(7):683–704.

Edginton AN, Schmitt W, Willmann S. Development and evaluation of a generic physiologically based pharmacokinetic model for children. *Clin Pharmacokinet* 2006;45(10):1013–1034.

Edginton AN, Willmann S. Physiology-based simulations of a pathological condition: prediction of pharmacokinetics in patients with liver cirrhosis. *Clin Pharmacokinet* 2008;47(11):743–752.

El-Masri HA, Kenyon EM. Development of a human physiologically based pharmacokinetic (PBPK) model for inorganic arsenic and its mono- and dimethylated metabolites. *J Pharmacokinet Pharmacodyn* 2008;35(1):31–68. doi:10.1007/s10928-007-9075-z.

Espie P, Tytgat D, Sargentini-Maier M, Poggesi I, Watelet J. Physiologically based pharmacokinetics (PBPK). *Drug Metab Rev* 2009;41(3):391–407.

European Medicines Agency (EMA) 2013. Ivabradine: Summary of Product Characteristics. http://www.ema.europa.eu/docs/en_GB/document_library/EPAR_-_Product_Information/human/000597/WC500043590.pdf. Accessed December 14, 2013.

Funck-Brentano C. Pharmacokinetic and pharmacodynamic profiles of d-sotalol and d,l-sotalol. *Eur Heart J* 1993;14:30–35.

Gallo JM, Vicini P, Orlansky A, Li S, Zhou F, Ma J et al. Pharmacokinetic model-predicted anticancer drug concentrations in human tumors. *Clin Cancer Res* 2004;10(23):8048–8058. doi:10.1158/1078-0432.CCR-04-0822.

Gastroplus. Advanced absorption, pharmacokinetic and pharmacodynamic simulation software. <http://www.simulations-plus.com/Products.aspx?grpID=3&clD=16&plD=11>. Accessed December 16, 2013.

Gentilcore D, Hausken T, Horowitz M, Jones KL. Measurements of gastric emptying of low- and high-nutrient liquids using 3D ultrasonography and scintigraphy in healthy subjects. *Neurogastroenterol Motil* 2006;18(12):1062–1068.

Germani M, Crivori P, Rocchetti M, Burton PS, Wilson AGE, Smith ME et al. Evaluation of a basic physiologically based pharmacokinetic model for simulating the first-time-in-animal study. *Eur J Pharm Sci* 2007;31(3-4):190–201.

Ginsberg G, Hattis D, Russ A, Sonawane B. Physiologically based pharmacokinetic (PBPK) modeling of caffeine and theophylline in neonates and adults: implications for assessing children's risks from environmental agents. *J Toxicol Environ Health A* 2004;67(4):297–329.

Graff J, Brinch K, Madsen JL. Gastrointestinal mean transit times in young and middle-aged healthy subjects. *Clin Physiol* 2001;21(2):253–259.

Grass GM, Sinko PJ. Physiologically-based pharmacokinetic simulation modelling. *Adv Drug Deliv Rev* 2002;54(3):433–451.

Hamelin G, Charest-Tardif G, Truchon G, Tardif R. Physiologically based modeling of n-hexane kinetics in humans following 2,5-hexanedione in urine and on n-hexane in alveolar air. *J Occup Environ Hyg* 2005;2(2):86-97; quiz D6-7. doi:10.1080/15459620590909673.

Hanyok JJ. Clinical pharmacokinetics of sotalol. *Am J Cardiol* 1993;72(4):19A-26A.

Hays SM, Elswick BA, Blumenthal GM, Welsch F, Conolly RB, Gargas ML. Development of a physiologically based pharmacokinetic model of 2-methoxyethanol and 2-methoxyacetic acid disposition in pregnant rats. *Toxicol Appl Pharmacol* 2000;163(1):67–74. doi:10.1006/taap.1999.8836.

Holt DW, Tucker GT, Jackson PR, McKenna WJ. Amiodarone pharmacokinetics. *Br J Clin Pract Suppl* 1986;44:109–114.

International Conference on Harmonisation; guidance on E11 clinical investigation of medicinal products in the pediatric population; availability. Notice. *Fed Regist* 2000;65(242):78493–78494.

Jadhav PR, Kern SE. The need for modeling and simulation to design clinical investigations in children. *J Clin Pharmacol* 2010;50(9 Suppl):121S-129S.

Jamei M, Marciniak S, Feng K, Barnett A, Tucker G, Rostami-Hodjegan A. The Simcyp population-based ADME simulator. *Expert Opin Drug Metab Toxicol* 2009;5(2):211–223.

Jamei M, Turner D, Yang J, Neuhoff S, Polak S, Rostami-Hodjegan A et al. Population-based mechanistic prediction of oral drug absorption. *AAPS J* 2009;11(2):225–237.

Johnson TN, Boussery K, Rowland-Yeo K, Tucker GT, Rostami-Hodjegan A. A semi-mechanistic model to predict the effects of liver cirrhosis on drug clearance. *Clin Pharmacokinet* 2010;49(3):189–206. doi:10.2165/11318160-000000000-00000.

Johnson TN, Rostami-Hodjegan A. Resurgence in the use of physiologically based pharmacokinetic models in pediatric clinical pharmacology: parallel shift in incorporating the knowledge of biological elements and increased applicability to drug development and clinical practice. *Paediatr Anaesth* 2011;21(3):291–301.

Johnson TN, Rostami-Hodjegan A, Tucker GT. Prediction of the clearance of eleven drugs and associated variability in neonates, infants and children. *Clin Pharmacokinet* 2006;45(9):931–956.

Jones HM, Parrott N, Ohlenbusch G, Lave T. Predicting pharmacokinetic food effects using biorelevant solubility media and physiologically based modelling. *Clin Pharmacokinet* 2006;45(12):1213–1226.

Kahela P, Anttila M, Tikkanen R, Sundquist H. Effect of food, food constituents and fluid volume on the bioavailability of sotalol. *Acta Pharmacol Toxicol (Copenh)* 1979;44(1):7–12.

Kawahara M, Nanbo T, Tsuji A. Physiologically based pharmacokinetic prediction of p-phenylbenzoic acid disposition in the pregnant rat. *Biopharm Drug Dispos* 1998;19(7):445–453.

Kersting G, Willmann S, Wurthwein G, Lippert J, Boos J, Hempel G. Physiologically based pharmacokinetic modelling of high- and low-dose etoposide: from adults to children. *Cancer Chemother Pharmacol* 2012;69(2):397–405.

Khalil F, Laer S. Physiologically based pharmacokinetic models in the prediction of oral drug exposure over the entire pediatric age range-sotalol as a model drug. *AAPS J* 2014;16(2):226–239. doi: 10.1208/s12248-013-9555-6.

Khalil F, Laer S. Physiologically based pharmacokinetic modeling: methodology, applications, and limitations with a focus on its role in pediatric drug development. *J Biomed Biotechnol* 2011;2011:907461. doi: 10.1155/2011/907461.

Khin M, Bolin TD, Tin-Oo, Thein-Win-Nyunt, Kyaw-Hla S, Thein-Thein-Myint. Investigation of small-intestinal transit time in normal and malnourished children. *J Gastroenterol* 1999;34(6):675–679.

Kimura M, Umemura K, Ikeda Y, Kosuge K, Mizuno A, Nakanomyo H et al. Pharmacokinetics and pharmacodynamics of (+/-)-sotalol in healthy male volunteers. *Br J Clin Pharmacol* 1996;42(5):583–588.

Kowey PR, Marinchak RA, Rials SJ, Bharucha D. Pharmacologic and pharmacokinetic profile of class III antiarrhythmic drugs. *Am J Cardiol* 1997;80(8A):16G-23G.

Laer S, Barrett JS, Meibohm B. The in silico child: using simulation to guide pediatric drug development and manage pediatric pharmacotherapy. *J Clin Pharmacol* 2009;49(8):889–904.

Laer S, Elshoff J, Meibohm B, Weil J, Mir TS, Zhang W et al. Development of a safe and effective pediatric dosing regimen for sotalol based on population pharmacokinetics and pharmacodynamics in children with supraventricular tachycardia. *J Am Coll Cardiol* 2005;46(7):1322–1330.

Laer S, Neumann J, Scholz H. Interaction between sotalol and an antacid preparation. *Br J Clin Pharmacol* 1997;43(3):269–272.

Lalloz MR, Byfield PG, Greenwood RM, Himsworth RL. Binding of amiodarone by serum proteins and the effects of drugs, hormones and other interacting ligands. *J Pharm Pharmacol* 1984;36(6):366–372.

Liebau. Versuche zur Wechselwirkung zwischen Sotalol und Colestyramin bei Menschen. Degree “Maguna cum laude”, Faculty of Medicine, University of Hamburg, 1999.

Li J, Gwilt PR. The effect of age on the early disposition of doxorubicin. *Cancer Chemother Pharmacol* 2003;51(5):395–402. doi:10.1007/s00280-002-0554-z.

Liu X, Smith BJ, Chen C, Callegari E, Becker SL, Chen X et al. Use of a physiologically based pharmacokinetic model to study the time to reach brain equilibrium: an

experimental analysis of the role of blood-brain barrier. *J Pharmacol Exp Ther* 2005;313(3):1254–1262. doi:10.1124/jpet.104.079319.

Maharaj AR, Barrett JS, Edginton AN. A Workflow Example of PBPK Modeling to Support Pediatric Research and Development: Case Study with Lorazepam. *AAPS J* 2013.

Manolis E, Osman TE, Herold R, Koenig F, Tomasi P, Vamvakas S et al. Role of modeling and simulation in pediatric investigation plans. *Paediatr Anaesth* 2011;21(3):214–221.

Manolis E, Pons G. Proposals for model-based paediatric medicinal development within the current European Union regulatory framework. *Br J Clin Pharmacol* 2009;68(4):493–501.

Martinez C, Garcia-Martin E, Blanco G, Gamito FJG, Ladero JM, Agundez JAG. The effect of the cytochrome P450 CYP2C8 polymorphism on the disposition of (R)-ibuprofen enantiomer in healthy subjects. *Br J Clin Pharmacol* 2005;59(1):62–69.

MATLAB: Mathworks. <http://www.mathworks.com/products/matlab/>. Accessed December 16, 2013.

McDevitt DG. Comparison of pharmacokinetic properties of beta-adrenoceptor blocking drugs. *Eur Heart J* 1987;8 Suppl M:9–14.

Meier J. Pharmacokinetic comparison of pindolol with other beta-adrenoceptor-blocking agents. *Am Heart J* 1982;104(2 Pt 2):364–373.

Nestorov I. Whole body pharmacokinetic models. *Clin Pharmacokinet* 2003;42(10):883–908.

Nestorov I. Whole-body physiologically based pharmacokinetic models. *Expert Opin Drug Metab Toxicol* 2007;3(2):235–249.

Nestorov IA, Aarons LJ, Arundel PA, Rowland M. Lumping of whole-body physiologically based pharmacokinetic models. *J Pharmacokinet Biopharm* 1998;26(1):21–46.

Ochs HR, Greenblatt DJ, Arendt RM, Schafer-Korting M, Mutschler E. Single-dose kinetics of oral propranolol, metoprolol, atenolol, and sotalol: relation to lipophilicity. *Arzneimittelforschung* 1985;35(10):1580–1582.

Ohyama K, Nakajima M, Nakamura S, Shimada N, Yamazaki H, Yokoi T. A significant role of human cytochrome P450 2C8 in amiodarone N-deethylation: an approach to predict the contribution with relative activity factor. *Drug Metab Dispos* 2000;28(11):1303–1310.

Paixao P, Gouveia LF, Morais JAG. Prediction of the in vitro intrinsic clearance determined in suspensions of human hepatocytes by using artificial neural networks. *Eur J Pharm Sci* 2010;39(5):310–321.

Parrott N, Davies B, Hoffmann G, Koerner A, Lave T, Prinssen E et al. Development of a physiologically based model for oseltamivir and simulation of pharmacokinetics in neonates and infants. *Clin Pharmacokinet* 2011;50(9):613–623.

Parrott N, Jones H, Paquereau N, Lave T. Application of full physiological models for pharmaceutical drug candidate selection and extrapolation of pharmacokinetics to man. *Basic Clin Pharmacol Toxicol* 2005;96(3):193–199.

Parrott N, Lave T. Applications of physiologically based absorption models in drug discovery and development. *Mol Pharm* 2008;5(5):760–775.

PK-Sim. <http://www.systems-biology.com/products/pk-sim.html>. Accessed December 16, 2013.

Poirier JM, Jaillon P, Lecocq B, Lecocq V, Ferry A, Cheymol G. The pharmacokinetics of d-sotalol and d,l-sotalol in healthy volunteers. *Eur J Clin Pharmacol* 1990;38(6):579–582.

Portoles A, Calvo A, Terleira A, Laredo L, Resplandy G, Gorostiaga C et al. Lack of pharmacokinetic interaction between omeprazole or lansoprazole and ivabradine in healthy volunteers: an open-label, randomized, crossover, pharmacokinetic interaction clinical trial. *J Clin Pharmacol* 2006;46(10):1195–1203.

Poulin P, Theil FP. A priori prediction of tissue:plasma partition coefficients of drugs to facilitate the use of physiologically-based pharmacokinetic models in drug discovery. *J Pharm Sci* 2000;89(1):16–35.

Pourbaix S, Berger Y, Desager JP, Pacco M, Harvengt C. Absolute bioavailability of amiodarone in normal subjects. *Clin Pharmacol Ther* 1985;37(2):118–123.

PubChem Compound Database; CID= 2157: Amiodarone. National Center for Biotechnology Information. http://pubchem.ncbi.nlm.nih.gov/summary/summary.cgi?cid=2157&loc=ec_rcs. Accessed December 16, 2013.

PubChem Compound Database; CID = 132999: Ivabradine. National Center for Biotechnology Information. <http://pubchem.ncbi.nlm.nih.gov/summary/summary.cgi?cid=132999>. Accessed December 15, 2013.

PubChem Compound Database; CID= 5253: Sotalol. National Center for Biotechnology Information. <http://pubchem.ncbi.nlm.nih.gov/summary/summary.cgi?cid=5253>. Accessed December 16, 2013.

Ragueneau I, Laveille C, Jochemsen R, Resplandy G, Funck-Brentano C, Jaillon P. Pharmacokinetic-pharmacodynamic modeling of the effects of ivabradine, a direct sinus node inhibitor, on heart rate in healthy volunteers. *Clin Pharmacol Ther* 1998;64(2):192–203.

Ramusovic S, Laer S, Meibohm B, Lagler FB, Paul T. Pharmacokinetics of intravenous amiodarone in children. *Arch Dis Child* 2013.

Reddy MB, Andersen ME, Morrow PE, Dobrev ID, Varaprath S, Plotzke KP et al. Physiological modeling of inhalation kinetics of octamethylcyclotetrasiloxane in humans during rest and exercise. *Toxicol Sci* 2003;72(1):3–18.

Rehm KD, Schnelle K, Dyde CJ, Blumner E, Arendts W. Plasma level and action of sotalol-HCL on the ECG interval after parenteral administration in healthy subjects. *Arzneimittelforschung* 1987;37(9):1058–1062.

Riddell JG, Harron DW, Shanks RG. Clinical pharmacokinetics of beta-adrenoceptor antagonists. An update. *Clin Pharmacokinet* 1987;12(5):305–320.

Rodgers T, Leahy D, Rowland M. Physiologically based pharmacokinetic modeling 1: predicting the tissue distribution of moderate-to-strong bases. *J Pharm Sci* 2005;94(6):1259–1276.

Rodgers T, Rowland M. Physiologically based pharmacokinetic modelling 2: predicting the tissue distribution of acids, very weak bases, neutrals and zwitterions. *J Pharm Sci* 2006;95(6):1238–1257.

Rodgers T, Rowland M. Mechanistic approaches to volume of distribution predictions: understanding the processes. *Pharm Res* 2007;24(5):918–933.

Rowland M, Peck C, Tucker G. Physiologically-based pharmacokinetics in drug development and regulatory science. *Annu Rev Pharmacol Toxicol* 2011;51:45–73.

Rowland YK, Jamei M, Yang J, Tucker GT, Rostami-Hodjegan A. Physiologically based mechanistic modelling to predict complex drug-drug interactions involving simultaneous competitive and time-dependent enzyme inhibition by parent compound and its metabolite in both liver and gut -the effect of diltiazem on the time-course of exposure to triazolam. *Eur J Pharm Sci* 2010;39(5):298–309.

Ruell JA, Tsinman O, Avdeef A. Acid-base cosolvent method for determining aqueous permeability of amiodarone, itraconazole, tamoxifen, terfenadine and other very insoluble molecules. *Chem Pharm Bull (Tokyo)* 2004;52(5):561–565.

Salazar DE, Much DR, Nichola PS, Seibold JR, Shindler D, Slugg PH. A pharmacokinetic-pharmacodynamic model of d-sotalol Q-Tc prolongation during intravenous administration to healthy subjects. *J Clin Pharmacol* 1997;37(9):799–809.

Sasaki Y, Wagner HN JR. Measurement of the distribution of cardiac output in unanesthetized rats. *J Appl Physiol* 1971;30(6):879–884.

Schmitt W. General approach for the calculation of tissue to plasma partition coefficients. *Toxicol In Vitro* 2008;22(2):457–467.

Sheiner LB, Beal SL. Some suggestions for measuring predictive performance. *J Pharmacokinet Biopharm* 1981;9(4):503–512.

Shiga T, Tanaka T, Irie S, Hagiwara N, Kasanuki H. Pharmacokinetics of intravenous amiodarone and its electrocardiographic effects on healthy Japanese subjects. *Heart Vessels* 2011;26(3):274–281.

Shiran MR, Proctor NJ, Howgate EM, Rowland-Yeo K, Tucker GT, Rostami-Hodjegan A. Prediction of metabolic drug clearance in humans: in vitro-in vivo extrapolation vs allometric scaling. *Xenobiotica* 2006;36(7):567–580.

Simcyp. <http://www.simcyp.com>. Accessed December 16, 2013.

Smith SC JR, Feldman TE, Hirshfeld JW JR, Jacobs AK, Kern MJ, King SB3 et al. ACC/AHA/SCAI 2005 Guideline Update for Percutaneous Coronary Intervention-Summary Article: A Report of the American College of Cardiology/American Heart Association Task Force on Practice Guidelines (ACC/AHA/SCAI Writing Committee to Update the 2001 Guidelines for Percutaneous Coronary Intervention). *J Am Coll Cardiol* 2006;47(1):216–235.

Somberg JC, Preston RA, Ranade V, Molnar J. Developing a safe intravenous sotalol dosing regimen. *Am J Ther* 2010;17(4):365–372.

Staelens S, van den Driessche M, Barclay D, Carrie-Faessler A, Haschke F, Verbeke K et al. Gastric emptying in healthy newborns fed an intact protein formula, a partially and an extensively hydrolysed formula. *Clin Nutr* 2008;27(2):264–268.

Summary of Product Characteristics, Corlentor® 5. mg-(EMA). http://www.ema.europa.eu/docs/en_GB/document_library/EPAR_-_Product_Information/human/000598/WC500035341.pdf. Accessed December 16, 2013.

Sundquist, H.; Anttila, M.; Simon, A.; Reich, J. W. (1979): Comparative bioavailability and pharmacokinetics of sotalol administered alone and in combination with hydrochlorothiazide. In: *J Clin Pharmacol* 19 (8-9 Pt 2), S. 557–564.

Sun H, Pang KS. Physiological modeling to understand the impact of enzymes and transporters on drug and metabolite data and bioavailability estimates. *Pharm Res* 2010;27(7):1237–1254. doi:10.1007/s11095-010-0049-2.

Tardif J, Ponikowski P, Kahan T. Efficacy of the I(f) current inhibitor ivabradine in patients with chronic stable angina receiving beta-blocker therapy: a 4-month, randomized, placebo-controlled trial. *Eur Heart J* 2009;30(5):540–548.

Taylor PJ, Cruickshank JM. Distribution coefficients of atenolol and sotalol. *J Pharm Pharmacol* 1985;37(2):143–144.

Tjandramaga TB. Altered pharmacokinetics of beta-adrenoceptor blocking drugs in patients with renal insufficiency. *Arch Int Pharmacodyn Ther* 1980;Suppl:38–53.

Uematsu T, Kanamaru M, Nakashima M. Comparative pharmacokinetic and pharmacodynamic properties of oral and intravenous (+)-sotalol in healthy volunteers. *J Pharm Pharmacol* 1994;46(7):600–605.

Vadiei K, Troy S, Korth-Bradley J, Chiang ST, Zimmerman JJ. Population pharmacokinetics of intravenous amiodarone and comparison with two-stage pharmacokinetic analysis. *J Clin Pharmacol* 1997;37(7):610–617.

Valentin J. Basic anatomical and physiological data for use in radiological protection: reference values: ICRP Publication 89. *Annals of the ICRP* /9//;32(3-4):1–277.

van Den Driessche M, Veereman-Wauters G. Gastric emptying in infants and children. *Acta Gastroenterol Belg* 2003;66(4):274–282.

Veronese ME, McLean S, Hendriks R. Plasma protein binding of amiodarone in a patient population: measurement by erythrocyte partitioning and a novel glass-binding method. *Br J Clin Pharmacol* 1988;26(6):721–731.

Vossen M, Sevestre M, Niederalt C, Jang IJ, Willmann S, Edginton AN. Dynamically simulating the interaction of midazolam and the CYP3A4 inhibitor itraconazole using individual coupled whole-body physiologically-based pharmacokinetic (WB-PBPK) models. *Theor Biol Med Model* 2007;4:13.

Wada DR, Harashima H, Ebling W, Osaki EW, Stanski DR. Effects of thiopental on regional blood flows in the rat. *Anesthesiology* 1996;84(3):596–604.

Wang RYGaLL. Calculating partition coefficient by atom-additive method: *Perspectives in Drug Discovery and Design* 19.1 (2000): 47-66.

Ward KW, Blumenthal GM, Welsch F, Pollack GM. Development of a physiologically based pharmacokinetic model to describe the. *Toxicol Appl Pharmacol* 1997;145(2):311–322. doi:10.1006/taap.1997.8170.

Willmann S, Lippert J, Sevestre M, Solodenko J, Fois F, Schmitt W. PK-Sim®: a physiologically based pharmacokinetic ‘whole-body’ model. *BIOSILICO* 2003;1(4):121–4.

Willmann S. [The in silico Child. Can computer simulations replace clinical pharmacokinetic. *Pharm Unserer Zeit* 2009;38(1):62–67. doi:10.1002/pauz.200800297.

Willmann S, Lippert J, Schmitt W. From physicochemistry to absorption and distribution: predictive mechanistic modelling and computational tools. *Expert Opin Drug Metab Toxicol* 2005;1(1):159–168.

Willmann S, Schmitt W, Keldenich J, Lippert J, Dressman JB. A physiological model for the estimation of the fraction dose absorbed in humans. *J Med Chem* 2004;47(16):4022–4031.

Woods PB, Robinson ML. An investigation of the comparative liposolubilities of beta-adrenoceptor blocking agents. *J Pharm Pharmacol* 1981;33(3):172–173.

Yang F, Tong X, McCarver DG, Hines RN, Beard DA. Population-based analysis of methadone distribution and metabolism using an age-dependent physiologically based pharmacokinetic model. *J Pharmacokinet Pharmacodyn* 2006;33(4):485–518. doi:10.1007/s10928-006-9018-0.

Yang Y, Faustino PJ, Volpe DA, Ellison CD, Lyon RC, Yu LX. Biopharmaceutics classification of selected beta-blockers: solubility and permeability class membership. *Mol Pharm* 2007;4(4):608–614.

Zhang X, Quinney SK, Gorski JC, Jones DR, Hall SD. Semiphysiologically based pharmacokinetic models for the inhibition of midazolam clearance by diltiazem and its major metabolite. *Drug Metab Dispos* 2009;37(8):1587–1597. doi:10.1124/dmd.109.026658.

Zhi J, Moore R, Kanitra L, Mulligan TE. Effects of orlistat, a lipase inhibitor, on the pharmacokinetics of three highly lipophilic drugs (amiodarone, fluoxetine, and simvastatin) in healthy volunteers. *J Clin Pharmacol* 2003;43(4):428–435.

XII. Curriculum Vitae

PERSONAL DETAILS:

Name: Feras Khalil
Date/Place of birth: 01.01.1983; Bochum, Germany
Address: Heinrich-Heine-University of Düsseldorf
Institute of Clinical Pharmacy and Pharmacotherapy
Building: 26.22 Room: 02.21
Universitätsstrasse. 1, 40225 Düsseldorf
Telephone: 004917684464099
eMail: feras.khalil@uni-duesseldorf.de

EMPLOYMENT

15 Oct. 2009–present Under contract as a research associate/teaching assistant at the Institute of Clinical Pharmacy and Pharmacotherapy at the Heinrich-Heine-Universität, Düsseldorf, Germany.

EDUCATION

June 2009–present PhD student at the institute of Clinical Pharmacy and Pharmacotherapy at the Heinrich-Heine-Universität, Düsseldorf, Germany.

Sept. 2008–June 2009 Thesis research (Master thesis equivalent) in preparation of a PhD thesis at the Institute of Clinical Pharmacy and Pharmacotherapy at the Heinrich-Heine-Universität, Düsseldorf, Germany.

Apr. 2007–Feb. 2008 German language courses and exams culminating in successful completion of the “TestDaF” at the Ruhr-Universität, Bochum, Germany.

2007 Syrian colloquium for pharmacy (National Total Test).

2000–2006 Doctor of Pharmacy “PharmD” Degree from Faculty of Pharmacy, Jordan University of Science and Technology, Irbid, Jordan. Good grade (73.2%).

1997-2000 Secondary education at 'Mustafa Khallouf' Secondary School in Tartous, Syria. [Certificate of Secondary Education (GSCE) with General Points Average of 85.8/100 (scientific section)].

TRAINING:

Oct. 05–June 2006 Hospital training (clinical clerkship) in various medical wards during the last graduation year as a graduation requirement to obtain PharmD degree, King Abdullah Hospital, Irbid, Jordan.

June 05–Sept. 2005 Training as a community pharmacist in 'Zat Al-Nitaqain' Pharmacy, Irbid, Jordan.

PUBLICATIONS:

2014 Khalil F, Läer S. Modeling and simulation to support neonatal clinical trials. A book chapter in "Neonatal Pharmacology and Nutrition Update": a volume in the series "Pediatric and Adolescent Medicine". In press.

2014 Khalil F, Läer S. Physiologically based pharmacokinetic models in the prediction of oral drug exposure over the entire pediatric age range – sotalol as a model drug. *AAPS J.* 2014;16(2):226-239. doi: 10.1208/s12248-013-9555-6.

2011 Khalil F, Läer S. Physiologically Based Pharmacokinetic Modeling: Methodology, Applications, and Limitations with a Focus on Its Role in Pediatric Drug Development. *J Biomed Biotechnol.* 2011;2011:907461. doi: 10.1155/2011/907461.

ORAL PRESENTATIONS:

Mar. 2013 Khalil F, Läer S. Physiologically based pharmacokinetic models to describe oral sotalol exposure from adults to children: A comparison of two modeling software

- programs. Presented at a national meeting for pharmacometrics: „Pharmacometrics in NRW”, Cologne, Germany (2013).
- Sept. 2011 Khalil F, Läer S. Physiology based pharmacokinetic modeling as a tool to explore drug disposition in newborns and infants and point to a new area of research. Presented at Clinical Trials in Pediatrics – 7th edition; SEMINAR “Pharmacokinetics & Pharmacodynamics in Pediatrics”, Genoa, Italy (2011).
- June 2011 Khalil F, Läer S. Physiologically-based pharmacokinetic modeling as a tool to explore drug disposition in newborns and infants and point to a new area of research. Presented at the 13th ESDPPP Congress, Oslo, Norway (2011).
- Sept. 2010 Khalil F, Läer S. Pediatric drug trials and clinical practice – challenges for clinical pharmacists; Presented at the 2nd Expert Workshop: ‘Can the "in silico Child" help to develop better medicines for our children?’, Genoa, Italy (2010).
- POSTERS:**
- Oct. 2013 Khalil F, Läer S. A bottom-approach to simulate amiodarone pharmacokinetics in children. Presented at a national meeting for pharmacometrics: „Pharmacometrics in NRW”, Cologne, Germany (2013).
- Mar. 2012 Khalil F, Läer S. Assembling of a multicenter and multinational data base to develop and validate a physiologically based pharmacokinetic sotalol model for pediatric extrapolation. Presented at the 2012 ASCPT Annual Meeting, National Harbor, Maryland, USA (2012).
- June 2009 Khalil F, Läer S. Development of a physiologically based pharmacokinetic model for a typical “kidney drug” –

Sotalol – in adults and children. Presented at the 12th ESDPPP Congress; Chamonix, France (2009).

ATTENDED WORKSHOPS OF INTERDISCIPLINARY GRADUATE AND RESEARCH ACADEMY

DÜSSELDORF (IGRAD):

- June 2013 “Get into teaching for doctoral researchers” – an iGrad workshop (credited as 16 work units), at the Heinrich-Heine Universität, Düsseldorf, Germany.
- Apr. 2013 “Job Hunting and Interview skills” – an iGrad workshop (credited as 16 work units), at the Heinrich-Heine Universität, Düsseldorf, Germany.
- Oct. 2012 “Presenting Science 1 – Comprehensive, Competent and Convincing” – an iGrad workshop (credited as 16 work units), at the Heinrich-Heine Universität, Düsseldorf, Germany.
- Nov. 2012 “Optimizing Writing Strategies for Publishing in English” – an iGrad workshop (credited as 16 work units), at the Heinrich-Heine Universität, Düsseldorf, Germany.
- Aug. 2012 “Introduction to Good Scientific Practice” – an iGrad workshop (credited as 6 work units), at the Heinrich-Heine Universität, Düsseldorf, Germany.

SELECTED WORKSHOPS, COURSES, AND SEMINARS:

- June 2013 GRIP Roadshow-Training Course: Medicines in children-what you need to know; Attended at the 14th biennial ESDP congress, Salzburg, Austria.
- Apr. 2013 “Introduction to R”, a compact course at the Heinrich-Heine Universität, Düsseldorf, Germany.
- May 2012 Simcyp™ Focused workshop on Parameter Estimation and Pharmacodynamics, Sheffield, UK.

- Dec. 2011 “Project Management Tools and Leadership for Young Professionals”. Seminar at Heinrich-Heine Universität, Düsseldorf, Germany.
- Sept. 2011 Clinical trials in pediatrics – 7th edition, Seminar “Pharmacokinetics & Pharmacodynamics in Pediatrics”, Genoa, Italy.
- June 2011 CME-Course on Drug therapy in Pregnancy, Neonates, Infants and Children. Challenges in Treatment, Assessment, and ADRs; Attended at the 13th biennial ESDP congress, Oslo, Norway
- Sept. 2010 Workshop on ‘Concepts and Applications of Predicting ADME, Pharmacokinetics and Population Variability’ at Simcyp 11th Consortium Meeting & Workshops, Sheffield, UK.

OTHER SKILLS

- Languages: Arabic: native speaker; German and English: Fluent both written and spoken.
- Computer skills: Microsoft office® (Excel, Word, Powerpoint), SimCYP®, PK-SIM®, MATLAB®, Simbiology, R®, SPSS®, Phoenix® WinNonlin®.
